DESIGN AND FORMULATION OF HYBRID BIOACTIVE COATINGS USING THERMAL SPRAY PROCESS

A
Thesis Report

Submitted in partial fulfilment of the requirement for the award of Degree of

MASTER OF ENGINEERING
IN
CAD/CAM and ROBOTICS

Submitted By
Harpreet Singh
Roll no. 800881009

Under the guidance of

Dr. Rahul Chhibber
Assistant Professor
Mechanical Engineering Department
Thapar University
Patiala

Dr. A.K. Chattopadhyay
Professor and Head
Mechanical Engineering Department
Mody Institute of Technology and Science
Lakshmangarh, Rajasthan

DEPARTMENT OF MECHANICAL ENGINEERING
THAPAR UNIVERSITY
PATIALA-147004, INDIA

CERTIFICATE

This is to certify that the work which is being presented in this thesis entitled "**Design and formulation of hybrid bioactive coatings using thermal spray process**", in partial fulfilment of requirement for the award of the Master Degree in CAD/CAM and Robotics, submitted in the Mechanical Engineering Department, Thapar University, Patiala, is an authentic record of the research work carried out by me under the guidance of **Dr. Rahul Chhibber, Assistant Professor, Mechanical Engineering Department, Thapar University, Patiala and Dr. A.K. Chattopadhyay, Professor and Head, Mechanical Engineering Department, Mody Institute of Technology and Science, Lakshmangarh, Rajasthan.**

The matter embodied in this report has not been submitted in part or full to any other university or institute for the award of any other degree.

Harpreet Singh

Dated: 15 July 2010 **(Harpreet Singh)**

This is to certify that the above statement made by the candidate concerned is correct to the best of my knowledge & belief.

Rahul Chhibber

Dr. RAHUL CHHIBBER
Assistant Professor
Mechanical Engineering Department
Thapar University
Patiala

Dr. A.K. CHATTOPADHYAY
Professor and Head
Mechanical Engineering Department
Mody Institute of Technology and Science
Lakshmangarh, Rajasthan

Countersigned by

Dr. S.K. MOHAPATRA
Professor and Head
Mechanical Engineering Department
Thapar University, Patiala

Dr. R.K. SHARMA
Dean of Academic Affairs
Thapar University
Patiala

ACKNOWLEDGEMENT

I am highly grateful to the authorities of Thapar University, Patiala for providing me this opportunity to carry out the seminar work.

I would first like to extend my deepest thank to my advisors, Dr. Rahul Chhibber and Dr. A.K. Chattopadhyay, for not only the research opportunity they have given me, but also their guidance. Their assistance extends far beyond the call of duty as they have also supplied the support, motivation, knowledge and the most importantly patience that have helped me complete this seminar report.

I would like to offer my sincere thanks to Dr. S.K. Mohapatra (H.O.D.) of Mechanical Engineering Department, Thapar University, Patiala for allowing me to work in the research lab after college working hours.

I would also like to thank the individuals who have helped me through my journey to this point: Dr. Harpreet Singh (Assistant Professor, Indian Institute of Technology, Ropar) and Mr.Tarun Nanda (Assistant Professor, Mechanical Engineering Department, Thapar University, Patiala).

Special thanks must be given to the M.S. Harhsa Vardhan (Chief Executive Officer, SVX Powder M Surface Engineering (Pvt.) Limited, Greater Noida) for providing me their support to accomplish coating process.

Final thanks must also be extended to my family, friends and lab-mates, particularly my mother and father.

HARPREET SINGH

ABSTRACT

Hydroxyapatite $Ca_{10}(PO_4)_6(OH)_2$, commonly referred to as HA, has attracted wide spread interest from both the orthopaedic and dental fields due to its excellent biocompatibility and tissue bioactivity properties. Hydroxyapatite is chemically similar to the mineral component of bones and hard tissues in mammals. It is one of the few materials that are considered bioactive, meaning that it will support bone growth when used in orthopaedic and dental applications.

Despite excellent properties as a biomaterial, the ceramic nature and the inherent mechanical properties of HA specifically brittleness, poor tensile strength and poor impact resistance have restricted its application in many load-bearing applications. In order for the HA coating to be effective and reliable, it must be strongly bonded to the metallic surface. Substitution of other elements has shown the potential to improve the bioactivity of HA. Titanium oxide (TiO_2) and Aluminium oxide (Al_2O_3) are added in HA powder to prevent corrosion and wear of metallic surface.

In the present investigation, an attempt is made to develop HA powder from Chicken eggshell, a natural apatite rich substance through heat treatment method. Eggshell, a cheaper source of HA is generated as waste material during egg processing. Fourier transform-infrared spectroscopy (FT-IR) and X-ray diffraction (XRD) techniques are employed to investigate the proof of formation of HA phase. The blood clotting test shows that both the powders are efficient and compatible with human blood.

The coating of Hybrid powder using HA, TiO_2, Al_2O_3 is developed on SS 304L metal substrate by using detonation gun spray technique. Coated samples are obtained at various D-Gun parameters. Samples are tested for Wear, Micro structural analysis, Hardness, Micro hardness, etc., to find the optimum D-Gun parameters.

LIST OF FIGURES

LIST OF TABLES

CONTENTS

Chapter 1 INTRODUCTION

Implants

An implant is a medical device manufactured to replace a missing biological structure, or to support a damaged biological structure. The surface of implants that contact the body might be made of a biomedical material such as titanium, silicone or apatite. In orthopaedic surgery, implants may refer to devices that are placed over or within bones to hold a fracture reduction while prosthesis would be the more appropriate term for devices that replace a part. Common areas of application including orthopaedic re-constructive prosthesis, cardiac prosthesis (artificial heart valves) and dental implant are shown in Fig1.1.

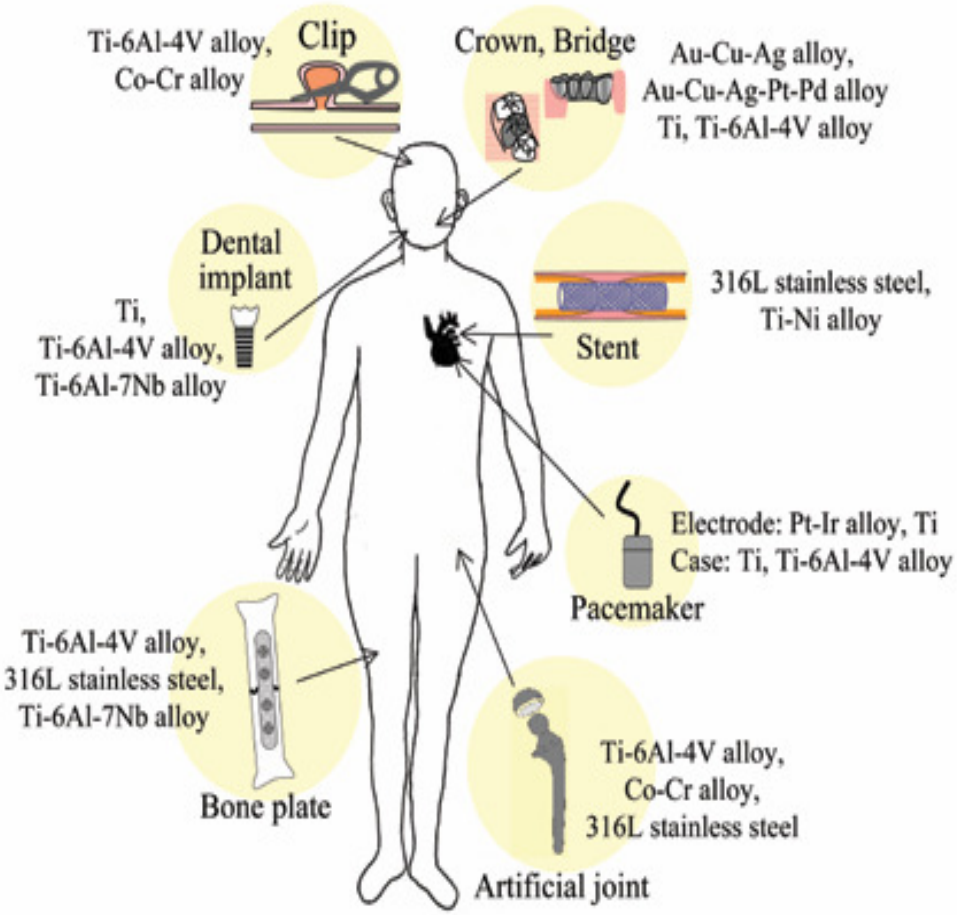

Fig1.1 Metallic devices and metallic biomaterials in human body [25].

1.1 Bio materials for implants

Biomaterials are materials used for making devices that can interact with biological systems. Williams (1981) defined biomaterials as "Any nonliving materials used in medical devices, intended to interact with the biological systems". Biomaterials are widely used in repair, or replacement of damaged parts of the musculoskeletal system such as bones, joints and teeth. A majority of the applications are summarized in Fig1.2 (Hench 1985). The fundamental requirement of a biomaterial is that the material and the tissue environment of the body should coexist without having any undesirable effect on each other [20].

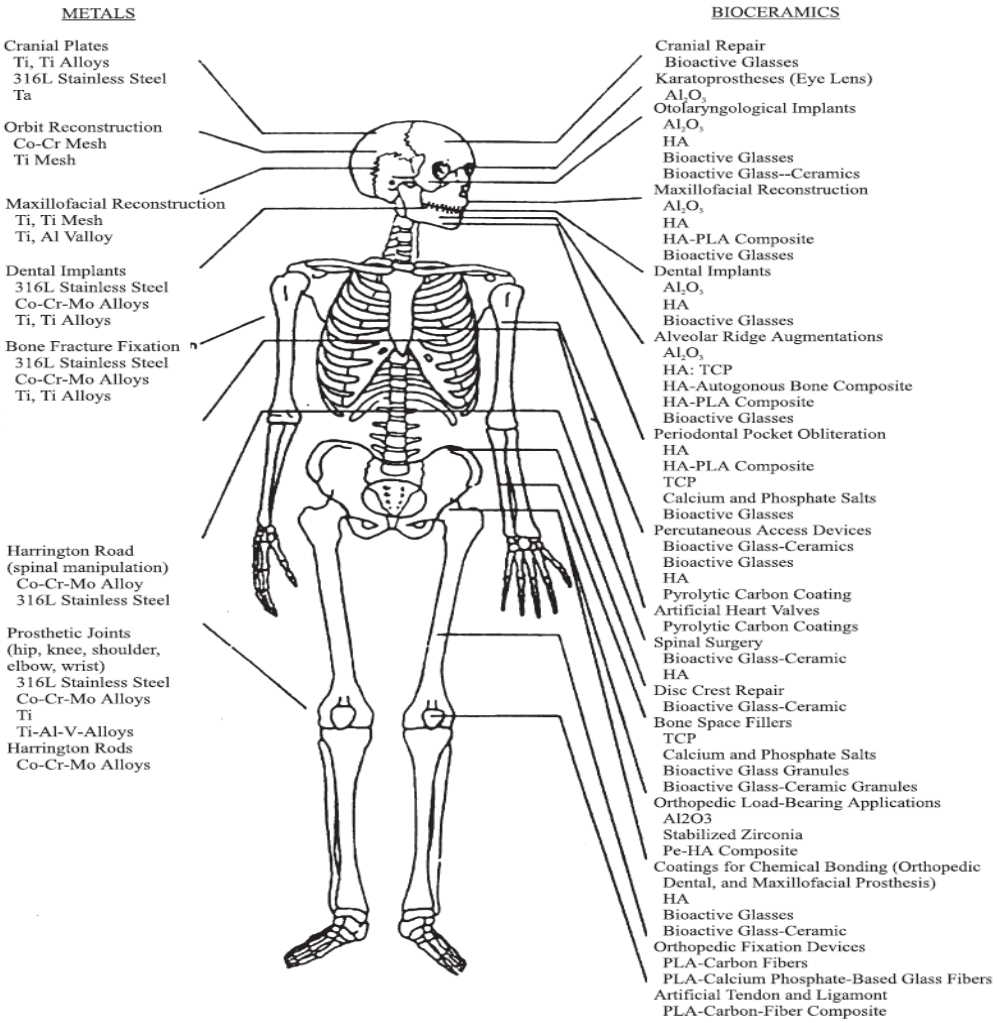

Fig1.2 Clinical uses of inorganic biomaterials (Hench, 1985) [20].

Ceramics

Ceramics are inorganic compounds that can be classified into five categories of biomaterials by their macroscopic surface characteristics or by their chemical stability in the body environment. They are carbon, alumina, zirconia, bioactive glass (glass ceramics) and calcium phosphate. The limitations of ceramic materials are their low tensile strength and fracture toughness. Their use in bulk form is therefore limited to functions in which only compressive loads are applied.

Polymers

Polymers are considered for implant applications in various forms such as fibres, textiles, rods and viscous liquids. Recently, polymers have been introduced for hip socket replacement in orthopaedic implant applications due to its close resemblance to natural polymeric tissue components. However, polymers undergo degradation in the body environment due to biochemical and mechanical factors. This results in ionic attack and formation of hydroxyl ions and dissolved oxygen, leading to tissue irritation and decrease in mechanical properties.

Composites

Composites are materials obtained by combining two or more materials or phases with a view to take advantage of the salient features of each constituent. It is essential that each component of the composite be biocompatible to avoid degradation between interfaces of the constituents. Fibre-reinforced polymers (FRP) are the most widely investigated composites for biomedical applications.

Metals and alloys

Metals and alloys have a wide range of applications including as devices for fracture fixation, partial and total joint replacement. The high modulus and yield point coupled with the ductility of metals make them suitable for load-bearing without leading to large deformations and permanent dimensional changes. The implant materials may corrode or wear, leading to the generation of particulate debris. The application of metals and alloys is very important in orthopaedic, as they play a very important role in fulfilling almost every difficult factor that arises in implant applications.

Currently used metallic implant materials

The fundamental criterion for choosing a metallic implant material is that it should possess biocompatibility. Metals and alloys have been widely used in various forms as implants, which provide the required mechanical strength and reasonable corrosion resistance. Metallic implants are usually made of one of the three types of materials: austenitic stainless steels, cobalt–chromium alloys and titanium and its alloys (Sivakumar *et al* 1992, 1994). The mechanical properties of these metals and alloys as recommended by ASTM are given in Table1.1 and compositions of common metal alloys are given in Table1.2. These materials are accepted by the body environment because of their inert oxide layer formed on the surface. Cobalt–chromium alloys have the excellent corrosion resistance property. However, they are not recommended for joint prosthesis because of their poor frictional properties with itself or with other materials.

Amongst all these materials, titanium and its alloys are the most corrosion resistant materials. Titanium alloys provide sufficient strength and corrosion resistance: Ti-6Al-4V, Ti-5Al-2.5Fe, Ti-6Al-7Nb, etc. However, the main disadvantages are their high cost, inferior wear properties, diffusion of oxygen into titanium during fabrication and heat treatment. These deficiencies in applications have demanded the surface modification of the material, which would enhance corrosion and wear resistance without altering the mechanical properties.

Material	Tensile strength $(MN/m)^2$	Yield strength $(MN/m)^2$	Elongation at fracture	Vickers hardness (H_v)	Young's modulus $(GN/m)^2$	Fatigue limit $(GN/m)^2$
316L SS (annealed)	650	280	45	190	211	0·28
Wrought Co–Cr alloy	1540	1050	9	450	541	0·49
Cast Co–Cr alloy	690	490	8	300	241	0·30
Titanium	710	470	30	–	121	0·30
Ti-6Al-4V	1000	970	12	–	121	–
Human bone	137·3	–	1·49	26·3	30	–

Table1.1 Mechanical Properties of current implant materials [20].

Element %	Co-Cr-Mo (1)	Co-Cr-Mo (2)	Stainless Steel GradeI/II (max) (3)	Stainless Steel (max) (4)	Stainless Steel (max) (5)	Ti-6Al-4V (max) (6)
Aluminum	-	0-0.30	-	-	-	5.5-6.50
Boron	-	0-0.01	-	-	-	-
Carbon	0-0.35	0-0.35	0.08/0.030	0.03	0.08	0.08
Chromium	27.0-30.0	27.0-30.0	17.019.0/17.0-19.0	17.0-19.0	19.5-22.0	-
Cobalt	Balance	Balance	-	-	-	-
Copper	-	-	0.50/0.50	0.5	0.25	-
Hydrogen	-	-	-	-	-	0.012
Iron	0-0.75	0-0.75	Balence/Balence	Balance	Balance	0.25
Manganese	0-1.0	0-1.0	2.0/2.0	2	2.0-4.25	-
Molybendeum	5.0-7.0	5.0-7.0	2.0-3.0/20-3.0	2.25-3.0	2.0-3.0	-
Nickle	0-1.0	0-1.0	13.0-15.5/13.0-15.5	13.0-15.0	9.0-11.0	-
Nitrogen	-	0-0.25	0.10/0.10	0.1	0.25-0.8	0.05
Oxygen	-	-	-	-	-	0.13
Phosphorous	-	-	0.025/0.025	0.025	0.025	-
Silicon	0-1.0	0-1.0	0.75/0.75	0.75	0.75	-
Sulfur	-	0-0.019	0.010/0.010	0.01	0.01	-
Titanium	-	-	-	-	-	Balance
Tungsten	-	0-0.20	-	-	-	-
Vanadium	-	-	-	-	-	3.5-4.5

1. ASTM F75-92-Cobalt-Chromium-Molybdenum Alloy.
2. ASTM F75-98- Cobalt-28 Chromium-6 Molybdenum Casting Alloy and Cast.
3. ASTM F138-92-Stainless Steel Bar and Wire (Special Quality).
4. ASTM 139-96-Wrought-18 Chromium-14 Nickel-2.5 Molybdenum Stainless Sheet and Strip.
5. ASTM F1586-Wrought Nitrogen Strengthened-21 Chromium-10 Nickel-3 Maganese-2, 5 Molybdenum Stainless Steel Bar.
6. ASTM F136-96-Wrought Titanium-6-Aluminium-4-Vanadium ELI (Extra low Interstitial) Alloy.

Table1.2 Composition of common metal alloys used in orthopaedic implants [31]

1.2 The requirements of biomaterials can be grouped into four broad categories[28]

I) Biocompatibility: The material must not disturb or induce un-welcoming response, but rather promote good tissue-implant integration. An initial burst of inflammatory response is expected and is sometimes considered essential in the healing process. However, prolonged inflammation is not desirable as it may indicate incompatibility.

II) Sterilizability: The material must be able to undergo sterilization. Sterilization techniques include gamma, gas (ethylene oxide (ETO)) and steam autoclaving. Some polymers such as polyacetal will depolymerize and give off the toxic gas formaldehyde when subjected under high energy radiation by gamma. These polymers are thus best sterilized by ETO.

III) Functionability: The functionability of a medical device depends on the ability of the material to be shaped to suit a particular function. The material must therefore be able to be shaped economically using engineering fabrication processes.

IV) Manufacturability: It is often the last step, the manufacturability of the material that hinders the actual production of the medical device.

1.3 Causes of implant failure

I) Fatigue and Wear: Fatigue is caused by repeated load and time fluctuations, whereas wear is due to adhesion and abrasion of particulates between two articulating bearing surfaces. Wear is affected by many factors including the type of materials, contact stresses, surface hardness and roughness, type of articulation due to motion, number of cycles, solution particle count and distribution, oxidation of materials, and surface abrasions of both metal and polyethylene particulates.

II) Corrosion: Corrosion is the unwanted chemical reaction of metal with its environment, resulting in its continued degradation to oxides, hydroxides, or other compounds. Tissue fluid in human body contains water, dissolved oxygen, proteins, and various ions such as chloride and hydroxide. As the result, the human body presents a very aggressive environment for metals used for implantations. Corrosion resistance of a metallic implant material is consequently an important aspect of its

biocompatibility. The metals and alloys often used for biomedical applications, such as 316L stainless steel, titanium, Ti-6Al-4V, Co-Cr-Mo and Ni-Ti, do indeed form surface oxide films within the human body, which usually provide good corrosion resistance. Problems can arise if the oxide film is damaged. As well as causing weakening of the implant. Corrosion has the undesirable consequence of releasing possibly toxic metal ions into the body [26,27]. The types of corrosion that are pertinent to the currently used alloys are pitting, crevice, galvanic, intergranular, stress-corrosion cracking, corrosion fatigue and fretting corrosion.

1.4 Hydroxyapatite Coatings for Biomedical Implants

Hydroxyapatite (HA), Ca_{10} $(PO_4)_6(OH)_2$, is a commonly used biomaterial for prostheses encompassing orthopedic, maxillofacial and dental applications. HA is chemically similar to the mineral component of bone. It is applied to metallic implants of titanium alloys and stainless steels in order to promote bone ingrowths. Key issues are the adhesion of the coating to the metallic substrate and the control of coating composition and microstructure during deposition. HA is thermodynamically unstable at the high temperatures used in plasma spraying and this promotes the formation of CaO, which reacts with water and has a high solubility in body fluids. High temperature deposition processes are also responsible for the formation of amorphous phases that reduce the coating-metal interfacial strength. Therefore recent developments have concentrated on improving coating stability and adhesion [21].

It is bioactive, means that it can integrate into bone structures and support growth without breaking down or dissolving in the human body. Implants need to be coated to trick the body; if this was not done, and the body would identify an implant as a foreign object and work to isolate it instead of incorporating it. Hydroxyapatite can also be used in instances where there are bone voids or defects. This process involves powders, blocks, or beads of the mineral being placed into or on the affected of areas of bone. Since it is bioactive, it encourages the bone to grow and correct the problem.

1.5 Thermal Spray Coating techniques

Thermal spraying is a group of coating processes in which finely divided metallic or nonmetallic materials are deposited in a molten or semi-molten condition to form a coating. The coating material may be in the form of powder, ceramic-rod, wire, or molten materials.

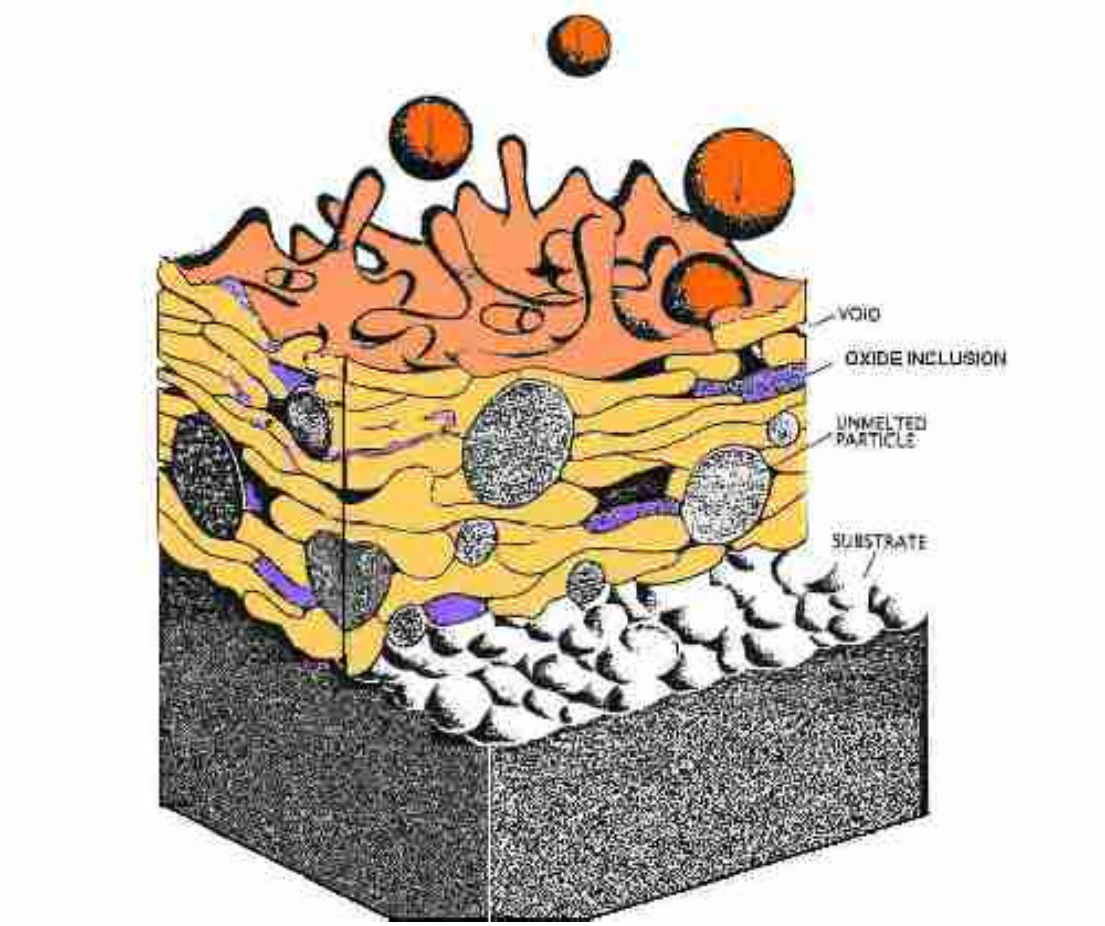

Fig.1.3 Schematic Diagram of Thermal Spray Metal Coating [29]

Different types of thermal spray process are shown in Fig.1.4.

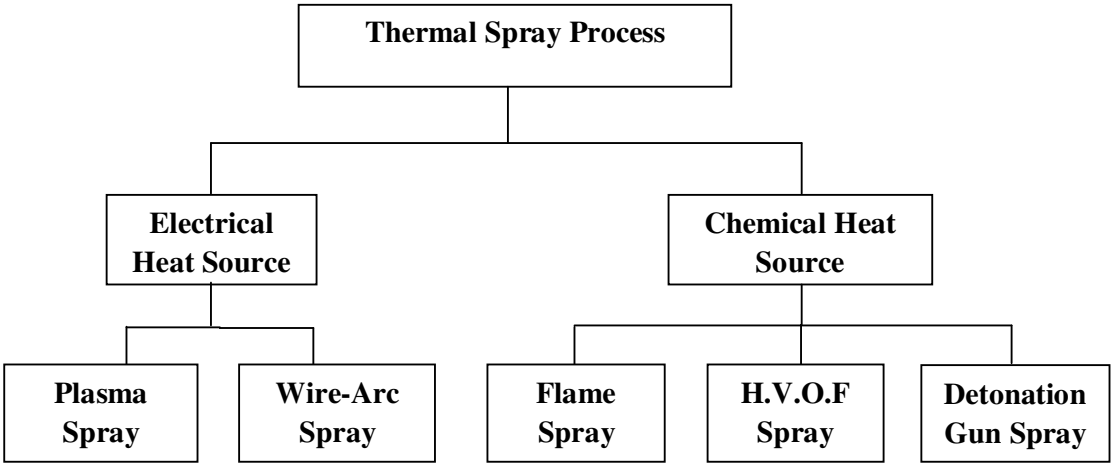

Fig1.4 Different Thermal Spray Processes.

1.5.1 Plasma Spray Process

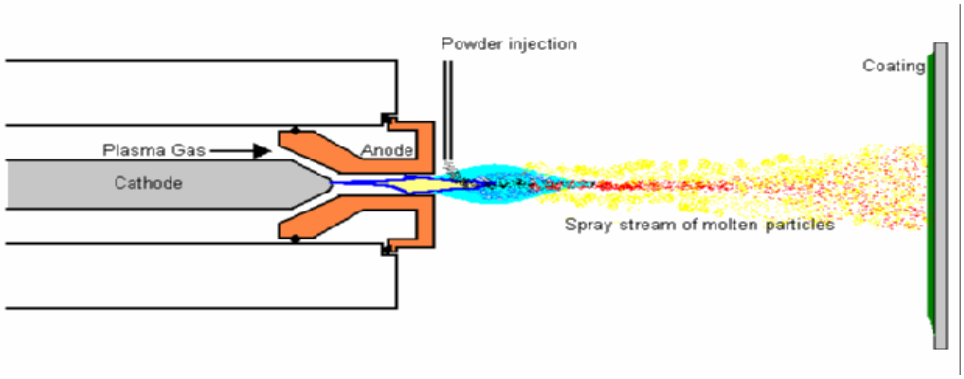

Fig1.5 Schematic Diagram of the Plasma Spray Process [29]

The Plasma Spray Process is basically the spraying of molten or heat softened material onto a surface to provide a coating. Material in the form of powder is injected into a very high temperature plasma flame, where it is rapidly heated and accelerated to a high velocity. The hot material impacts on the substrate surface and rapidly cools forming a coating. This plasma spray process carried out correctly is called a "cold process" (relative to the substrate material being coated) as the substrate temperature can be kept low during processing avoiding damage, metallurgical changes and distortion to the substrate material.

The plasma spray gun comprises a copper anode and tungsten cathode, both of which are water cooled. Plasma gas (argon, nitrogen, hydrogen, helium) flows around the cathode and through the anode which is shaped as a constricting nozzle. The plasma is initiated by a high voltage discharge which causes a conductive path for a DC arc to form between cathode and anode. The resistance heating from the arc causes the gas to reach extreme temperature, dissociate and ionise to form a plasma. The plasma exits the anode nozzle as a free or neutral plasma flame (plasma which does not carry electric current). When the plasma is stabilised ready for spraying the electric arc extends down the nozzle, instead of shorting out to the nearest edge of the anode nozzle. Cold gas around the surface of the water cooled anode nozzle being electrically non-conductive constricts the plasma arc, raising its temperature and velocity. Powder is fed into the plasma flame most commonly via an external powder port mounted near the anode nozzle exit. The powder is so rapidly heated and accelerated that spray distances can be in the order of 25 to 150 mm.

1.5.2 Arc Spray Process

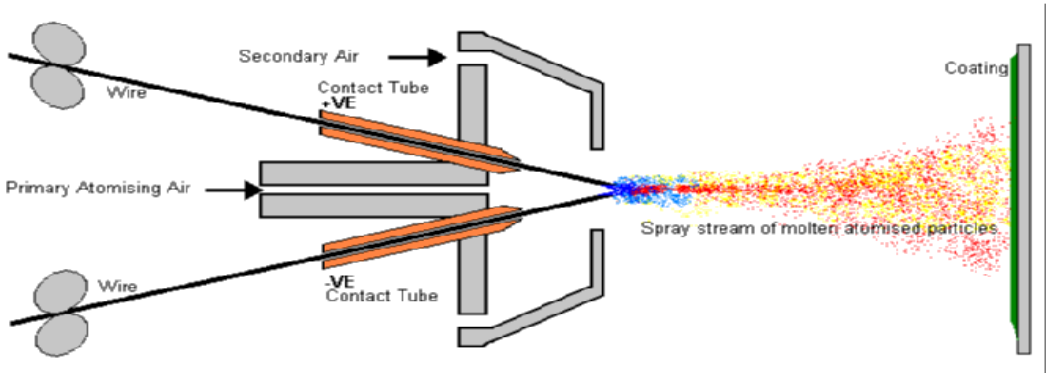

Fig1.6 Schematic Diagram of the Electric Arc Wire Thermal Spray Process [29]

In the Arc Spray Process a pair of electrically conductive wires is melted by means of an electric arc as shown in Fig1.6. The molten material is atomized by compressed air and propelled towards the substrate surface. The impacting molten particles on the substrate rapidly solidify to form a coating. This arc spray process carried out correctly is called a "cold process" (relative to the substrate material being coated) as the substrate temperature can be kept low during processing avoiding damage, metallurgical changes and distortion to the substrate material.

1.5.3 Combustion Powder Thermal Spray Process (Flame Spray Process)

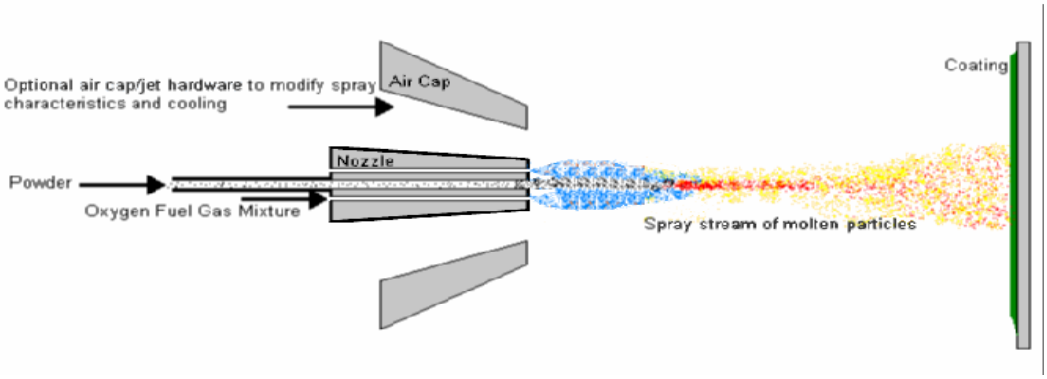

Fig1.7 Schematic Diagram of Combustion Powder Thermal Spray Process (also known as Powder Flame Spraying) [29]

This process is basically the spraying of molten material onto a surface to provide a coating. Material in powder form is melted in a flame (oxy-acetylene or hydrogen most common) to form a fine spray. When the spray contacts the prepared surface of a substrate material, the fine molten droplets rapidly solidify forming a coating. This flame spray process carried out correctly is called a "cold process" (relative to the substrate material being coated) as the substrate temperature can be kept low during processing avoiding damage, metallurgical changes and distortion to the substrate material.

1.5.4 High Velocity Oxygen Fuel Thermal Spray Process (HVOF)

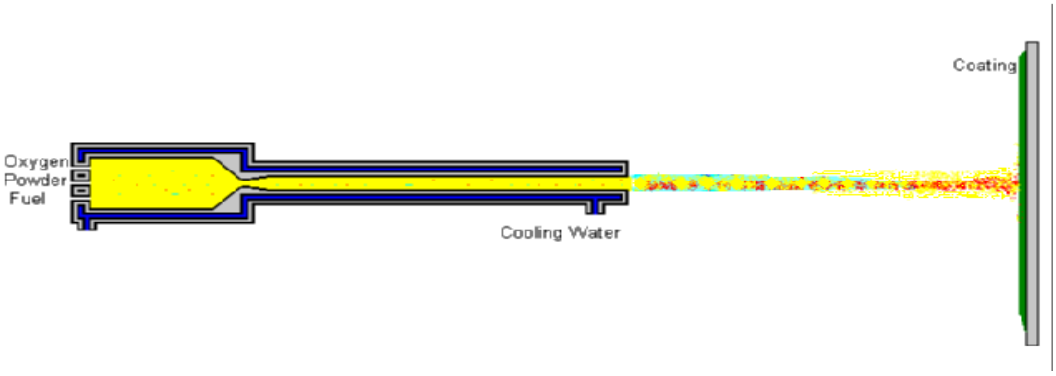

Fig1.8 Schematic Diagram of the HVOF Process [29]

There are a number of HVOF guns which use different methods to achieve high velocity spraying. One method is basically a high pressure water cooled HVOF

combustion chamber and long nozzle. Fuel (kerosene, acetylene, propylene and hydrogen) and oxygen are fed into the chamber; combustion produces a hot high pressure flame which is forced down a nozzle increasing its velocity. Powder may be fed axially as in Fig1.8 into the HVOF combustion chamber under high pressure or fed through the side of De laval type nozzle where the pressure is lower. Another method uses a simpler system of a high pressure combustion nozzle and air cap. Fuel gas (propane, propylene or hydrogen) and oxygen are supplied at high pressure, combustion occurs outside the nozzle but within an air cap supplied with compressed air. The compressed air pinches and accelerates the flame and acts as a coolant for the HVOF gun. Powder is fed at high pressure axially from the centre of the nozzle. The coatings produced by HVOF are similar to those produce by the detonation process. HVOF coatings are very dense, strong and show low residual tensile stress or in some cases compressive stress, which enable very much thicker coatings to be applied than previously possible with the other processes. The very high kinetic energy of particles striking the substrate surface does not require the particles to be fully molten to form high quality HVOF coatings. HVOF coatings are used in applications requiring the highest density and strength not found in most other thermal spray processes.

1.5.5 Detonation Thermal Spraying Process

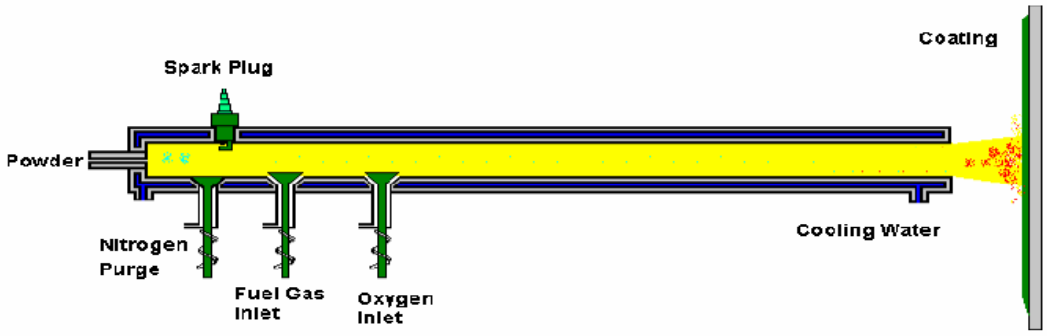

Fig1.9 Schematic Diagram of the Detonation Thermal Spray Process [29]

The Detonation gun basically consists of a long water cooled barrel with inlet valves for gases and powder. Oxygen and fuel (acetylene most common) is fed into the barrel along with a charge of powder. A spark is used to ignite the gas mixture and the resulting detonation heats and accelerates the powder to supersonic velocity down the

barrel. A pulse of nitrogen is used to purge the barrel after each detonation. This process is repeated many times a second. The high kinetic energy of the hot powder particles on impact with the substrate result in a build up of a very dense and strong coating.

Chapter 2 LITERATURE REVIEW

Following are the persons who are involved in the research work of development of Hydroxyapatite powder and bioactive coatings. These studies however, can provide valuable information regarding the development of Hydroxyapatite through heat treatment process from eggshell, use of TiO_2 and its phase selection (from anatase, rutile and brookite) for high temperature.

K Prabakaran [1] *et al.,* developed hydroxyapatite powder from eggshell and phosphoric acid by heat treatment method. Fourier-transform infrared (FT–IR) and X-ray diffraction (XRD) techniques were employed to investigate the formation of the HA phase. Thermal analysis (TG–DTA) was carried out to investigate the thermal stability of HA powder. FTIR peaks indicate good crystallinity for the material heated at 900^0C as compared to 80^0C, 400^0C and 700^0C. This paper suggests that eggshell-originated HAP could be useful as an inexpensive ceramic for biomedical applications.

Csaba Balazsi [2] *et al.,* Calcium phosphates and hydroxyapatite nanopowders was prepared from eggshells and phosphoric acid at different mixing ratios. Raw eggshells were heated at 900^0C. Powder was crushed and reacted with phosphoric acid by exothermic reaction. The characteristic of the end product was influenced by different acid mixing ratio, milling time and heat treatment applied. Calcium phosphates foams resulted at higher acid mixing ratio, longer milling time with high specific surface area. At higher sintering temperatures calcium phosphate had been found with good adherence to hydroxyapatite substrate.

Su-Hee Lee [3] *et al.,* investigated hydroxyapatite (HA)–titania (TiO_2) hybrid coating for improvement of biocompatibility of titanium (Ti) implants. The HA predeposited layer on Ti via electron beam evaporation is subsequently treated by micro-arc oxidation (MAO) to produce an HA–TiO_2 hybrid layer on Ti. By means of MAO treatment, a rough and porous TiO_2 layer is formed beneath the HA layer. Due to the HA precoating, high concentrations of Ca and P are preserved on the coating surface. The cell propagation rate on the hybrid coatings is not much different from that on

pure Ti or simple MAO-treated Ti. However, the alkaline phosphatase (ALP) activity of the cells is significantly higher on the HA–TiO_2 hybrid coatings than on either the pure Ti or the simple MAO-treated specimen. It suggests that the cellular activity on the hybrid coatings is improved.

R.S. Lima [4] *et al.,* in this study, three types of Al_2O_3-13 wt.% TiO_2 powders were employed. One nanostructured and two conventional Al_2O_3-13 wt.% TiO_2 feedstock powders were employed in this work. The nanostructured Al_2O_3-13 wt.% TiO_2 feedstock was made by spray-drying. The result shows strong evidence for antiwear performance of the coatings made from the mixture of nanostructured and submicron particles when compared to those made by conventional materials. The high degree of Al_2O_3 and TiO_2 mixing in each hybrid agglomerate probably lowers its melting point. Addition of TiO_2 to Al_2O_3, produce a lowering of the particle viscosity and improve the interlamellar contact at impact during HVOF spraying.

Aravind Vadiraj [5] *et al.,* examined the fretting fatigue damage characterization of physical vapor deposition (PVD) TiN-coated biomedical titanium alloys subjected to cyclic loads. The damage profile was studied with optical and scanning electron microscopy (SEM) micrographs and friction coefficient curves. The PVD TiN layer delayed the damage because of superior tribological properties compared with uncoated alloys. Delamination and abrasive wear damage of TiN at contact caused failure of the alloy. PVD TiN coatings improved the fretting fatigue life of the titanium alloy. The TiN coating has shown better fretting resistance compared with uncoated alloy.

R. Jaworski [6] *et al.,* this paper describes the studies on TiO_2, hydroxyapatite and their composite multilayer coatings onto stainless steel, titanium and aluminum substrate using suspension plasma spraying. The suspensions were formulated with the use of fine commercial TiO_2 rutile and HA milled from commercial spray-dried powder. The injection of suspension to the plasma jet was studied carefully with the use of atomizer injector. The sprayed coatings were analyzed by using XRD. The content of anatase and rutile was calculated in the titanium oxide deposits. Scratch test enabled to characterize the adhesion of the coatings, their microhardness and friction coefficient.

Heleno R.A [7] *et al.,* studied HA coatings on substrates of 316L stainless steel applied by a high energy plasma spray gun (HEP). The evaluation of coating adhesion was conducted by scratch testing with progressive loads. The scratch test results show that the critical load for failure increases as the coating thickness increases. The clinical evaluation shows a very good HA thermal spray coating biocompatibility with human tissue. An inflammatory reaction occurred in only 3% of HA coated fixation pins whereas 30% of non-coated fixation pins produced an inflammatory reaction.

F-X. Ye [8] *et al.,* investigated the microstructures and compositions of plasma sprayed TiO_2, TiO_2-10%HA, TiO_2-30%HA and HA coatings. The addition of HA inhibited the phase transformation of anatase TiO_2 to rutile. This results in increase of photocatalytic activity of TiO_2. Under the arc current of 600 A, the anatase content in the TiO_2, TiO_2-10%HA and TiO_2-30%HA coatings was 11, 20 and 42%, respectively. With the increasing of the spraying distance from 70 to 110 mm, the anatase content in the TiO_2-30%Hap coatings decreased from 34 to 17% under arc current of 700 A. The photocatalytic activity of TiO_2-10%HAp coating was highest among TiO_2, TiO_2-10%HAp and TiO_2-30%HAp coatings sprayed under the arc current of 600 A.

Kobayashi Akira [9] *et al.,* in this paper titanium dioxide + 30vol% hydroxyapatite photo-catalytic coatings were deposited by atmospheric plasma spraying using powders with nano-sized grains. The injection tube of the powder was set at different positions along the axial direction outside the plasma torch. The phase compositions and microstructures of the coatings were characterized using XRD and SEM. The result showed that porosity and anatase content ratio in the coatings were increased with the powder injected in the relatively low temperature zone.

Celaletdin Ergun [10] *et al.,* studied the reaction of HA with metallic titanium and titanium oxide. HA composites with both metallic titanium powder and titanium oxide were prepared and sintered at 1100^0C for 2 h. According to DT analysis results, HA reacts with titania at approximately 960^0C in air. DT analysis indicate that HA decomposed to $Ca_3(PO_4)_3$ and H_2O at this temperature and reacted with titania forming $CaTiO_3$. XRD analysis shows larger amounts of titanium and HA exists in the composite structure when sintered in the vacuum environment.

M. Gaona [11] *et al.,* in this paper nanostructured titania feedstock powders were deposited via high velocity oxy-fuel (HVOF) spraying onto Ti–6Al–4V substrates. In-flight particle characteristics were observed, which shows that there is a linear dependence between particle temperature and particle velocity. The major phase of the nanostructured feedstock powder was anatase, whereas the major phase of the HVOF-sprayed coatings was rutile. Higher Vickers micro-hardness number was found for higher average particle temperature and velocity.

Arjun Dey [12] *et al.,* examined HA coatings on SS316L substrates by microplasma spraying. The XRD patterns of HAP coatings identify the presence of only HA peaks. In the FTIR analysis, mainly the peaks for phosphate and hydroxyl groups in the HA could be identified. The coating showed the characteristic heterogeneous microstructure comprising of ellipsoidal and spheroidal splats with large number of microcracks, pores and different types of defects. The nanohardness (H) and Young's modulus (E) of the coatings as measured by nanoindentation technique were 6 and 92 GPa, respectively.

P. Suresh Babu [13] *et al.,* analyzed the coatings WC (Tungsten Carbide)–12wt.% Co powder deposited on mild steel substrates using the detonation spray process at various oxygen-fuel (OF) ratio. The amount of various phases present in the WC–12Co coatings was computed from the XRD spectrum. The hardness and elastic modulus of the detonation sprayed WC–12Co coatings was measured as a function of OF ratio and understood in terms of the phases present in the coating. It was examined that the microstructure evolution in terms of nature of decomposition of WC–12wt.% Co coatings is dependent on variation of oxygen–fuel ratio.

Kantesh Balani [14] *et al.,* studied irregular HA powder blended with 4wt% multiwalled CNTs (Carbon Nanotube) in a mill for 18 hours. Plasma spraying of HA with and without CNTs was carried out using Praxair SG-100 gun with optimized spray parameters. CNTs were spread over HA particles as seen in the SEM image of the blended powder feedstock. CNT reinforcement in HA coating using plasma spray improves the fracture toughness by 56% and enhances crystallinity by 27%.Cell culture studies with human osteoblasts hFOB 1.19 cells were performed onto HA–

4wt% CNT plasma sprayed coating which shows its biocompatibility with living cells.

Dean-Mo Liu [15] *et al.,* in this report, 316L stainless steel was used as a substrate, dip coated with the sol solution. The coatings were annealed in air at 375^0C, 400^0C, and 500^0C. It was founded that the sol–gel HA coatings strongly attach to the 316L substrates after annealing temperatures as low as 375–400^0C. Surface morphology and interfacial microstructure of the coatings on the 316L substrates was examined in terms of annealing temperature. Apatitic structure developed within the coatings while, annealing at temperatures ≥400^0C. It was examined that a dense and adhesive apatite coating can be achieved through water-based sol–gel technology after short-term annealing at around 400^0C in air.

Harpreet Singh [16] *et al.,* studied wear characteristics of two ceramic coating powders, Al_2O_3 + *(40%)* TiO2 and Cr_2O_3 coated AISI 309 SS stainless steel. Two metallic powders were coated on AISI 309 SS steel by HVOF spray technique. The coatings were characterized by XRD and SEM analyses. SEM analysis revealed splat morphology with distinct boundaries for the sprayed coatings. The XRD analysis of the coating indicated the presence of Al_2O_3, TiO_2 and Cr_2O_3 phases in the coatings. The wear resistances of the 309 SS, Al_2O_3 + (40%) TiO_2, and Cr_2O_3 coatings followed the trend: Cr_2O_3 > Al_2O_3 + (40%) TiO_2 > 309 SS.

Maninder Kaur [17] *et al.,* investigated wear behavior of the bare Ni-20Cr and Ni_3Al coated 309 SS steel on a Pin-on-Disc Wear Test Rig. Two metallic powders namely Ni-20Cr and Ni_3Al were coated on 309 SS steel by shrouded plasma spray process. The wear tests were carried out at normal loads of 30 and 50 N with a sliding velocity of 1 m/s. Cumulative wear rate and coefficient of friction (μ) were calculated for all the cases. The μ value follows the order as: 309 SS < Ni-20Cr < Ni_3Al. It was concluded that the Ni_3Al coating is more wear resistant than the Ni-20Cr coating. The XRD analysis indicated the formation of Ni phase for the Ni-20Cr coating and Ni_3Al phase for the Ni_3Al coating.

G. Sundararajan [18] *et al.,* examined wide range (94) samples of 13 spray powders by using detonation gun on mild steel. For each coating composition, combination of properties had obtained by systematically varying the process parameters. The

resulting coatings were characterized in terms of phase content, porosity, microhardness, abrasion and sliding wear resistance. The hardness and tribological properties of the coatings were more strongly influenced by the coating process parameters. This paper leads to the conclusion that the any significant improvement in the coating properties should be possible only if the coating formation process is better understood.

Margaret A. McGee [19] *et al.,* this paper was derived from histological investigations on retrieval tissues and implants. In vivo and in vitro test provide strong support for this biological failure of joint replacement implants. Late loosening which is the major problem was related to wear of the prosthetic components. Result of retrieval studies was Ti femoral heads had the most wear, SS was intermediate between CoCr and Ti heads, and CoCr heads had least wear. From the retrieval and analysis of failed implants, hypotheses regarding the mechanism of wear-induced loosening and other causes for implant failure were developed.

U Kamachi Mudali [20] *et al.,* in this paper work is done on corrosion of bio implants as it is one of the major processes affecting the life and service of orthopedic devices made of metals and alloys used as implants in the body. Modified stainless steels are developed with the additions of alloying elements like nitrogen, titanium etc., for improving the corrosion resistance by ion implantation. The modified materials have shown improvement in high pitting corrosion resistance as compared to the currently used type 316L SS. HA was electrophoretically deposited on type 316L stainless steel alloy surface should be considered as a feasible alternative for improving the corrosion resistance .

J.J. Ramsden [21] *et al.,* this paper deals with the surfaces of objects designed to be introduced into the human body. This paper reviews the nature of the bio-environment and the essential features of protein adsorption. The relationship between the morphology and chemistry of the surface and the biological response was reviewed. The metrology of biomedical surfaces, essential for optimizing surface finish was considered in this paper. This paper suggested that surface treatment provides a means to overcome bio-incompatibility and stabilization with respect to corrosion and wear.

J.P. SIMON [22] *et al.,* studied various materials used in orthopedic implants. These material include metals, polymers and ceramics. Metals used in orthopedic implants include surgical grade stainless steel, cobalt-chromium alloys, titanium and titanium alloys. Polyethylene is the most popular polymer used in orthopedic implants. The ceramics used in orthopedic implants include aluminium oxide and calcium phosphates. These calcium phosphate implant coatings result in strong implant fixation.

Daniel Lin [23] *et al.,* this paper provides a review on the issues of mandibular and maxillary bone remodeling as a result of dental implantation. Bone remodeling is defined as a process where bone gradually alters its morphology in attempt to adapt to any new external load. In this paper, the published remodeling data was analyzed. The established relationships between bone density and corresponding mechanical properties were outlined. Finite element method had proven effective to capture the geometrical and material complexities involved.

Naresh Chaudhary [24] *et al.,* reported experimental and numerical method to explore the stresses generated around bone screws used in rigid internal fixation of mandibular fractures. The experimental screw pull out tests were done using bone screws embedded in a trilaminate standard polyurethane block. A finite element model of a human mandible was created. The mandibular model was loaded, and the forces exerted by the fixation plate onto the simplified screws were obtained .These forces were transferred to another finite element submodel of a screw implant embedded in a block with material properties of cortical and cancellous bone. The stress in the bone surrounding the screw implant was obtained. Results from the experimental and numerical screw pull out tests were correlated. The results of this study suggest that bicortical drilling can be avoided by using screws of a larger major diameter.

Chapter 3 PROBLEM FORMULATION

It was observed from the review of available literature that Hydroxyapatite is used extensively as a biomaterial for biomedical implant applications. Due to its structural and chemical similarities to human bone mineral, HA promotes growth of bone tissue directly on its surface. Hydroxyapatite [Ca_{10} $(PO_4)_6(OH)_2$] commonly referred to as HA, has attracted wide spread interest from both the orthopedic and dental fields due to its excellent biocompatibility and tissue bioactivity properties.

Despite excellent properties as a biomaterial, the ceramic nature and the inherent mechanical properties of HA specifically brittleness, poor tensile strength and poor impact resistance have restricted its application in many load bearing applications. Therefore, the concept of applying HA on to metallic implants as a coating was developed and the HA coated implants combine good strength and ductility of the metal with excellent biocompatibility and bioactivity of the HA.

The interface between HA and a metallic implant has been matter of concern in terms of the mechanical properties and biocompatibility of the implant. In order for the HA coating to be effective and reliable, it must be strongly bonded to the metallic surface. Substitution of other elements has shown the potential to improve the bioactivity of HA. Hybrid coating with hydroxyapatite (HA) and titanium dioxide (TiO_2) and aluminium oxide (Al_2O_3) have attracted particular attention over the last decade. TiO_2 and Al_2O_3 prevent corrosion and wear of metallic surface.

Therefore, the concept of applying Hybrid coatings using HA, TiO_2 and Al_2O_3 on to metallic implants is to be explored under this research work, as not much work has been reported on development of hybrid coatings till now.

Chapter 4 EXPERIMENTATION

4.1 Powder Preparation

In the present investigation, an attempt was made to develop Hydroxyapatite (HA) powder from eggshell, a natural apatite rich substance through heat treatment method. Eggshell, a cheaper source of HA is generated as waste material during egg processing. Fourier transform-infrared spectroscopy (FT-IR) and X-ray diffraction (XRD) techniques were employed to investigate the proof of formation of HA phase.

Commercially HA powder is very costly, so an attempt is made to prepare the powder from eggshell as these sources consider as waste material. It is easily available and free of cost.

TiO_2 and Al_2O_3 were added in eggshell powder to enhance their properties, to facilitate coating of these powders.

4.1.1 Steps for preparation of HA powder from Chicken Eggshells

1) Eggshells are collected from the boiled egg sellers in the *Tripuri Town market* and from *Hostels of Thapar University*, Patiala as shown in Fig.4.1.

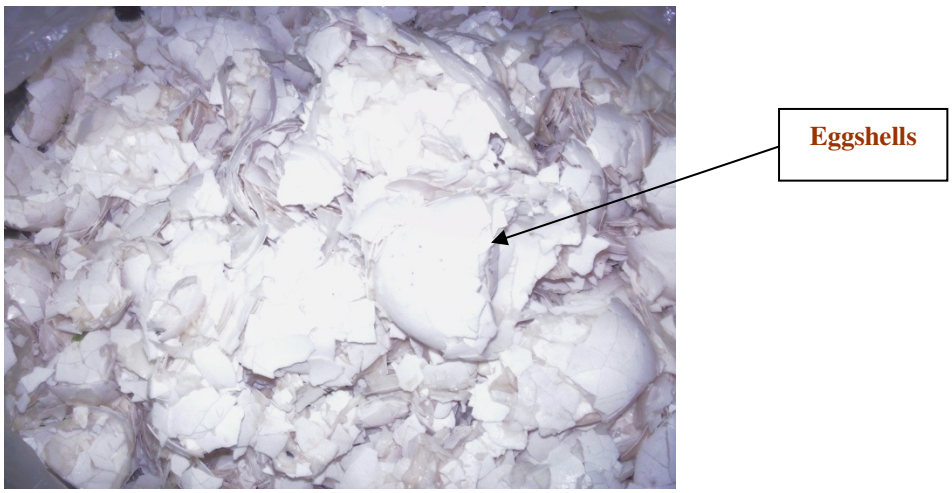

Fig.4.1 Chicken eggshells

2) The eggshells were washed in hot water for 30 minutes as shown in Fig.4.2.

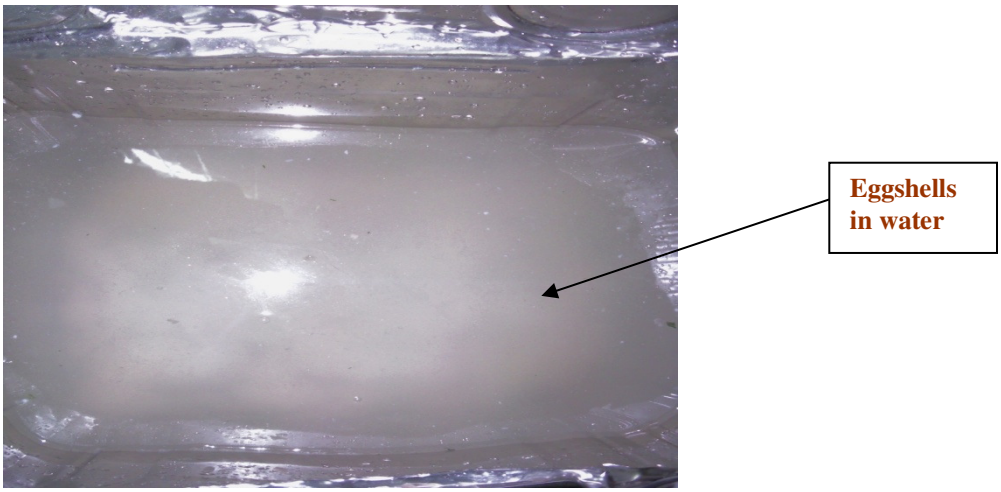

Fig.4.2 Washing of Chicken eggshells

3) The eggshells after washing were dried in sunlight for 2 hours to make them dry as shown in Fig.4.3.

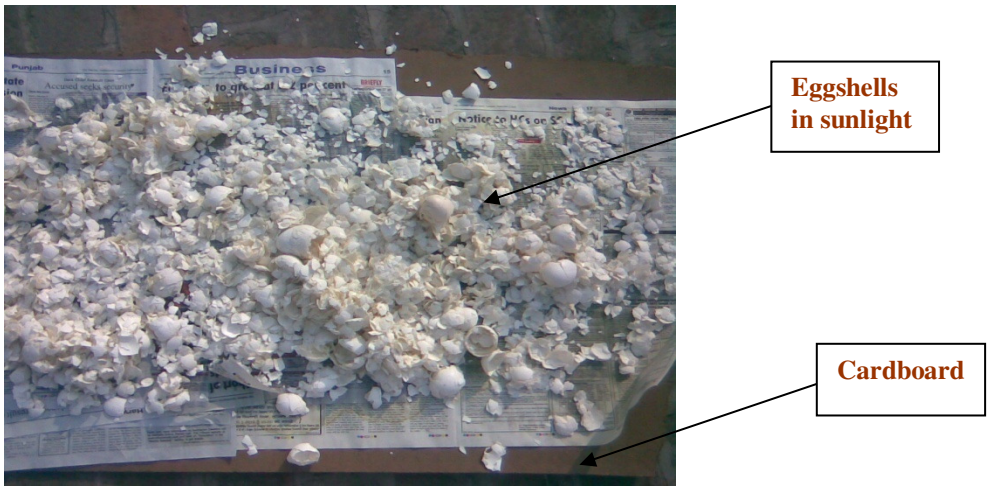

Fig.4.3 Drying of Chicken eggshells

4) The eggshells were heated in a muffle furnace at 900^0C for 3 hours by using crucible made from alumina as shown in Fig.4.4. The ceramic crucible for heating at this temperature in a muffle furnace was purchased from ANTS Ceramics, Nashik.

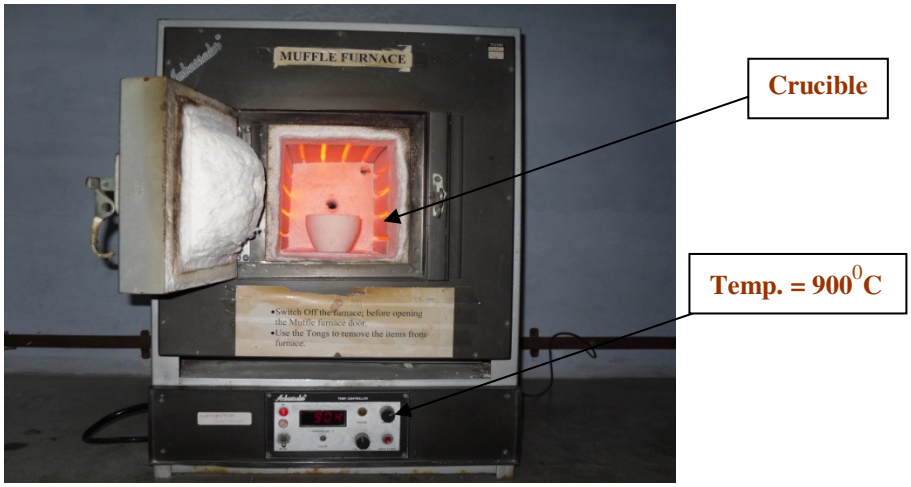

Fig.4.4 Muffle furnace

After a short time (30 min), the colour of eggshells turned to black, and after 3 hour they changed to white. The colour change suggested that most of the organic materials were burnt out.

The crucible is then placed in a desiccator for 20 minutes to prevent heated eggshells from humidity as in shown in Fig.4.5. The appearance of eggshells after this heat treatment is shown in Fig.4.6.

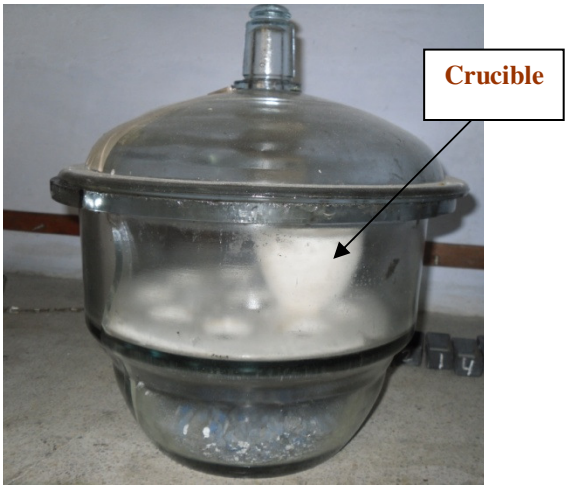

Fig.4.5 Desiccator

Fig.4.6 Eggshells powder at 900^{0}C

Initial the powder was also heated at 300^0C and 600^0C. At 300^0C the colour of eggshells is found to be reddish and at 600^0C it is of black colour. The appearance of eggshells after heating at 300^0C and 600^0C are shown in Fig.4.7 and Fig.4.8 respectively.

Fig.4.7 Eggshells powder at 300^0C

Fig.4.8 Eggshells powder at 600^0C

5) It is then crushed with spice grinder of which sieve is made of size 40 micron. Mesh of sieve is purchased from Bright Industries, Ambala (Fig.4.9). Powder is crushed by grinder blades which rotate about horizontal axis. At the bottom of which the sieve is fixed so to pass powder of size 40 micron (Fig.4.10).

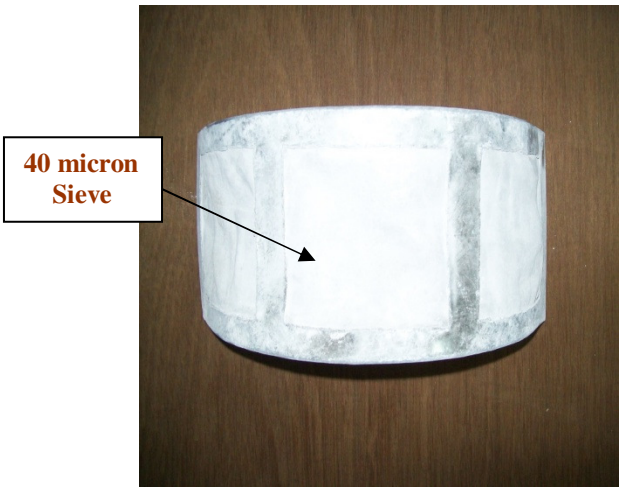

Fig.4.9 Grinder Sieve

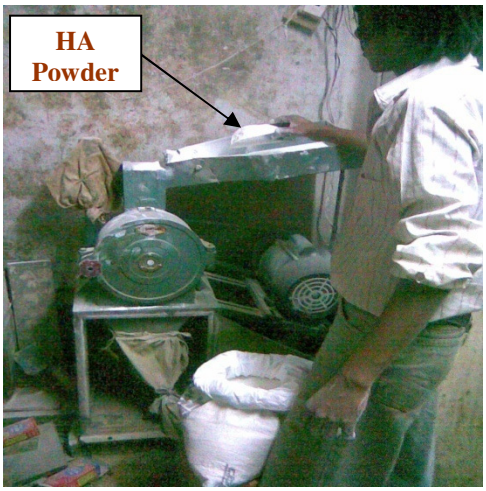

Fig.4.10 Grinder

4.2 Testing of Powder

Before coating of the powder on the metal substrate, the following tests are done on both the powders to show the presence of HA phase and to know the compatibility with human blood.

1) X-ray Powder Diffraction (XRD)
2) FT IR
3) Blood Clotting test

4.2.1 X-ray Powder Diffraction (XRD)

X-ray powder diffraction (XRD) is a rapid analytical technique primarily used for phase identification of a crystalline material and can provide information on unit cell dimensions. The analyzed material is finely ground, homogenized, and average bulk composition is determined.

Max von Laue, in 1912, discovered that crystalline substances act as three-dimensional diffraction gratings for X-ray wavelengths similar to the spacing of planes in a crystal lattice. X-ray diffraction is now a common technique for the study of crystal structures and atomic spacing.

X-ray diffraction is based on constructive interference of monochromatic X-rays and a crystalline sample. These X-rays are generated by a cathode ray tube, filtered to produce monochromatic radiation, collimated to concentrate, and directed toward the sample. The interaction of the incident rays with the sample produces constructive interference (and a diffracted ray) when conditions satisfy Bragg's Law ($n\lambda=2d \sin \theta$). This law relates the wavelength of electromagnetic radiation to the diffraction angle and the lattice spacing in a crystalline sample. These diffracted X-rays are then detected, processed and counted. By scanning the sample through a range of 2θangles, all possible diffraction directions of the lattice should be attained due to the random orientation of the powdered material. Conversion of the diffraction peaks to d-spacings allows identification of the mineral because each mineral has a set of unique d-spacings. Typically, this is achieved by comparison of d-spacings with standard reference patterns.

All diffraction methods are based on generation of X-rays in an X-ray tube. These X-rays are directed at the sample, and the diffracted rays are collected. A key component of all diffraction is the angle between the incident and diffracted rays.

X-ray diffractometers consist of three basic elements: an X-ray tube, a sample holder, and an X-ray detector. X-rays are generated in a cathode ray tube by heating a filament to produce electrons, accelerating the electrons toward a target by applying a voltage, and bombarding the target material with electrons. When electrons have sufficient energy to dislodge inner shell electrons of the target material, characteristic X-ray spectra are produced. These X-rays are collimated and directed onto the sample. As the sample and detector are rotated, the intensity of the reflected X-rays is recorded. When the geometry of the incident X-rays impinging the sample satisfies the Bragg Equation, constructive interference occurs and a peak in intensity occurs. A detector records and processes this X-ray signal and converts the signal to a count rate which is then output to a device such as a printer or computer monitor. The geometry of an X-ray diffractometer is such that the sample rotates in the path of the collimated X-ray beam at an angle θ while the X-ray detector is mounted on an arm to collect the diffracted X-rays and rotates at an angle of 2θ. The instrument used to maintain the angle and rotate the sample is termed a *goniometer*. For typical powder patterns, data is collected at 2θ from ~5° to 70°, angles that are preset in the X-ray scan.

4.2.1.1 Applications

X-ray powder diffraction is most widely used for the identification of unknown crystalline materials (e.g. minerals, inorganic compounds). Determination of unknown solids is critical to studies in geology, environmental science, material science, engineering and biology.

Other applications include:

- Characterization of crystalline materials.
- Identification of fine-grained minerals such as clays and mixed layer clays that are difficult to determine optically.

- Determination of unit cell dimensions.
- Measurement of sample purity.

With specialized techniques, XRD can be used to:

- Determine crystal structures.
- Determine of modal amounts of minerals (quantitative analysis).
- Characterize thin films samples by:
    - Determining lattice mismatch between film and substrate and to inferring stress and strain.
    - Determining dislocation density and quality of the film by rocking curve measurements.
    - Measuring super lattices in multilayered epitaxial structures.
    - Determining the thickness, roughness and density of the film using glancing incidence X-ray reflectivity measurements.
- Make textural measurements, such as the orientation of grains, in a polycrystalline sample.

To understand the phase formation or phase identification was carried out by X-ray diffractometer, X'PERT Pro-Panalytical using CuKα radiation. The XRD results of eggshell powder at 300^0C, eggshell powder at 600^0C, eggshell powder at 900^0C, TiO_2, Al_2O_3, Powder 1 (20%HA+40%TiO_2+40%Al_2O_3) and Powder 2 (30%HA+35%TiO_2+35%Al_2O_3) are shown in Fig.4.11, Fig.4.12, Fig.4.13 Fig.4.14, Fig.4.15, Fig.4.16 and Fig.4.17 respectively.

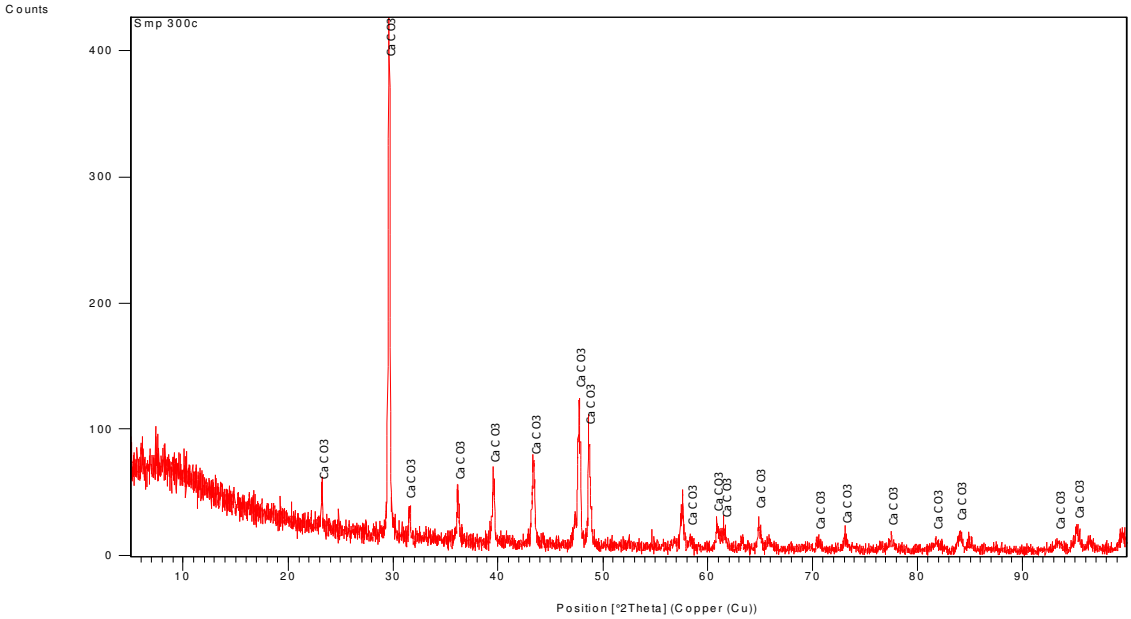

Fig.4.11 The XRD of Eggshell at 300^0C

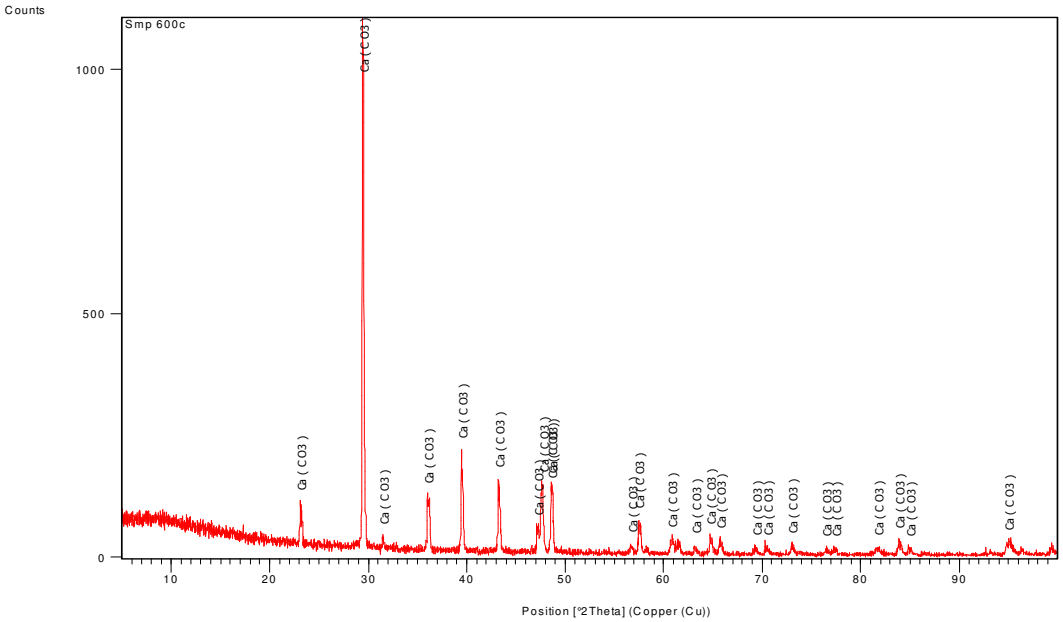

Fig.4.12 The XRD of Eggshell at 600^0C

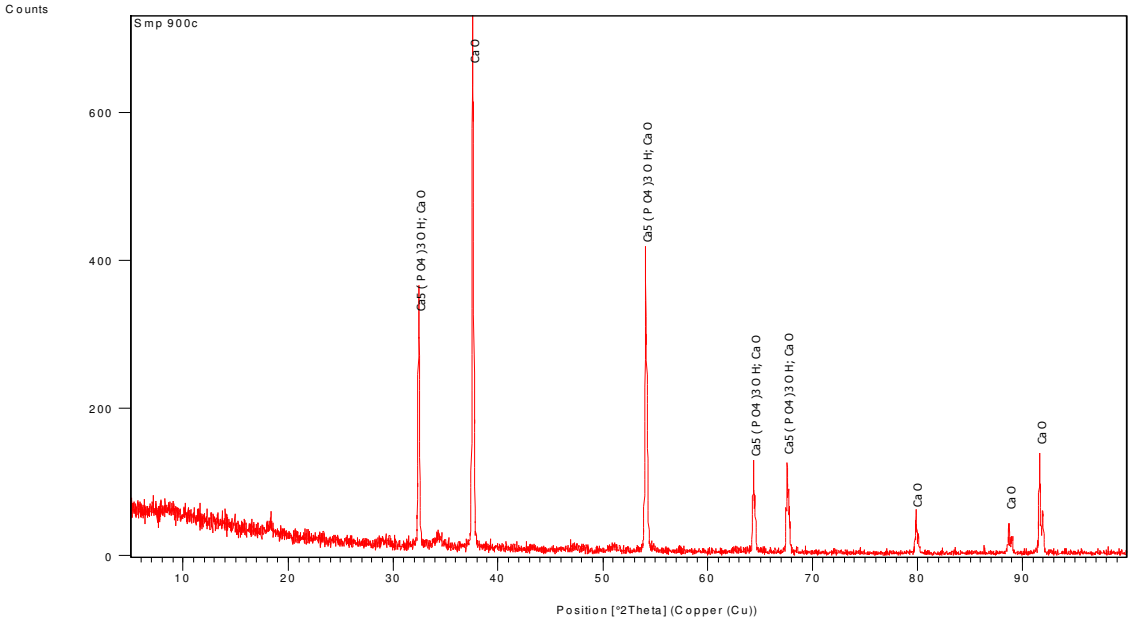

Fig.4.13 The XRD of Eggshell at 900^0C

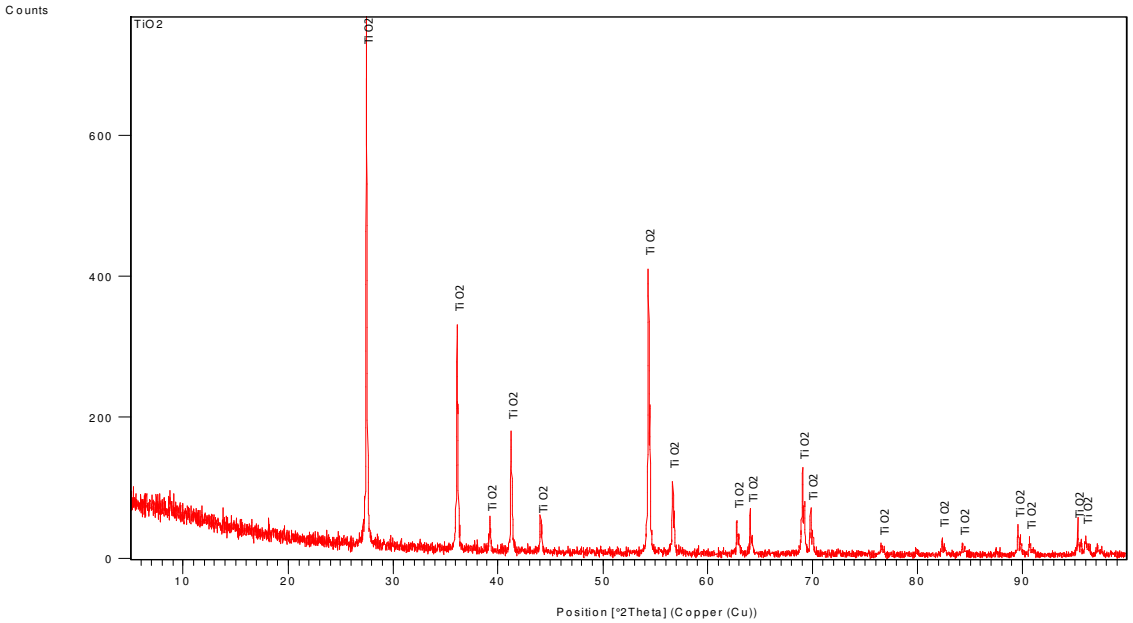

Fig.4.14 The XRD of TiO_2

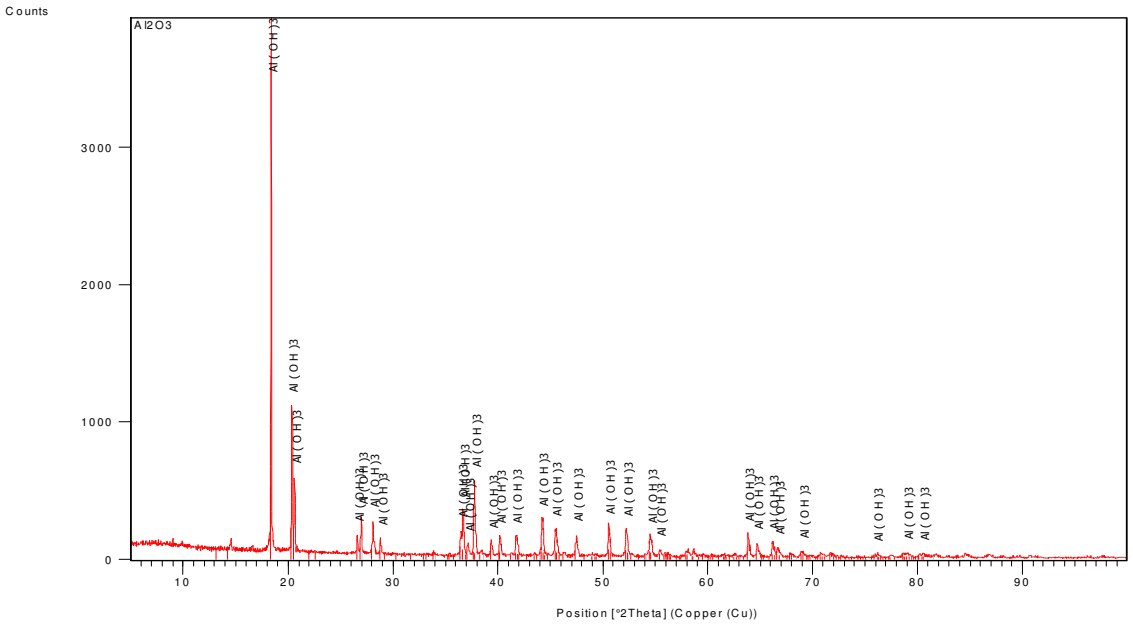

Fig.4.15 The XRD of Al_2O_3

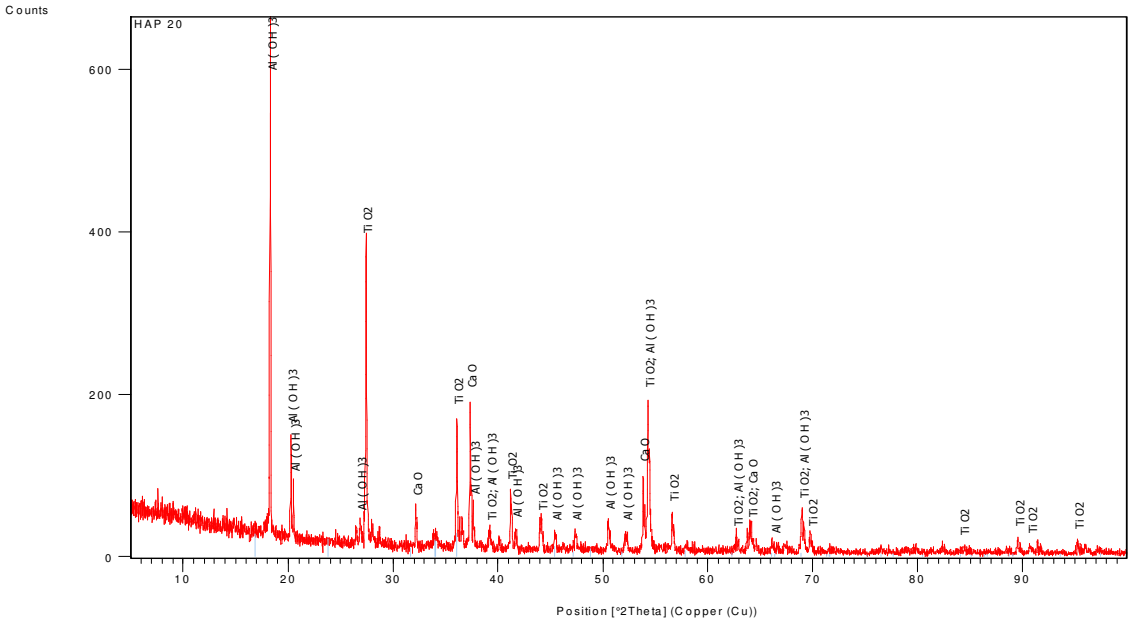

Fig.4.16 The XRD of Powder 1 (20%HA+40%TiO_2+40%Al_2O_3)

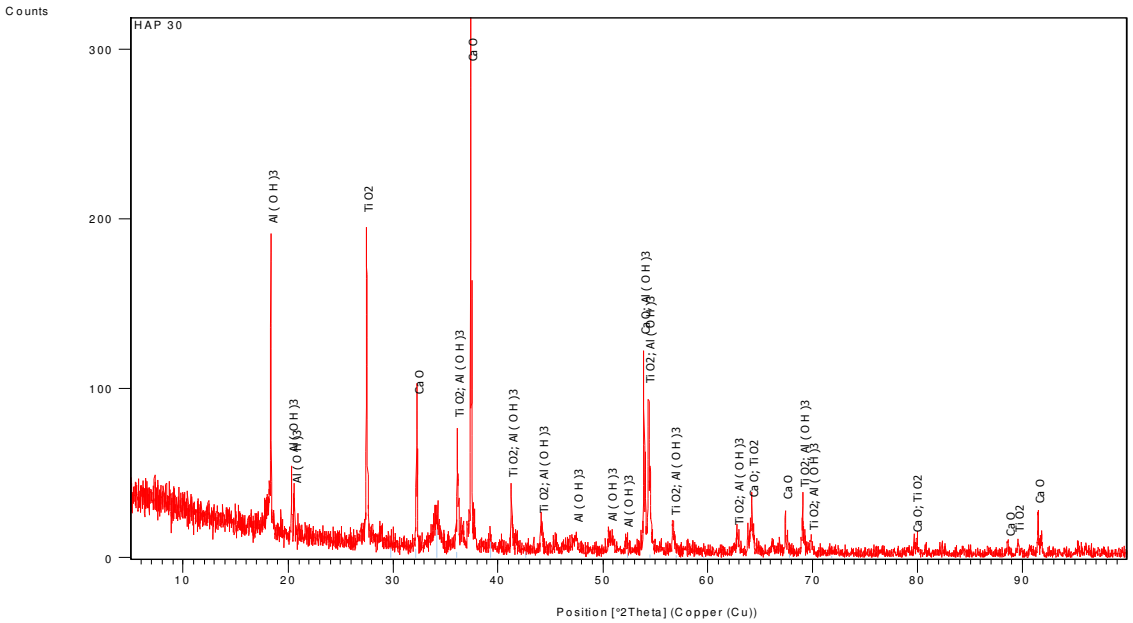

Fig.4.17 The XRD of Powder 2 (30%HA+35%TiO_2+35%Al_2O_3)

The XRD peaks of eggshell powder at 900^0C shows Hydroxyapatite (HA) as per following:

Peak No.1: 32.8 ^{o}

Peak No.2: 54.5 ^{o}

Peak No.3: 65.3 ^{o}

Peak No.4: 67.0 ^{o}

4.2.2 FTIR (Fourier Transform Infrared Spectrometry)

FT-IR stands for Fourier Transform Infrared, the preferred method of infrared spectroscopy. In infrared spectroscopy, IR radiation is passed through a sample. Some of the infrared radiation is absorbed by the sample and some of it is passed through (transmitted). The resulting spectrum represents the molecular absorption and transmission, creating a molecular fingerprint of the sample. Like a fingerprint no two unique molecular structures produce the same infrared spectrum. This makes infrared spectroscopy useful for several types of analysis.

- It can identify unknown materials
- It can determine the quality or consistency of a sample
- It can determine the amount of components in a mixture

Infrared spectroscopy has been a workhorse technique for materials analysis in the laboratory for over seventy years. An infrared spectrum represents a fingerprint of a sample with absorption peaks which correspond to the frequencies of vibrations between the bonds of the atoms making up the material. Because each different material is a unique combination of atoms, no two compounds produce the exact same infrared spectrum. Therefore, infrared spectroscopy can result in a positive identification (qualitative analysis) of every different kind of material. In addition, the size of the peaks in the spectrum is a direct indication of the amount of material present. With modern software algorithms, infrared is an excellent tool for quantitative analysis.

The original infrared instruments were of the dispersive type. These instruments separated the individual frequencies of energy emitted from the infrared source. This was accomplished by the use of a prism or grating. An infrared prism works exactly the same as a visible prism which separates visible light into its colors (frequencies). A grating is a more modern dispersive element which better separates the frequencies of infrared energy. The detector measures the amount of energy at each frequency which has passed through the sample. This results in a spectrum which is a plot of intensity vs. frequency.

Fourier Transform Infrared (FT-IR) spectrometry was developed in order to overcome the limitations encountered with dispersive instruments. The main difficulty was the slow

scanning process. A method for measuring all of the infrared frequencies simultaneously, rather than individually, was needed. A solution was developed which employed a very simple optical device called an interferometer. The interferometer produces a unique type of signal which has all of the infrared frequencies "encoded" into it. The signal can be measured very quickly, usually on the order of one second or so. Thus, the time element per sample is reduced to a matter of a few seconds rather than several minutes. Most interferometers employ a beamsplitter which takes the incoming infrared beam and divides it into two optical beams. One beam reflects off of a flat mirror which is fixed in place. The other beam reflects off of a flat mirror which is on a mechanism which allows this mirror to move a very short distance (typically a few millimeters) away from the beamsplitter. The two beams reflect off of their respective mirrors and are recombined when they meet back at the beamsplitter. Because the path that one beam travels is a fixed length and the other is constantly changing as its mirror moves, the signal which exits the interferometer is the result of these two beams "interfering" with each other. The resulting signal is called an interferogram which has the unique property that every data point (a function of the moving mirror position) which makes up the signal has information about every infrared frequency which comes from the source. This means that as the interferogram is measured, all frequencies are being measured simultaneously. Thus, the use of the interferometer results in extremely fast measurements. Because the analyst requires a frequency spectrum (a plot of the intensity at each individual frequency) in order to make an identification, the measured interferogram signal cannot be interpreted directly. A means of "decoding" the individual frequencies is required. This can be accomplished via a well-known mathematical technique called the Fourier transformation. This transformation is performed by the computer which then presents the user with the desired spectral information for analysis.

The process (Fig.4.18) is as follows:

1. The Source: Infrared energy is emitted from a glowing black-body source. This beam passes through an aperture which controls the amount of energy presented to the sample (and, ultimately, to the detector).

2. The Interferometer: The beam enters the interferometer where the "spectral encoding" takes place. The resulting interferogram signal then exits the interferometer.

3. The Sample: The beam enters the sample compartment where it is transmitted through or reflected off of the surface of the sample, depending on the type of analysis being accomplished. This is where specific frequencies of energy, which are uniquely characteristic of the sample, are absorbed.

4. The Detector: The beam finally passes to the detector for final measurement. The detectors used are specially designed to measure the special interferogram signal.

5. The Computer: The measured signal is digitized and sent to the computer where the Fourier transformation takes place. The final infrared spectrum is then presented to the user for interpretation and any further manipulation. The process layout is shown in Fig.4.18

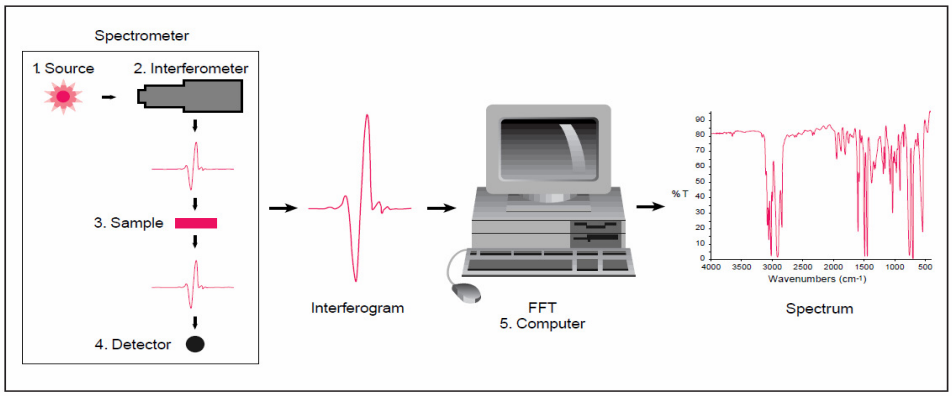

Fig.4.18 FTIR process [32]

4.2.2.1 FTIR comparison of powders with Hydroxyapatite

The FTIR reports of eggshell powder at 300^0C, 600^0C, 900^0C, TiO_2, Al_2O_3, two mixtures of powder (20%HA+40%TiO_2+40%Al_2O_3, 30%HA+35%TiO_2+35%Al_2O_3) and Hydroxyapatite are shown in Fig.4.19, Fig.4.20, Fig.4.21, Fig.4.22, Fig.4.23, Fig.4.24 , Fig.4.25 and Fig.4.26 respectively.

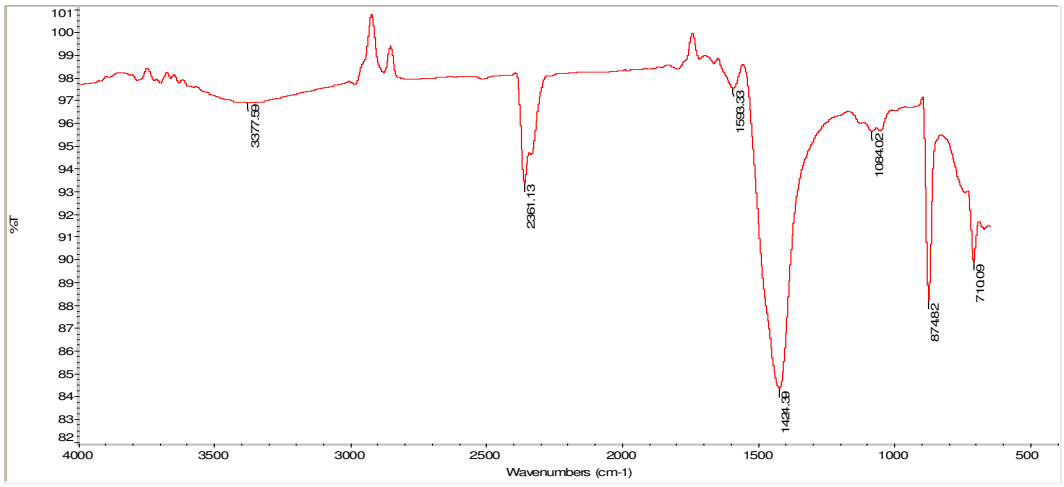

Fig.4.19 FTIR of eggshell powder at 300^0C

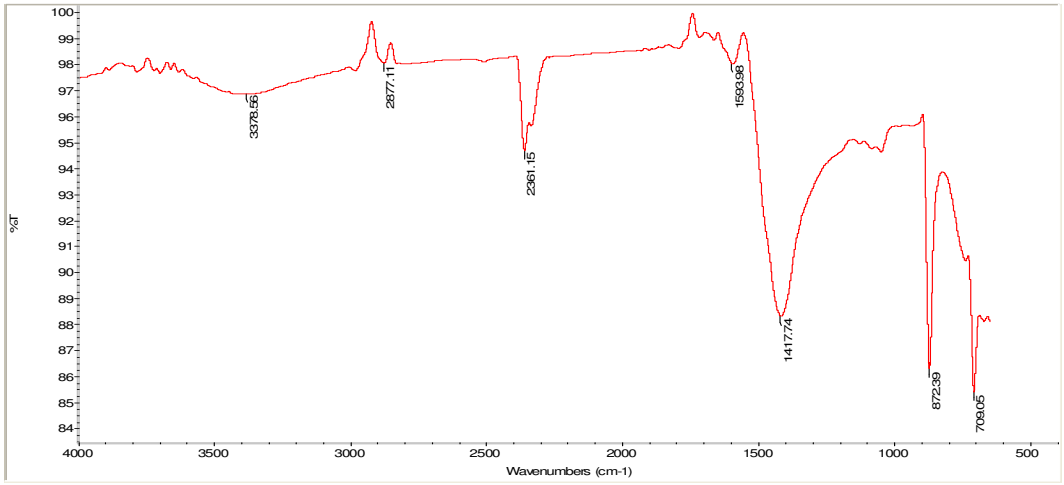

Fig.4.20 FTIR of eggshell powder at 600^0C

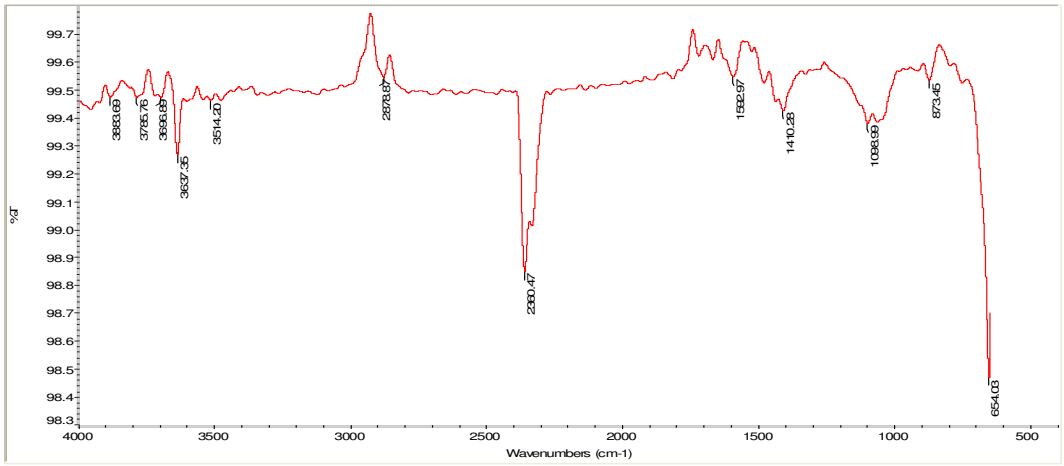

Fig.4.21 FTIR of eggshell powder at 900^0C

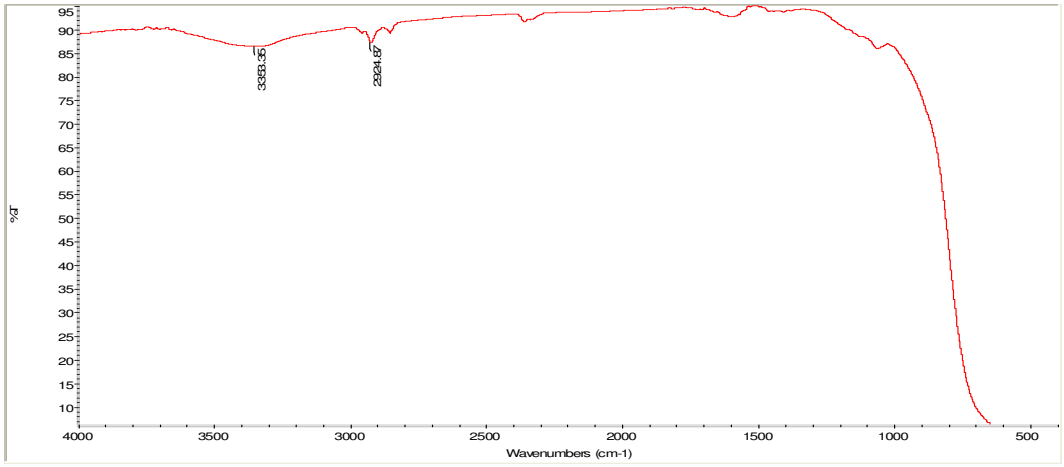

Fig.4.22 FTIR of TiO_2

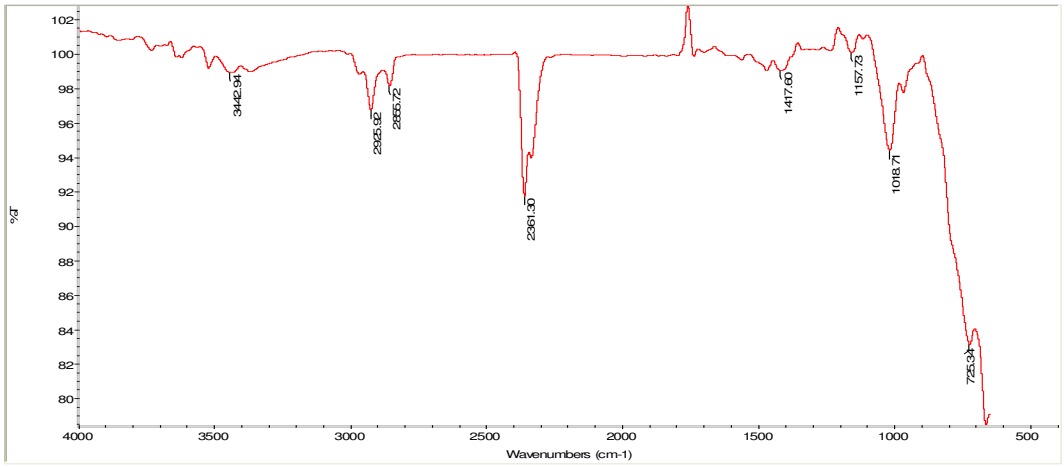

Fig.4.23 FTIR of Al_2O_3

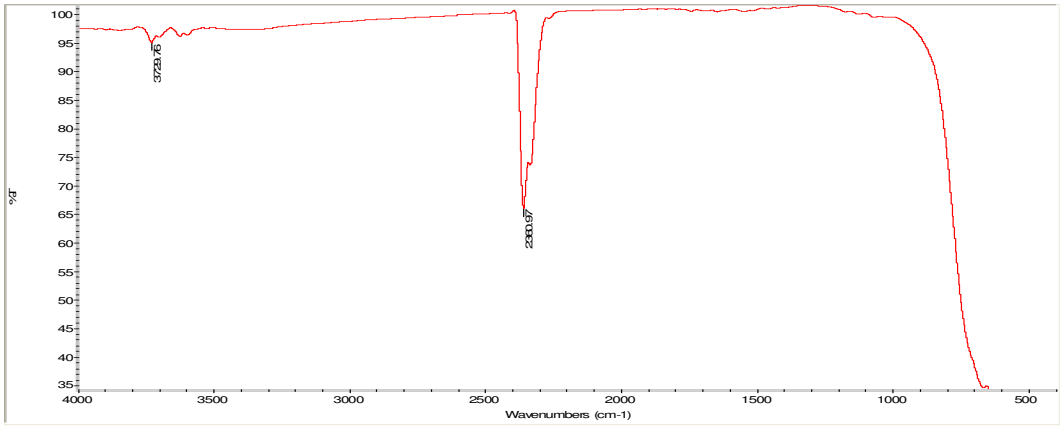

Fig.4.24 FTIR of Powder 1 (20%HA+40%TiO_2+40%Al_2O_3)

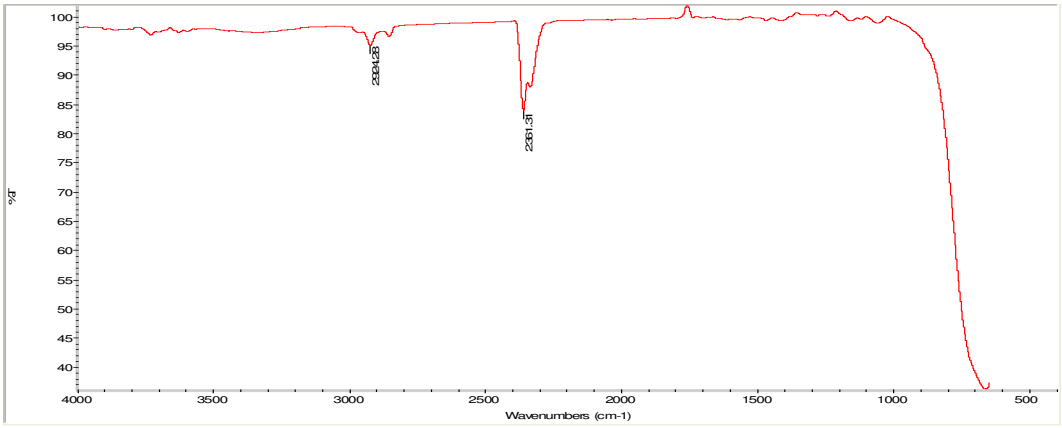

Fig.4.25 FTIR of Powder 2 (30%HA+35%TiO_2+35%Al_2O_3)

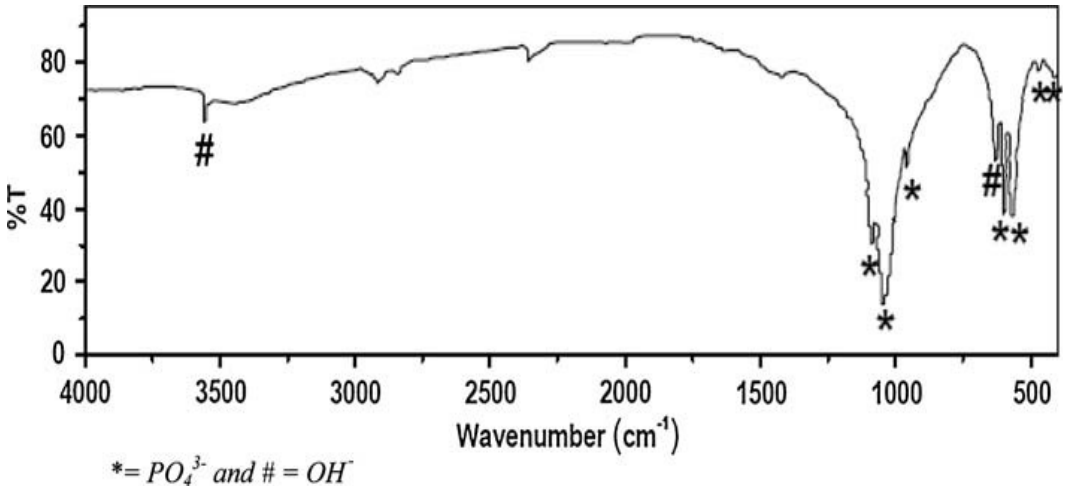

Fig.4.26 FTIR of HA powder [12]

The OH group is found at 3514.20cm^{-1} and 654.03 for eggshell powder at 900^0C, and the same peak is also traced in HA powder. Similarly, the P-O group is also found at 1084.02cm^{-1} and 874.82cm^{-1} for egg shell powder at 300^0C, 872.39cm^{-1} for eggshell powder at 600^0C, 1098.99cm^{-1} and 873.45cm^{-1} for eggshell powder at 900^0C and the same peak is also traced in HA powder. So, it is clear from the above comparison that both the powders shows the traces of HA phase.

4.2.3 Blood clotting test

Before preceding the coating, one of the most important tests is to know the compatibility of the powders with human blood.

When blood vessels are cut or damaged, the loss of blood from the system must be stopped before shock and possible death occur. This is accomplished by solidification of the blood, a process called coagulation or clotting. A blood clot consists of a plug of platelets.

Clotting also requires calcium ions (Ca^{2+}) (which is why blood banks use a chelating agent to bind the calcium in donated blood so the blood will not clot in the bag). Blood clotting is a natural process in which blood cells and fibrin strands rapidly form a clump to stop bleeding after a blood vessel has been injured. Eventually the clot will form a protective scab over a wounded blood vessel, allowing it to heal. If the body did not have the ability to form blood clot people would bleed to death after even a minor cut.

The blood clotting test is performed as follow:

1) First of all the blood sample is collected and place on test slide (Fig.4.27) and then mix the normal blood with anticoagulant (Sodium citrate solution 3.8 % W/V) . Note down the clotting time with the help of stop watch. The clotting time is 7 min. and 5 sec.

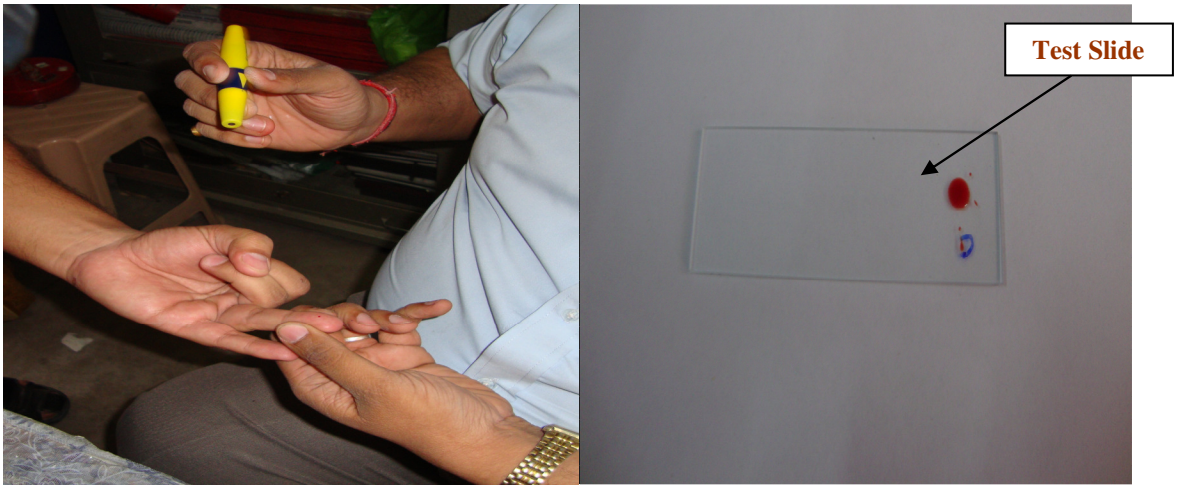

Fig.4.27 Blood sample collection

2) The test slide is seen under the microscope by using 10X (Fig.4.28) and 40X (Fig.4.29) magnifications.

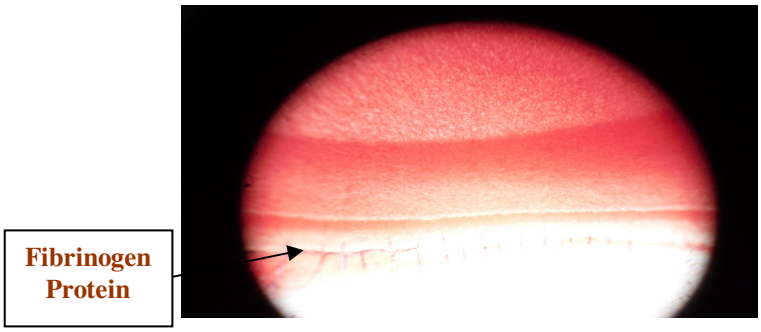

Fig.4.28 Normal Blood with anticoagulant at 10 X magnification

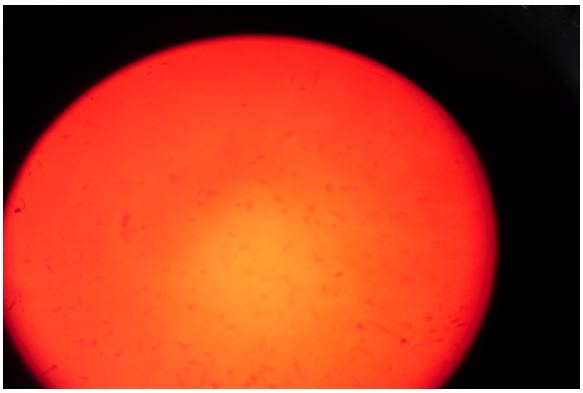

Fig.4.29 Normal Blood with anticoagulant at 40 X magnification

3) Mix the eggshell powder at 300^{0}C in the normal blood with anticoagulant immediately and note down the clotting time. In this case the clotting time is 63 seconds. Now see this under microscope by using 10X (Fig.4.30) and 40X (Fig.4.31).

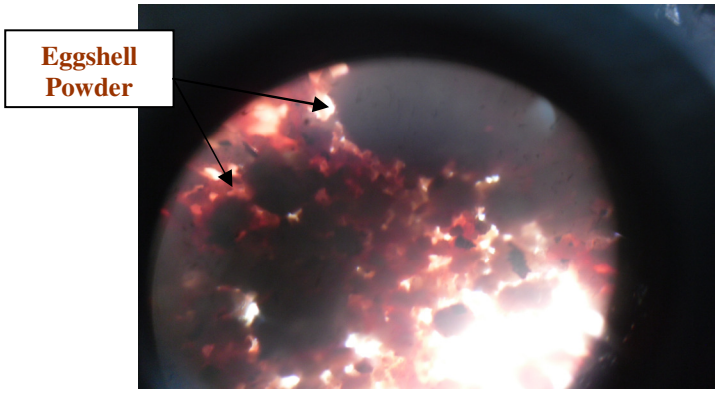

Fig.4.30 Normal Blood with anticoagulant and eggshell powder (300^{0}C) at 10 X

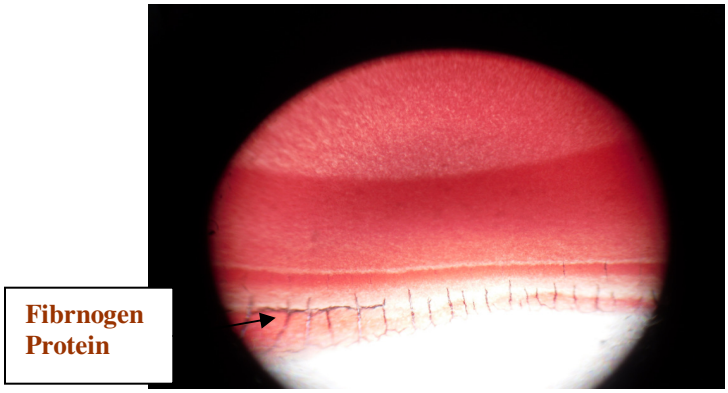

Fig.4.31 Normal Blood with anticoagulant and eggshell powder (300^{0}C) at 40 X

4) Mix the eggshell powder at 600^{0}C in the normal blood with anticoagulant immediately and note down the clotting time. In this case the clotting time is 54 seconds. Now see this under microscope by using 10X (Fig.4.32) and 40X (Fig.4.33).

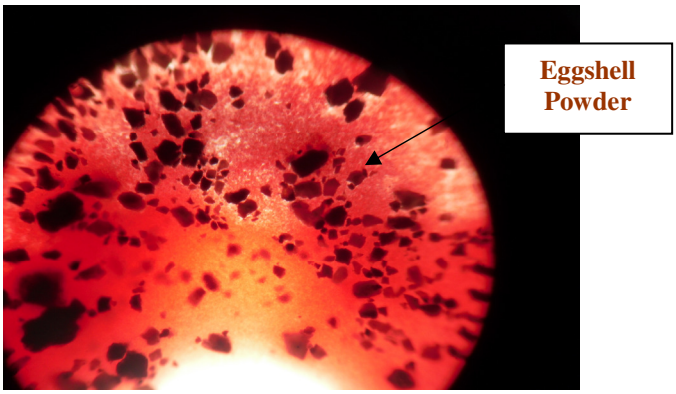

Fig.4.32 Normal Blood with anticoagulant and eggshell powder (600^{0}C) at 10 X

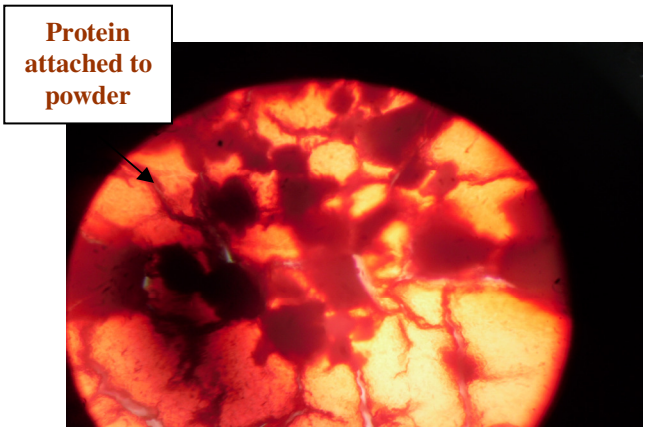

Fig.4.33 Normal Blood with anticoagulant and eggshell powder (600^{0}C) at 40 X

5) Now again mix the eggshell powder at 900^{0}C in the normal blood with anticoagulant immediately and note down the clotting time. In this case the clotting time is 44 seconds. Now see this under microscope by using 10X (Fig.4.34) and 40X (Fig.4.35).

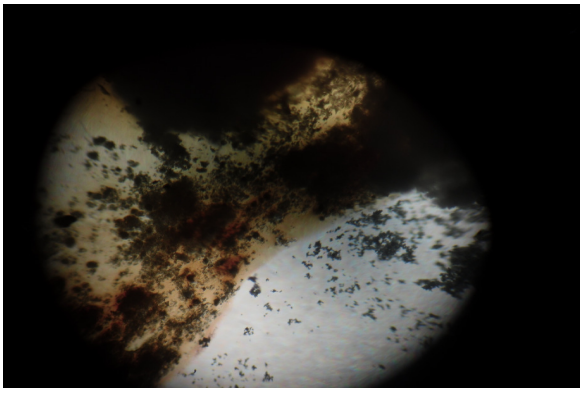

Fig.4.34 Normal Blood with anticoagulant and eggshell powder (900^{0}C) at 10 X

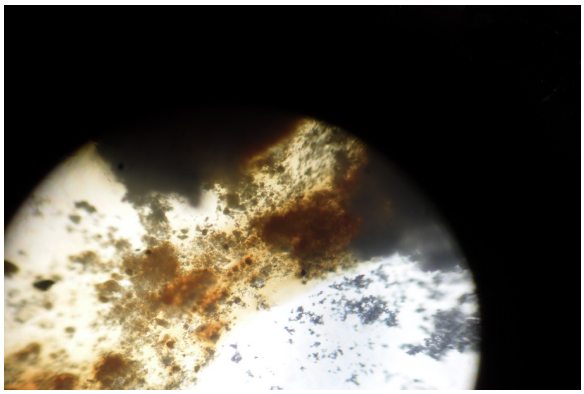

Fig.4.35 Normal Blood with anticoagulant and eggshell powder (900^0C) at 40 X

6) Now mix the (20%HA+40%TiO_2+40%Al_2O_3) powder in the normal blood with anticoagulant immediately and note down the clotting time. In this case the clotting time is 8 seconds. Now see this under microscope by using 10X (Fig.4.36) and 40X (Fig.4.37).

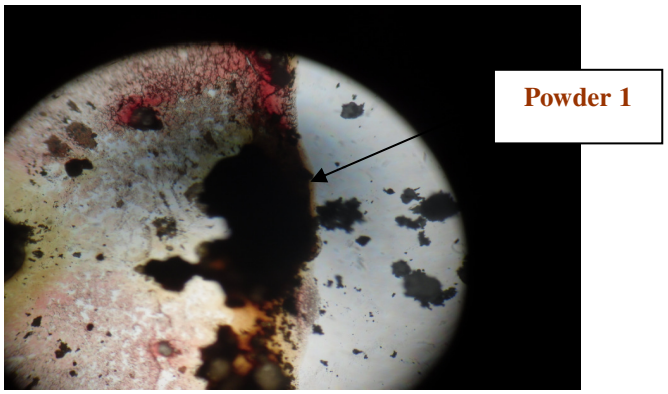

Fig.4.36 Normal Blood with anticoagulant and Powder 1 at 10 X

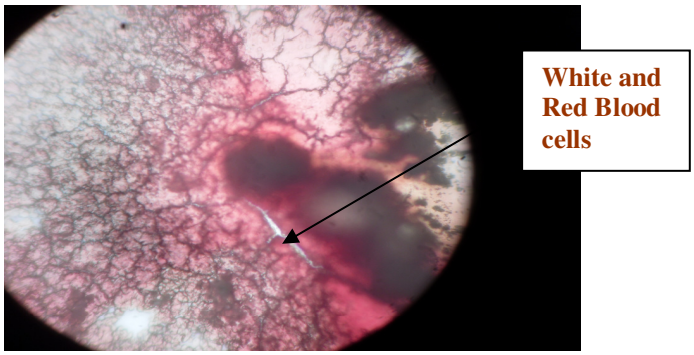

Fig.4.37 Normal Blood with anticoagulant and Powder 1 at 40 X

6) Now mix the (30%HA+35%TiO_2+35%Al_2O_3) in the normal blood with anticoagulant immediately and note down the clotting time. In this case the clotting time is 28 seconds. Now see this under microscope by using 10X (Fig.4.38) and 40X (Fig.4.39).

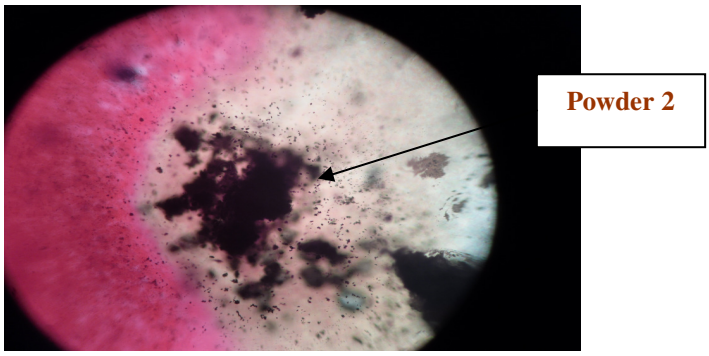

Fig.4.38 Normal Blood with anticoagulant and Powder 2 at 10 X

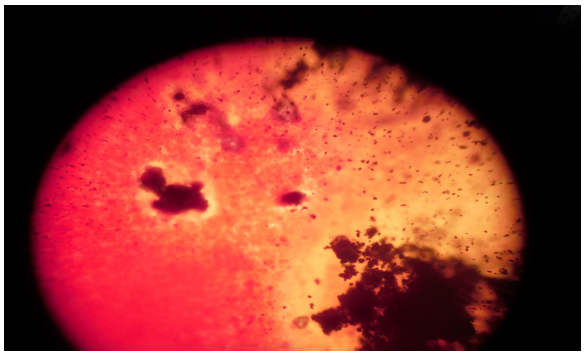

Fig.4.39 Normal Blood with anticoagulant and Powder 2 at 40 X

Clotting capacity is good if clotting time is small. Clotting capacity follows the trend (20%HA+40%TiO_2+40%Al_2O_3) > (30%HA+35%TiO_2+35%Al_2O_3) > Eggshell (900^{0}C) > Eggshell (600^{0}C) > Eggshell (300^{0}C). So, Powder 1 is more biocompatible as compared to other powders.

4.3 Powder Coating

Hydroxyapatite is increasingly used, as implant material for medical applications owing to its chemical composition very similar to that of a major component of human bone. The most interesting property of HA is its excellent biocompatibility i.e. it helps to form a direct bond with the neighbouring bone.

However, the low strength of calcium phosphate bio ceramics such as Hydroxyapatite (HA) have limited their scope of clinical applications and hence more research needs to be conducted to improve their mechanical properties.

Despite excellent properties as a biomaterial, the ceramic nature and the inherent mechanical properties of HA specifically brittleness, poor tensile strength and poor impact resistance have restricted it's application in many load bearing applications.

Therefore, the concept of applying hybrid coating using HA, TiO_2 and Al_2O_3 on to metallic implants as a surface is developed. TiO_2 and Al_2O_3 prevent corrosion and wear of metallic surface. Hydroxyapatite coatings on metal substrates such as Ti–6Al–4V and SS 304L are used often in orthopaedics.

In this research work SS 304L is used as base metal substrate. The composition of SS 304L is evaluated by using Spectrometer. The results are shown in Table 4.1.

Element	Weight %
C	0.0689
Mn	1.97
Si	0.508
Cr	18.1
Ni	8.22
P	0.0461
S	0.0169
Fe	69.9
Co	0.129
Cu	0.503

Nb	0.081
Ti	0.099
V	0.0489
W	0.0405

Table 4.1 The Composition of SS 304L

4.3.1 Preparation of metal substrate

The SS 304L is easily available at True Metals, Industrial area, Phase II, Chandigarh. The material is available in the form of long strips of 5 mm thickness and circular rods of 8mm diameter. The strip is cut into small rectangular pieces of 40mm x 40mm by Press. The circular rod is cut into small pieces (pins) of length 8mm by Center Lathe as shown in Fig.4.40.

Fig.4.40 Preparation of metal subtrate

4.3.2 Flow chart of Experimental plan

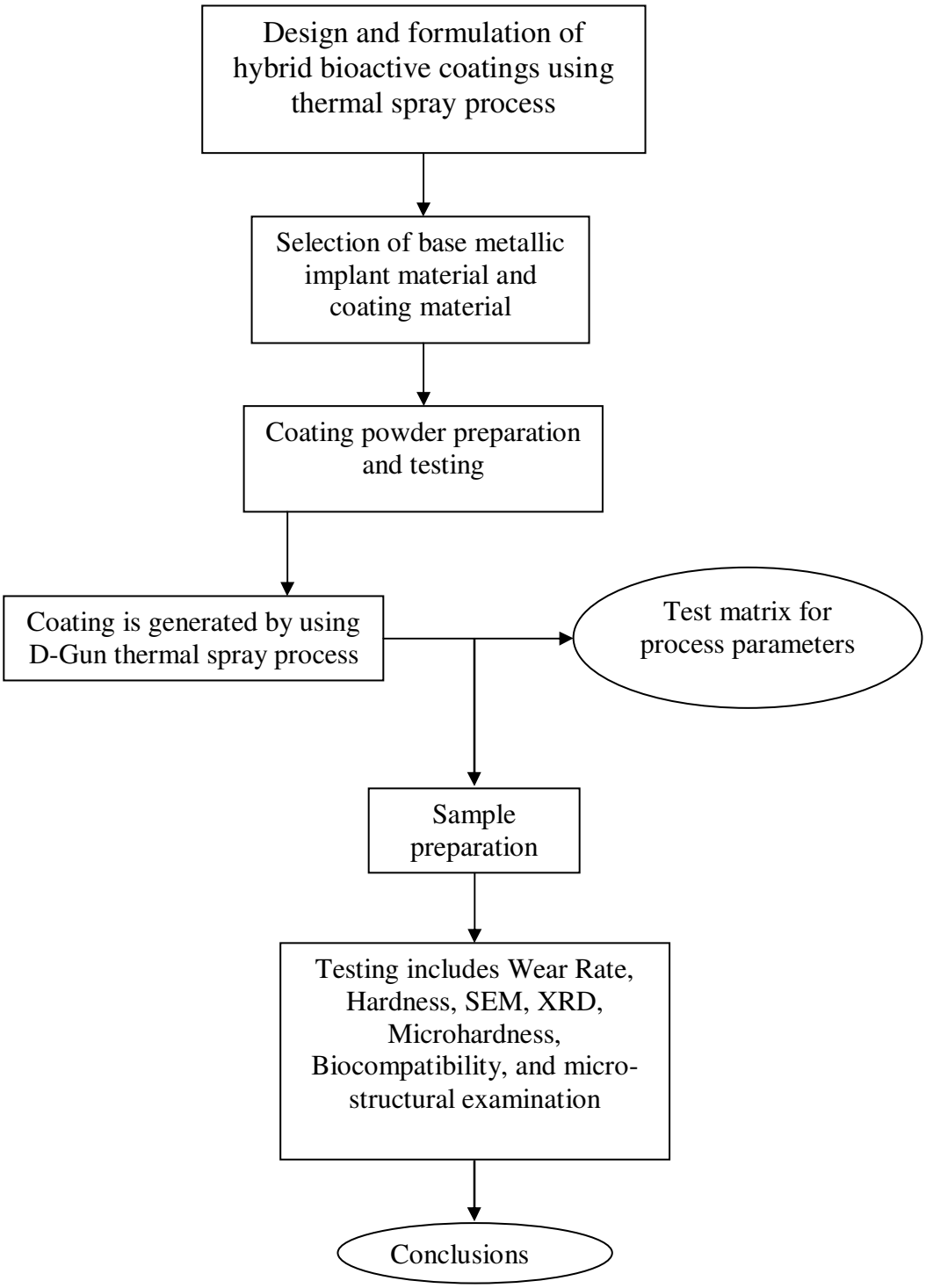

Fig.4.41 Flow chart of the Experimental plan

4.3.3 Detonation Gun (D-Gun) thermal spray process

After making the required sample size of metal substrate SS 304L , the next step is to develop coating of eggshell, aluminium oxide and Titanium oxide powders on it by using D-Gun thermal spray process. Coating is carried out at SVX Powder M Surface Engineering Pvt. Ltd, H-14,Site C, Surajpur Industrial Area, Greater Noida (U.P).

The following are the main steps:

1) First of all surface of metal substrate is prepared prior to coating using Sandblasting (Fig.4.42). Sandblasting means the act of propelling very fine bits of material at high-velocity to clean a surface.

Fig.4.42 Sandblasting

2) The eggshell, Al_2O_3 and TiO_2 powder mixture is placed in the powder feed mechanism (Fig.4.43).

Fig.4.43 Powder feeding

3) Adjust the flow rate of powder Acetylene, Nitrogen and Oxygen supply through control panel (Fig.4.44).

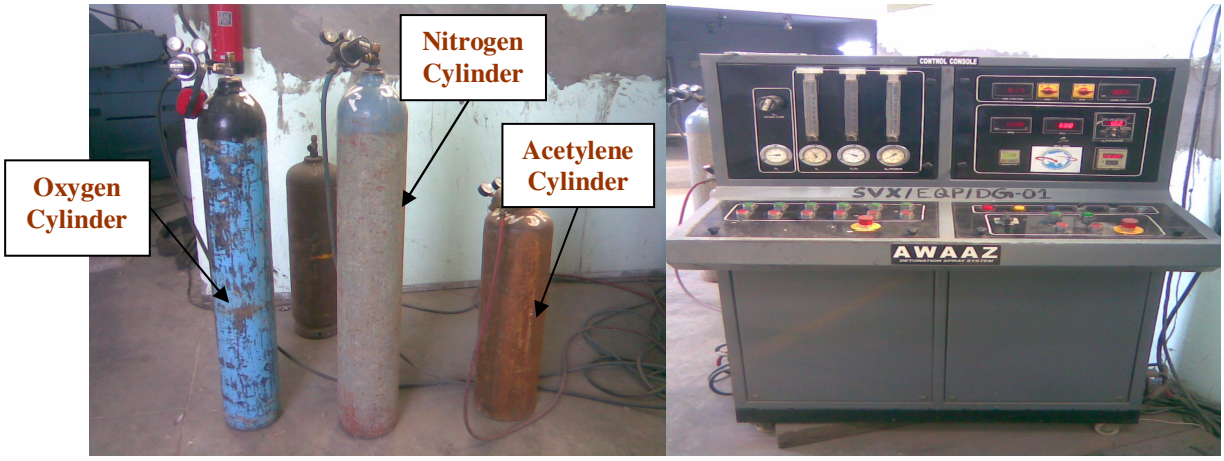

Fig.4.44 Control panel

4) Adjust the stand off distance between work piece and nozzle of detonation gun to 180mm.
5) Ignite the spark plug using control pannel and on the supply of powder, acetylene, oxygen and nitrogen gas to start the coating process (Fig.4.45).

Fig.4.45 Performing coating process

6) Obtain the large number of samples by varying the parameters like Acetylene flow rate, Nitrogen flow rate, Oxygen flow rate and Powder composition.

4.3.3.1 Coating Parameters

Coating is carried out by varying the following parameters using factorial design:

1) Oxygen flow rate

It is varied form 5120 SLPH to 5040 SLPH.

2) Acetylene flow rate

It is varied form 2240 SLPH to 2160 SLPH.

3) Nitrogen flow rate

It is varied form 800 SLPH to 720 SLPH.

4) Powder composition

It is varied form Powder 1 (20%HA+40%TiO_2+40%Al_2O_3) to Powder 2 (30%HA+35%TiO_2+35%Al_2O_3).

'SLPH' — 'Standard Litres per Hour'

The four factors Oxygen flow rate, Acetylene flow rate, Nitrogen flow rate and Powder composition is set to a low (-1) and a high level (+1).

Coating run resulting from the factorial experimental plan is shown in Table4.2

Sample No.	Oxygen flow rate (SPLH)	Acetylene flow rate (SPLH)	Nitrogen flow rate (SPLH)	Powder composition
1	5040	710	2160	Powder 1
2	5120	710	2160	Powder 1
3	5040	800	2160	Powder 1
4	5120	800	2160	Powder 1
5	5040	710	2160	Powder 1
6	5120	710	2160	Powder 1
7	5040	800	2160	Powder 1
8	5120	800	2160	Powder 1
9	5040	710	2240	Powder 2
10	5120	710	2240	Powder 2
11	5040	800	2240	Powder 2
12	5120	800	2240	Powder 2
13	5040	710	2240	Powder 2
14	5120	710	2240	Powder 2
15	5040	800	2240	Powder 2
16	5120	800	2240	Powder 2

Table4.2 Readings at different detonation parameters

Coating is carried out for both 16 samples of rods (8mm) and 16 samples of square (40 × 40 mm).

4.4 Sliding Wear

Wear is a process of removal of material from one or both of two solid surfaces in solid state contact. As the wear is a surface phenomenon and occurs mostly at outer surfaces, it is more appropriate and economical to make surface modification of existing alloys than using the wear resistant alloys.

4.4.1 Experimental procedure of wear test

Dry sliding wear tests for the uncoated and detonation coated 309 SS is conducted by using a pin-on-disc machine (Model: Wear & Friction Monitor TR-20) supplied by DUCOM, Bangalore. During the experiment room is 28-30^{0}C as shown in Fig.4.46.

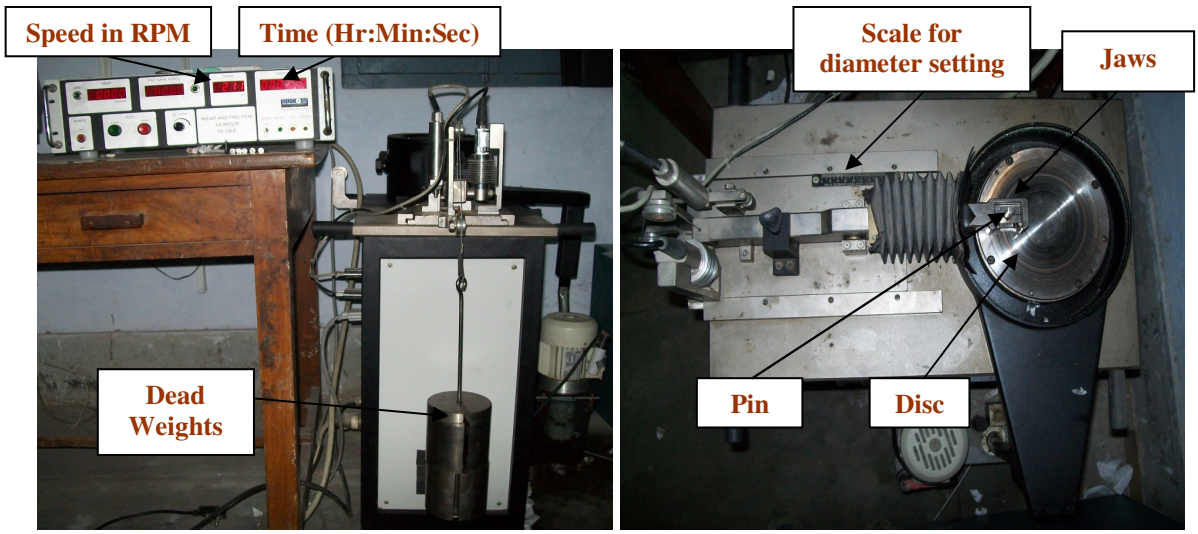

Fig.4.46 Wear & Friction Monitor TR-20

The pin is held against the counterface of a rotating disc at 100mm diameter. The pin is loaded against the disc through a dead weight loading system. The wear tests for coated as well as uncoated specimens are conducted under the normal loads of 110N and a fixed sliding velocity of 1 m/s.

Wear tests are carried out for a total sliding distance of 2700m under cyclic conditions for 9 cycles. Each cycle comprised 5 min sliding wear of the specimen on the pin-on-disc machine or in other words each cycle measured 300m. After each cycle, the specimen is removed from the jaws and brushed lightly to remove lose wear debris. Then weight loss for the pin is measured at the end of each cycle to determine the wear loss. The specimen after weighing is fixed again at exactly the same position in the jaws for the next cycle, so that the orientation of the sliding surface remains unchanged.

4.5 Hardness and Microhardness Measurement

The hardness is measured of all the coated samples by using Rockwell hardness tester. Five readings are taken at different points on 'A' scale by applying 60 Kg load for 10 sec for each sample.

Similarly micro hardness is calculated by using MVH-II digital micro hardness tester. Five readings are taken at different points by applying 200 grams load for 20 sec for each sample

5.1 Microscopic Behaviour

5.1.1 Microstructure Examination of coated samples

The microstructure examination of the coated samples is done with the help of metallurgical microscope by using magnification of 15X to show the presence of eggshell powder and its distribution on the metal surface. The microstructure of all the samples is shown Fig.5.1 to Fig.5.16:

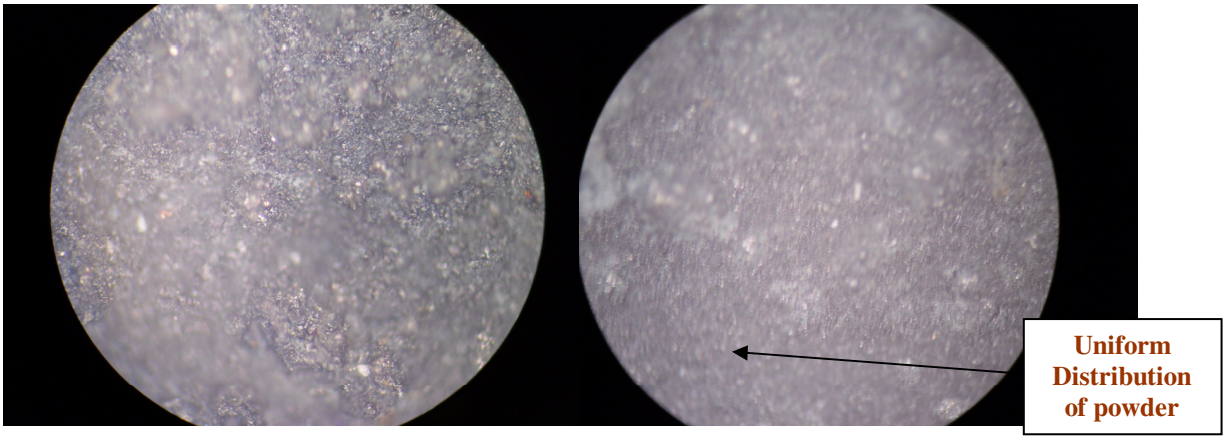

Fig.5.1 Microstructure image of Sample 1 Fig.5.2 Microstructure image of Sample 2

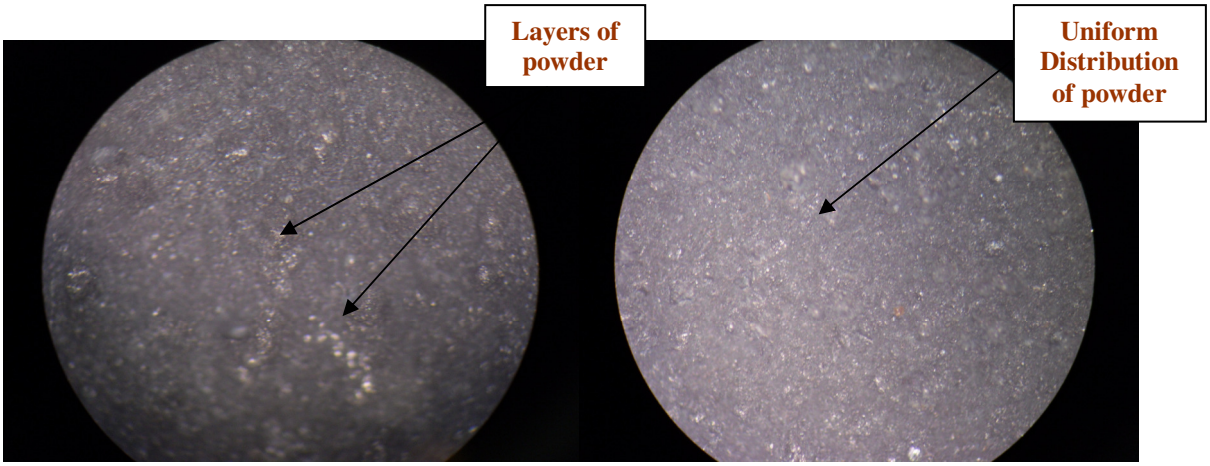

Fig.5.3 Microstructure image of Sample 3 Fig.5.4 Microstructure image of Sample 4

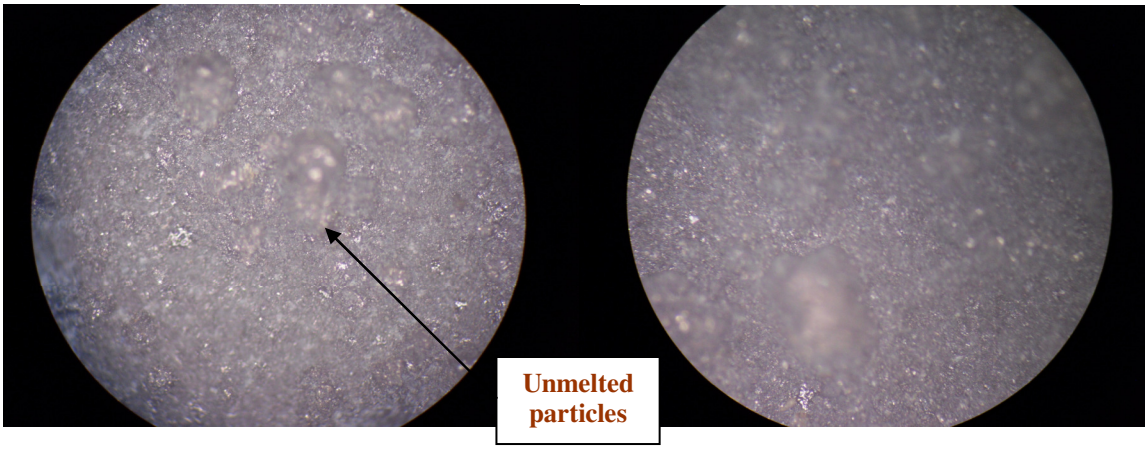

Fig.5.5 Microstructure image of Sample 5

Fig.5.6 Microstructure image of Sample 6

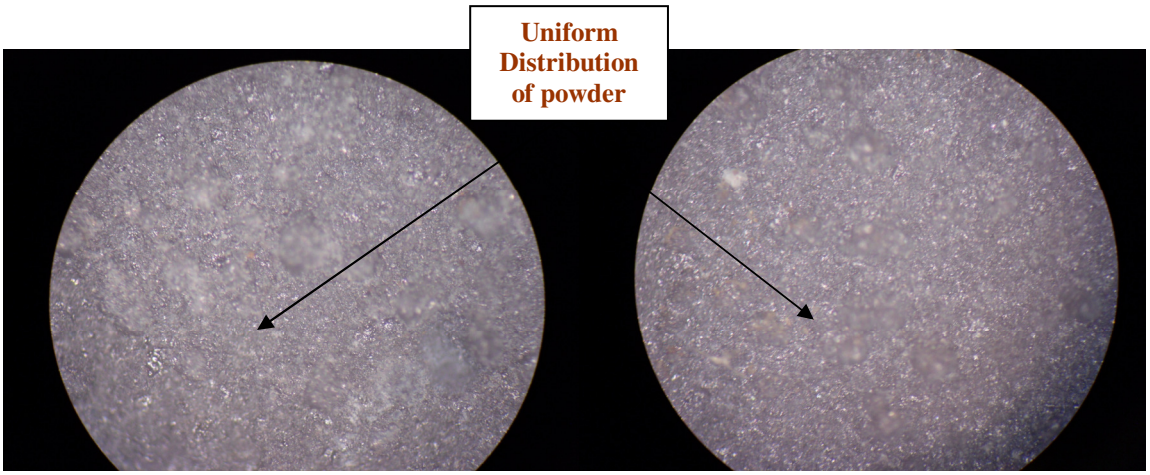

Fig.5.7 Microstructure image of Sample 7

Fig.5.8 Microstructure image of Sample 8

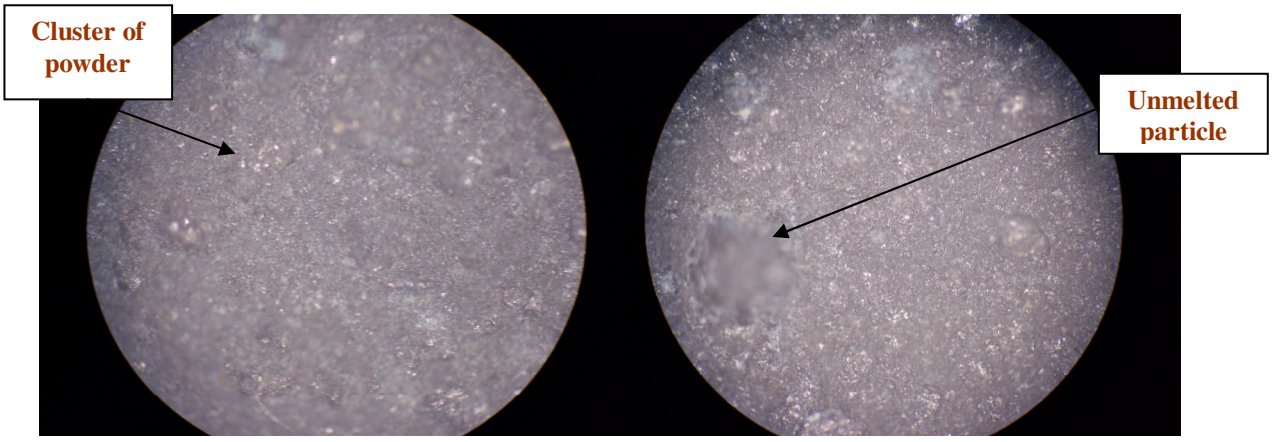

Fig.5.9 Microstructure image of Sample 9

Fig.5.10 Microstructure image of Sample 10

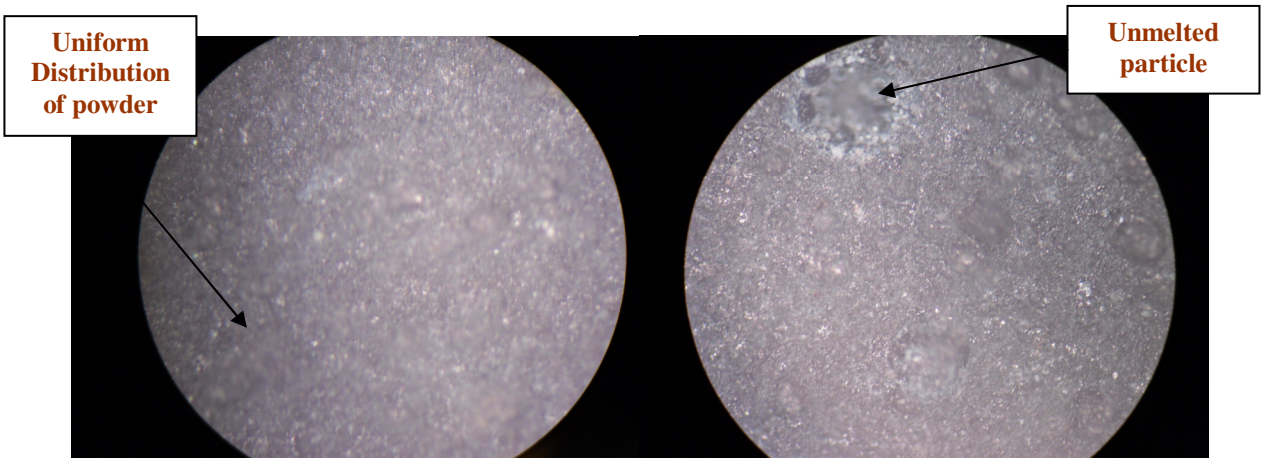

Fig.5.11 Microstructure image of Sample11 Fig.5.12 Microstructure image of Sample12

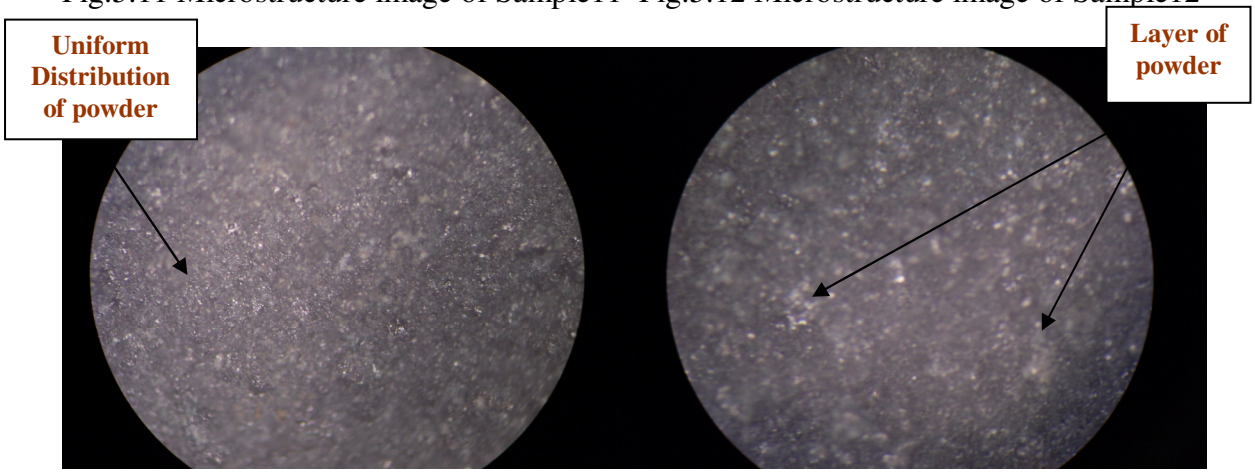

Fig.5.13 Microstructure image of Sample13 Fig.5.14 Microstructure image of Sample14

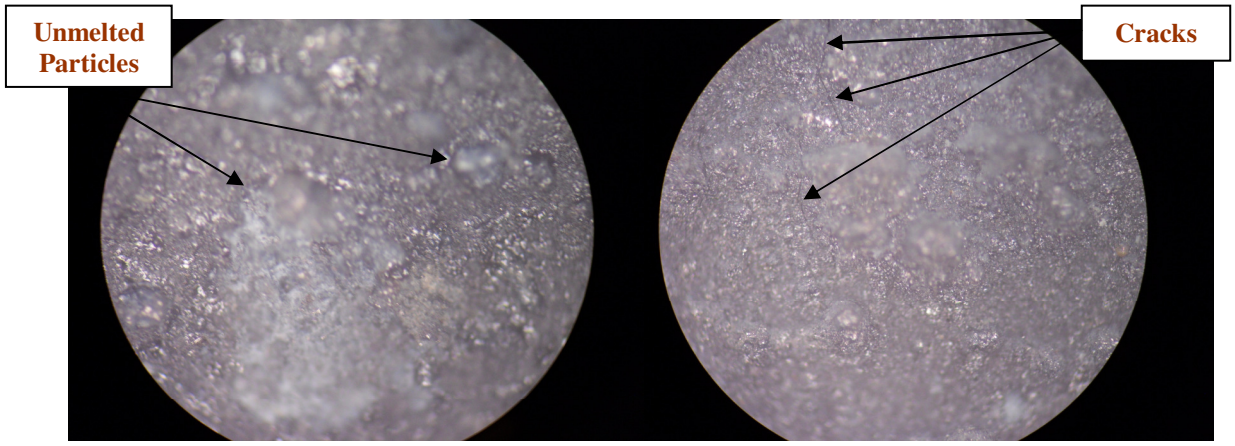

Fig.5.15 Microstructure image of Sample15 Fig.5.16 Microstructure image of Sample16

Result and discussion of microstructure examination

The microstructure examination of the coated samples shows the uniform distribution of Powder 1(20%HA+40%TiO_2+40%Al_2O_3) on SS 304L metal substrate. It is due to good flowability of Powder 1 as compared to Powder 2(30%HA+35%TiO_2+35%Al_2O_3).

5.1.2 X-ray Powder Diffraction (XRD) of coated samples

XRD images of coated samples are given in Fig.5.17 to Fig.5.32.

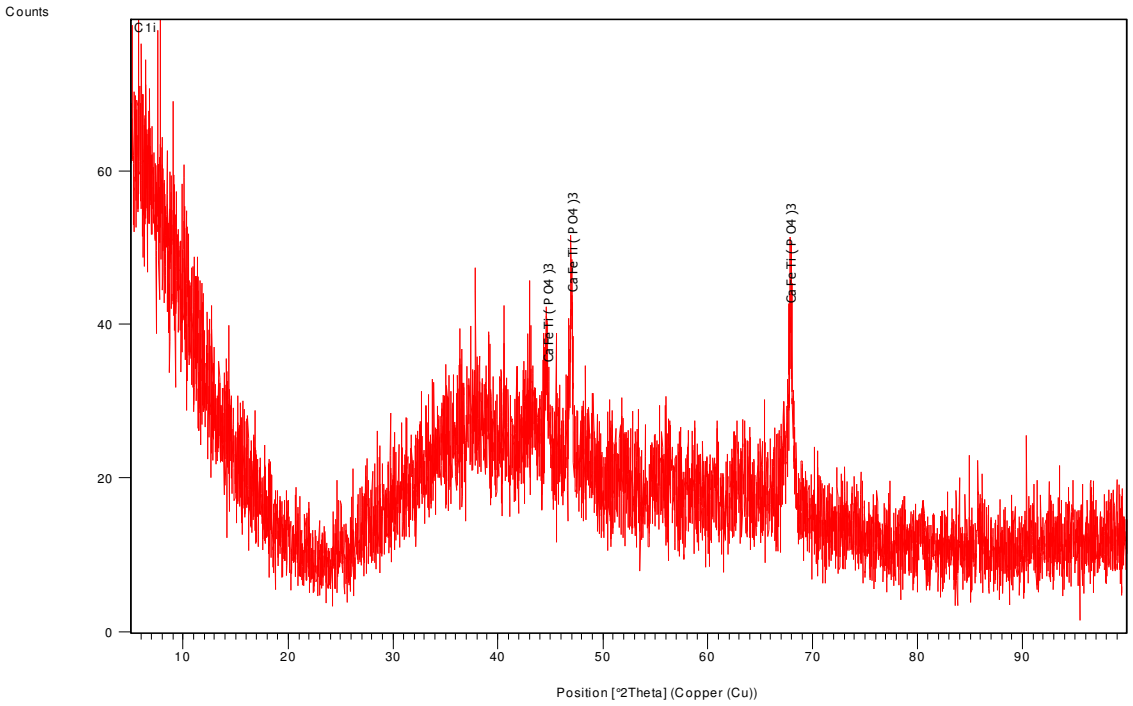

Fig.5.17 XRD image of Sample 1

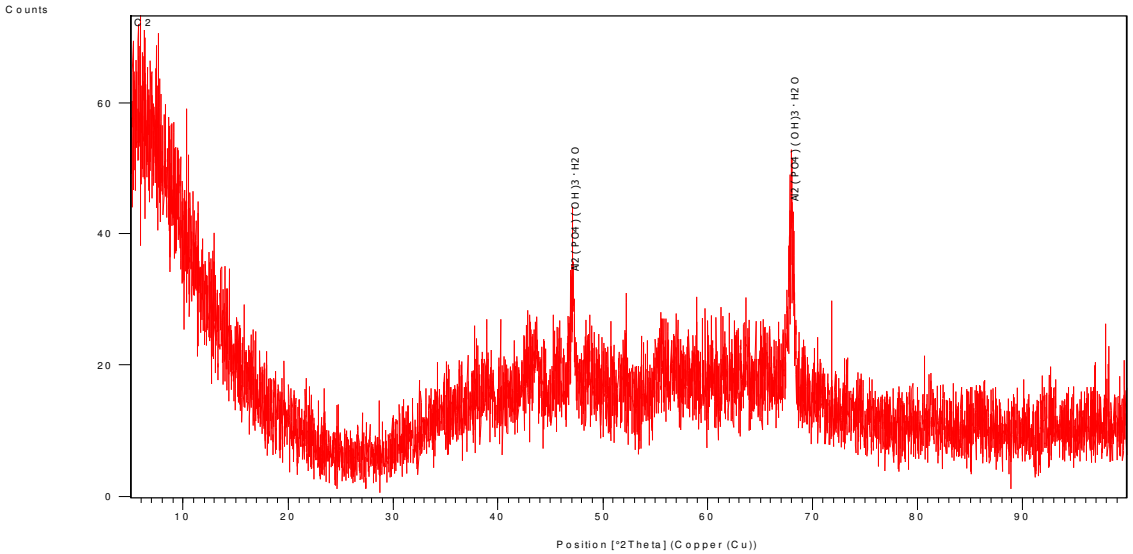

Fig.5.18 XRD image of Sample 2

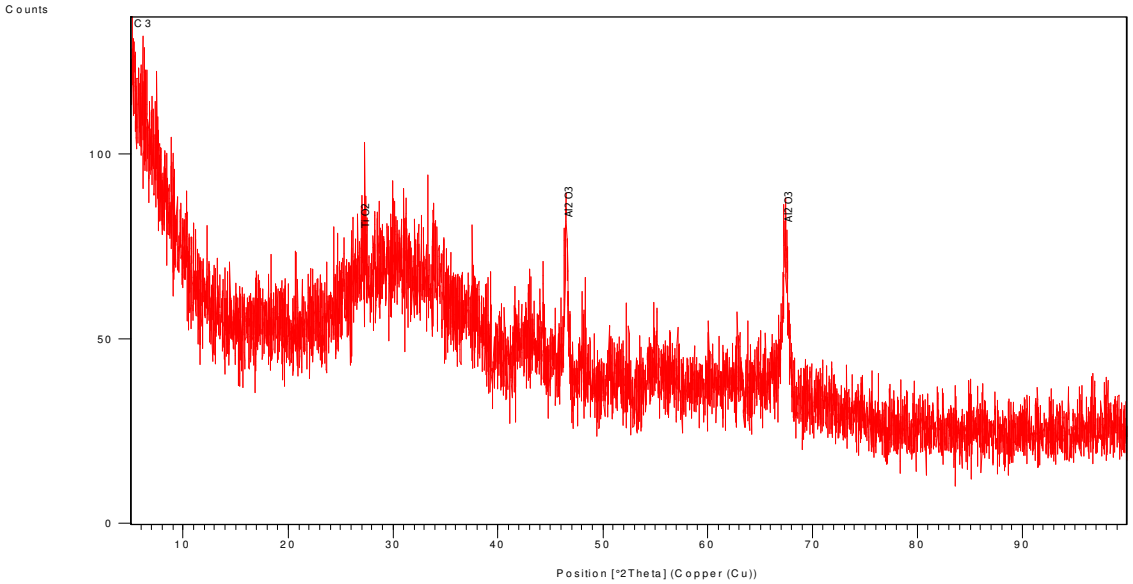

Fig.5.19 XRD image of Sample 3

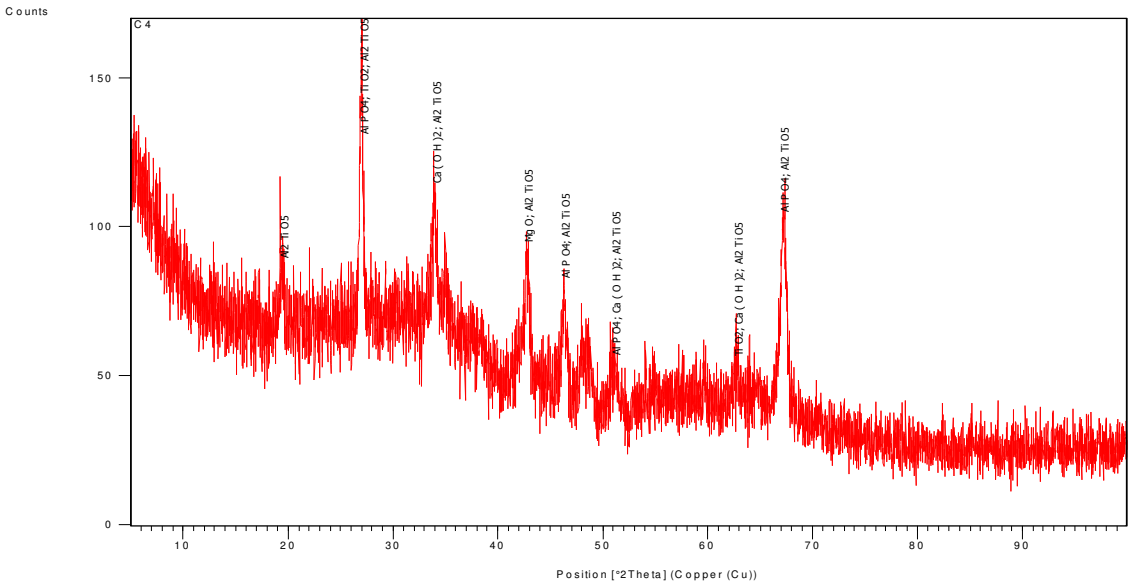

Fig.5.20 XRD image of Sample 4

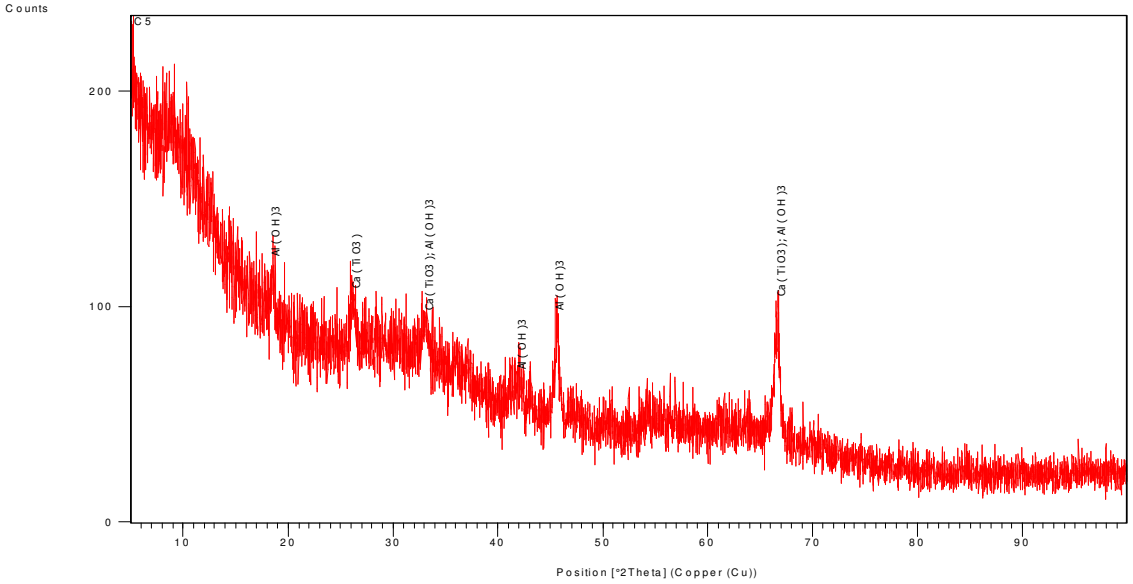

Fig.5.21 XRD image of Sample 5

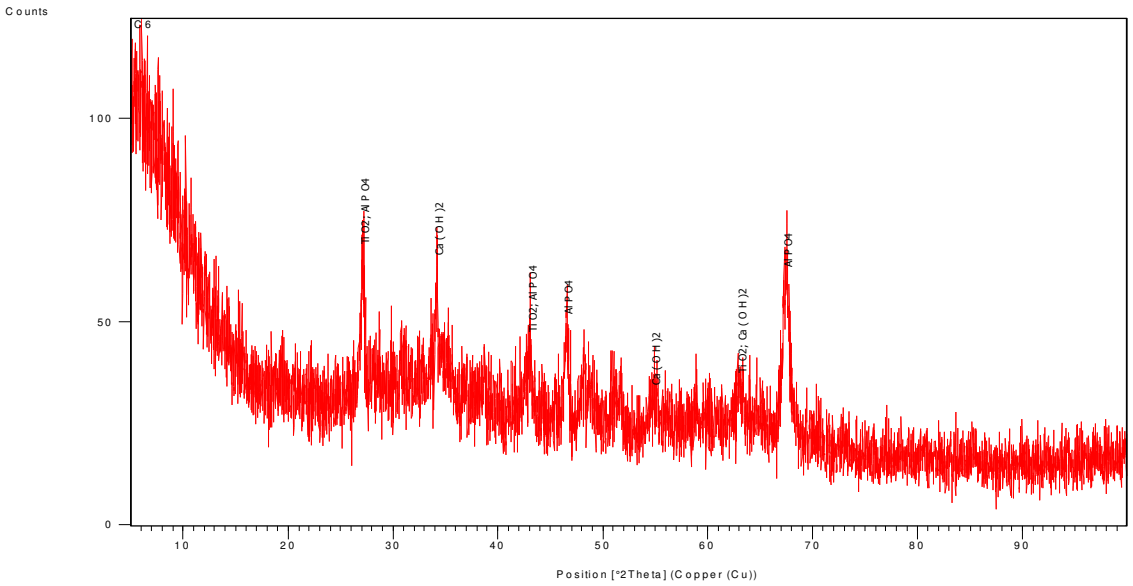

Fig.5.22 XRD image of Sample 6

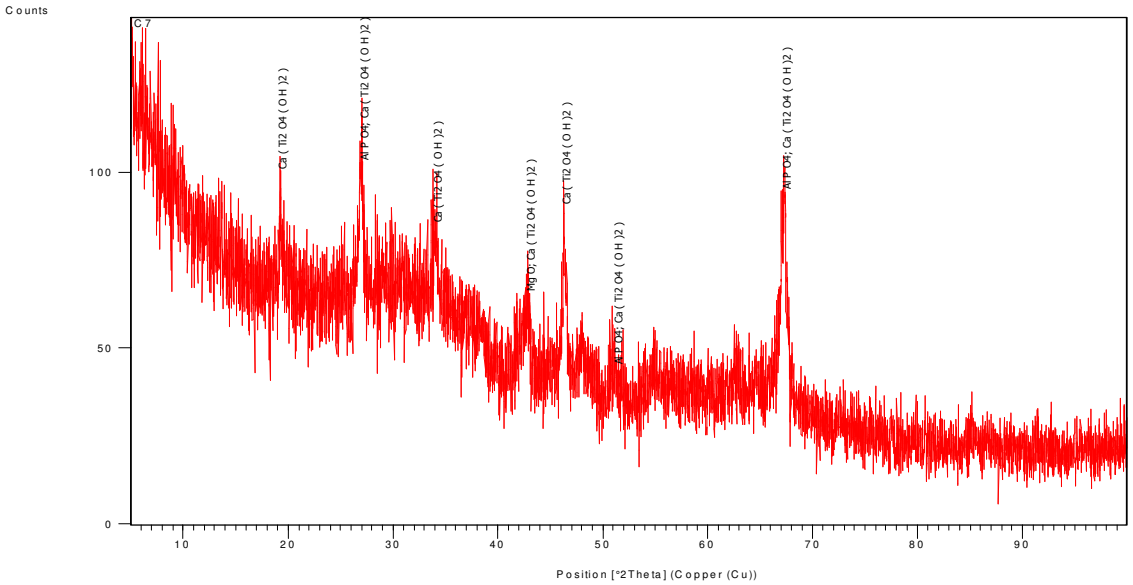

Fig.5.23 XRD image of Sample 7

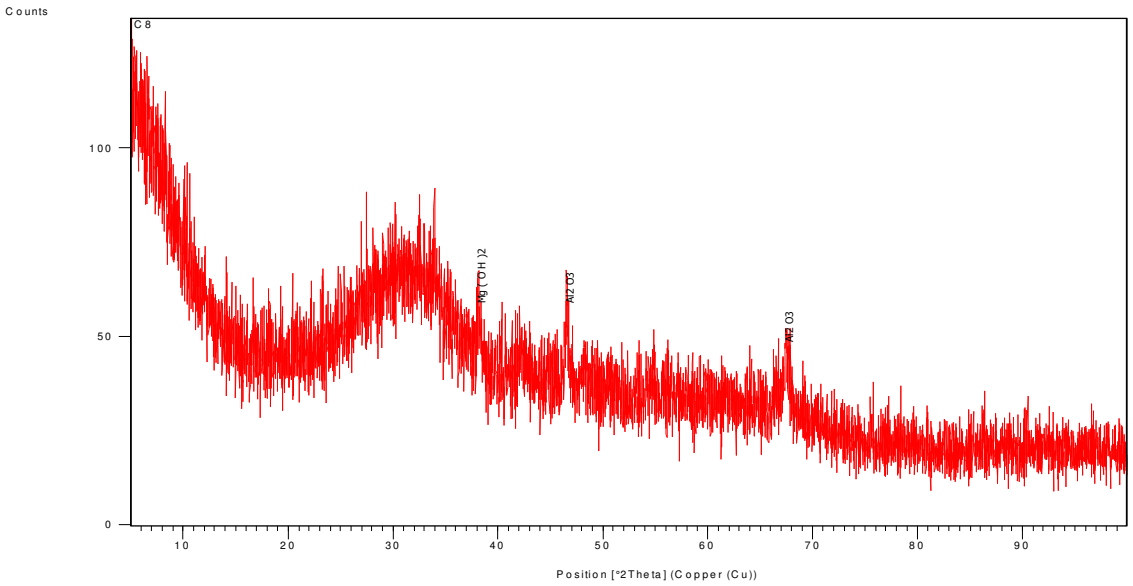

Fig.5.24 XRD image of Sample 8

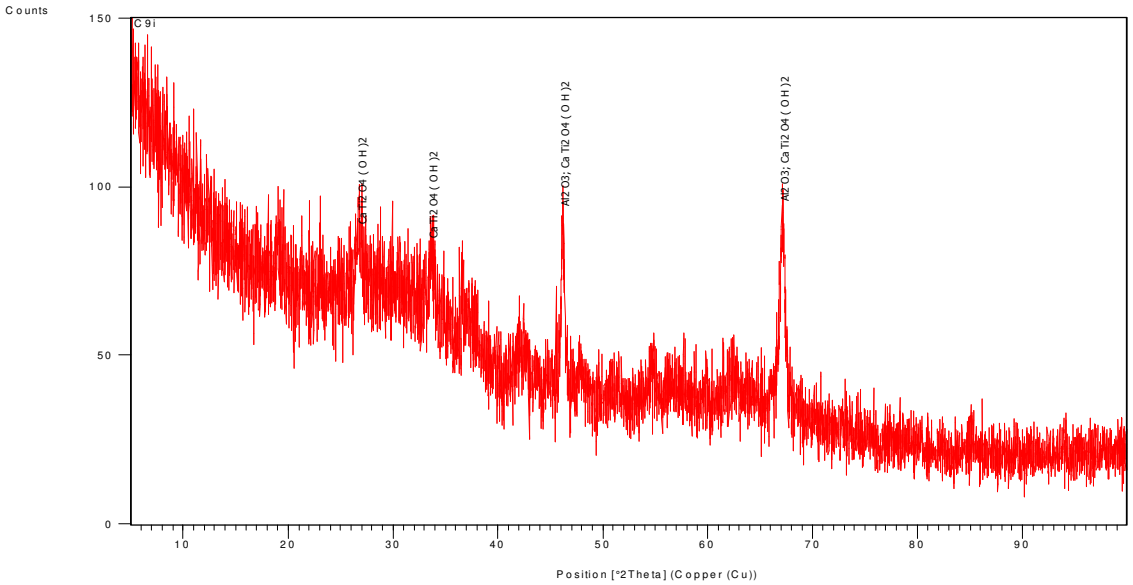

Fig.5.25 XRD image of Sample 9

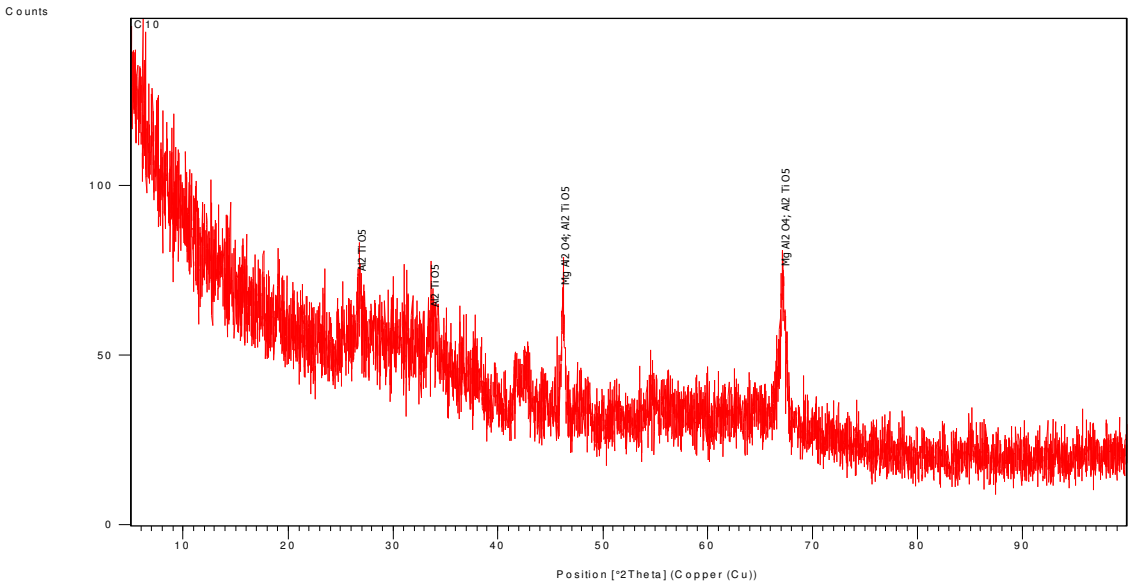

Fig.5.26 XRD image of Sample 10

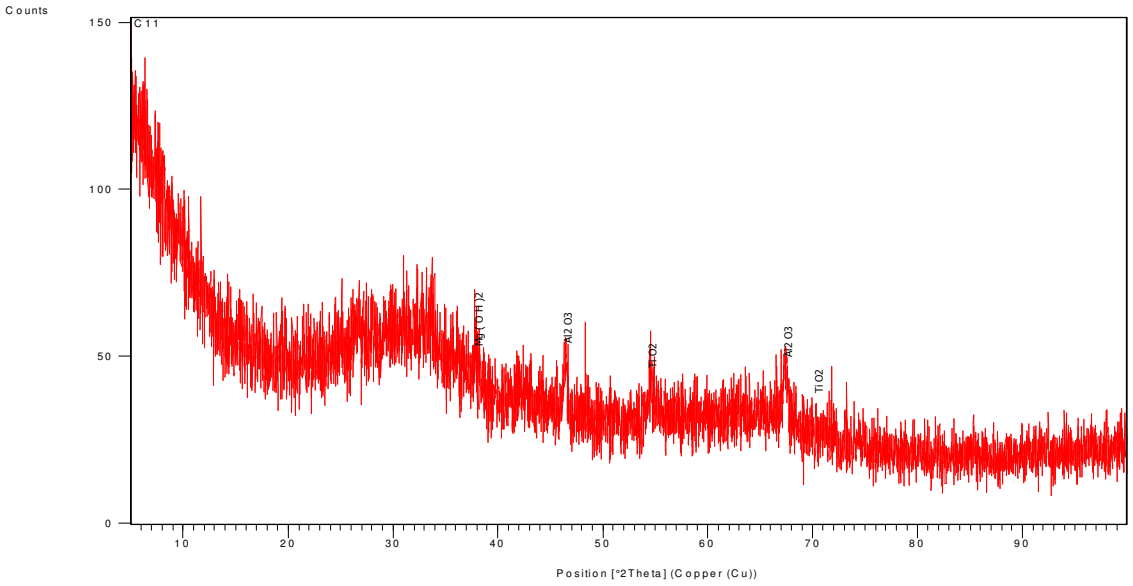

Fig.5.27 XRD image of Sample 11

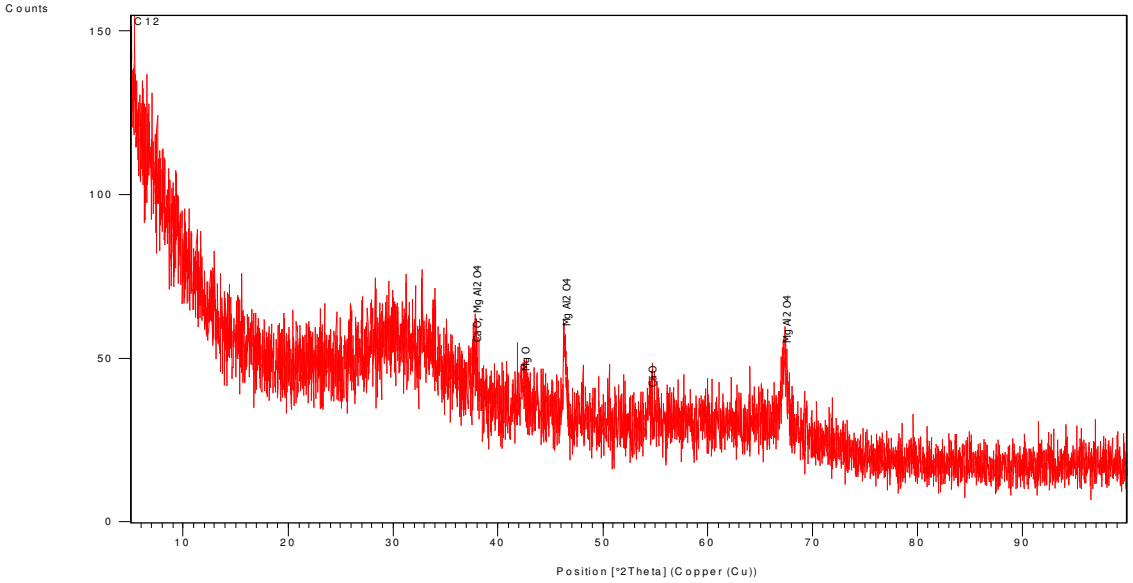

Fig.5.28 XRD image of Sample 12

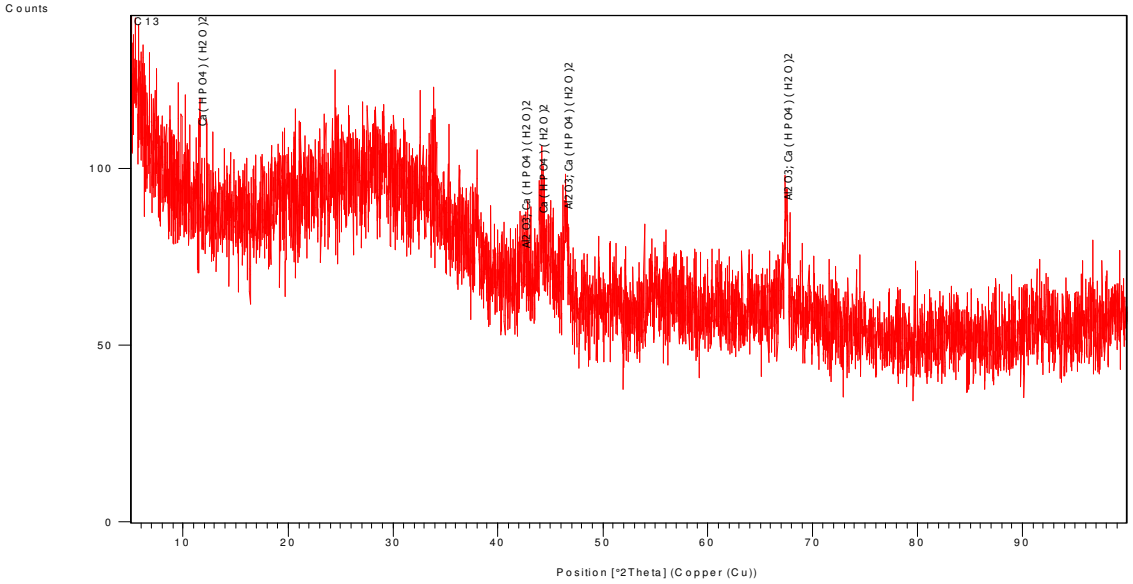

Fig.5.29 XRD image of Sample 13

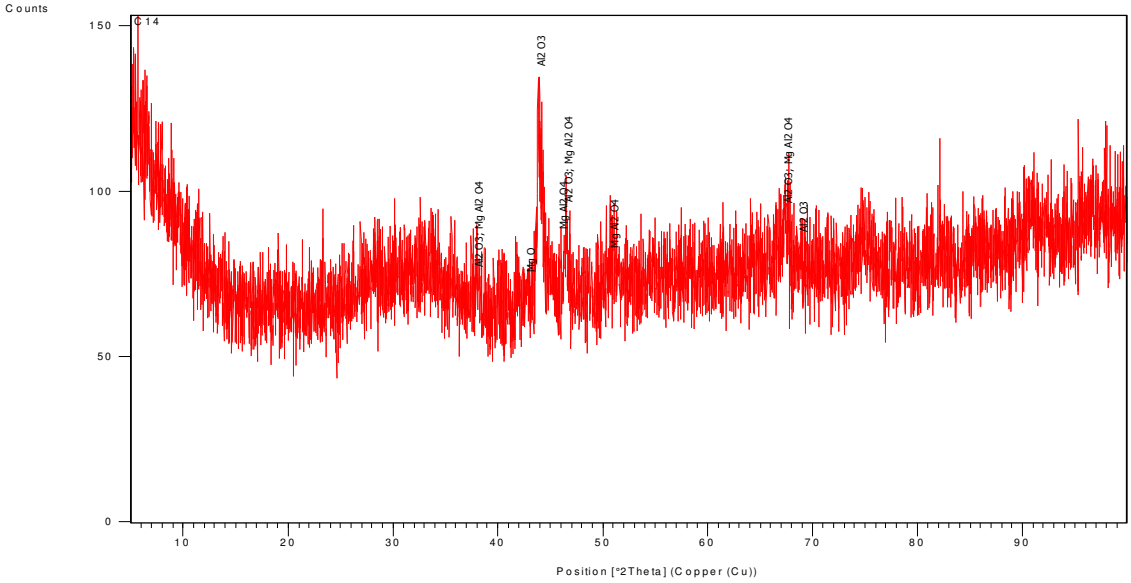

Fig.5.30 XRD image of Sample 14

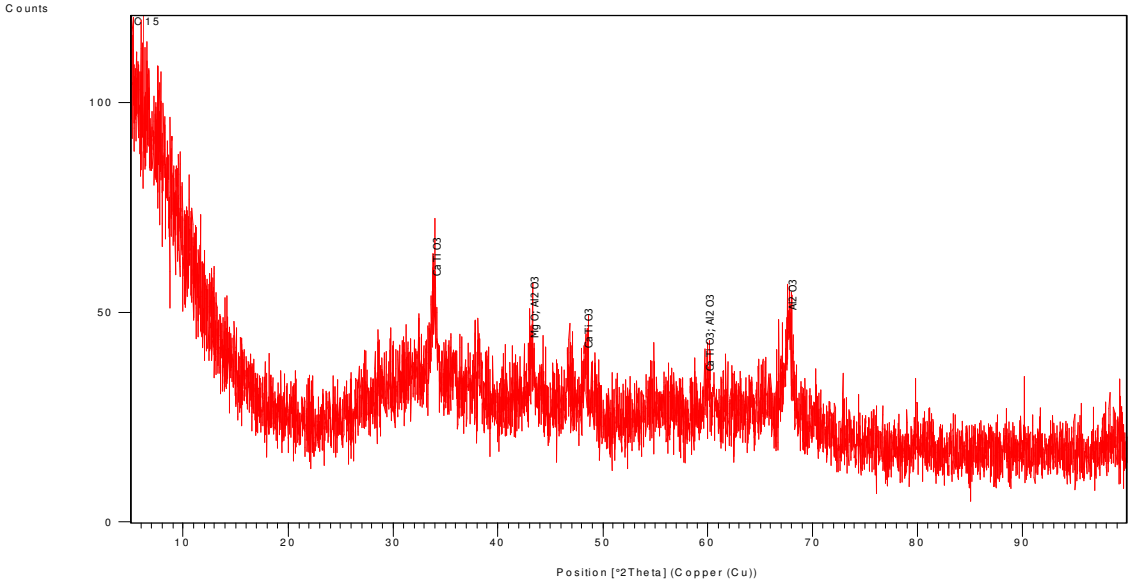

Fig.5.31 XRD image of Sample 15

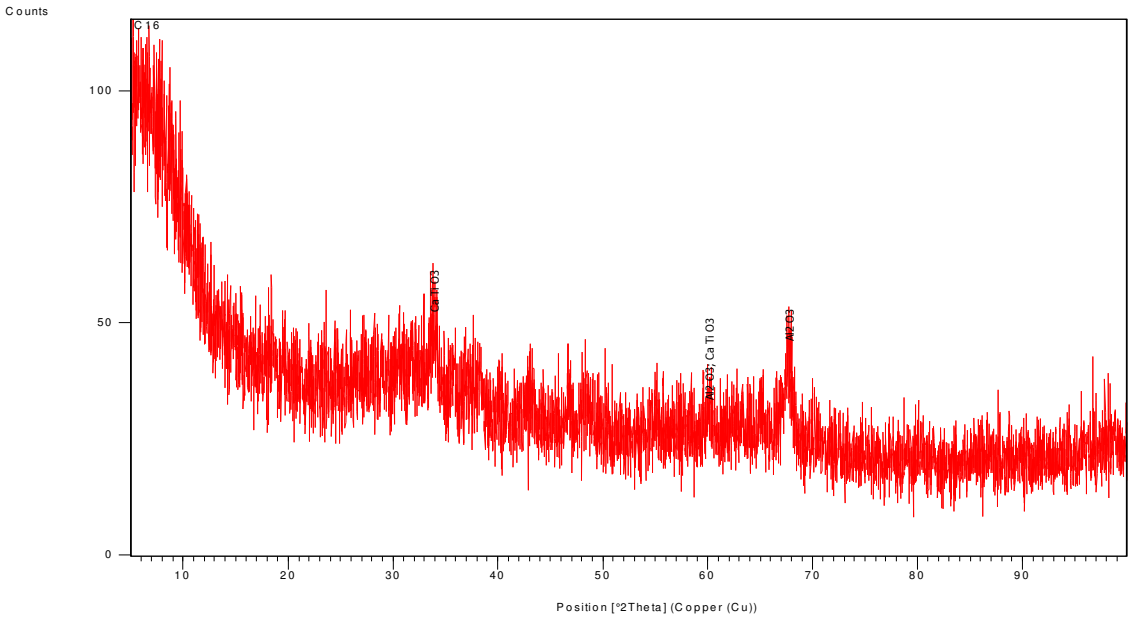

Fig.5.32 XRD image of Sample 16

Result and discussion of XRD of coated samples

The XRD peaks of coated samples shows formation of various elements from hybrid powder like $CaFeTi(PO_4)_3$, $Al_2(PO_4)(OH)_3{\cdot}H_2O$, $Ca(TiO_3)$, $Al(OH)_3$, $AlPO_4$, $CaTi_2O_4(OH)_2$, MgO, CaO, which are shown in Table 5.1.

Sample 1		
Pos. [°2Th.]	Rel. Int. [%]	Assignment
44.6798	53.80	$CaFeTi(PO_4)_3$
47.0068	85.54	$CaFeTi(PO_4)_3$
67.8800	100.00	$CaFeTi(PO_4)_3$
Sample 2		
47.1318	65.82	$Al_2(PO_4)(OH)_3{\cdot}H_2O$
68.0117	100.00	$Al_2(PO_4)(OH)_3{\cdot}H_2O$

Sample 3		
27.1640	55.62	TiO_2
46.5369	84.64	Al_2O_3
67.4315	100.00	Al_2O_3
Sample 4		
27.0495	100.00	TiO_2
33.9539	58.97	$AlPO_4$
42.7297	51.58	$AlPO_4$
46.2877	42.82	$AlPO_4$
67.1208	72.71	$AlPO_4$
Sample 5		
66.7385	100.00	$Ca(TiO_3)$
45.6171	72.50	$Al(OH)_3$
26.2362	52.60	$Al(OH)_3$
33.2280	51.61	$Ca(TiO_3)$
Sample 6		
27.1072	87.07	$AlPO_4$
34.1930	86.60	$Ca(OH)_2$
67.4380	100.00	$AlPO_4$
Sample 7		
67.2472	100.00	$AlPO_4$
27.0460	86.57	$AlPO_4$
46.2997	77.06	$AlPO_4$
Sample 8		
38.2147	87.14	$Mg(OH)_2$

46.5810	100.00	Al_2O_3
67.5660	93.07	Al_2O_3
Sample 9		
33.6419	55.72	Al_2O_3
46.1534	89.91	$CaTi_2O_4(OH)_2$
67.1185	100.00	Al_2O_3
Sample 10		
26.7704	58.89	$MgAl_2O_4$
67.1584	100.00	$MgAl_2O_4$
46.1784	77.12	$MgAl_2O_4$
Sample 11		
46.4404	100.00	Al_2O_3
67.4658	85.65	Al_2O_3
54.4945	66.25	TiO_2
Sample 12		
67.3155	100.00	$MgAl_2O_4$
46.3100	95.00	$MgAl_2O_4$
37.7839	58.70	$MgAl_2O_4$
Sample 13		
44.1052	73.99	Al_2O_3
46.5337	85.41	$Ca(HPO_4)(H_2O)_2$
67.4572	100.00	Al_2O_3
Sample 14		
43.8240	100.00	Al_2O_3
46.0301	34.99	$MgAl_2O_4$

41.8363	22.23	Al_2O_3
46.4933	45.42	$MgAl_2O_4$
Sample 15		
33.9113	100.00	$CaTiO_3$
67.8738	85.76	$CaTiO_3$
43.2107	58.99	$Al_2 O_3$
48.3860	57.51	$CaTiO_3$
Sample 16		
33.7157	100.00	$CaTiO_3$
59.9925	44.33	Al_2O_3
67.6254	96.70	Al_2O_3

Table 5.1 XRD results of coated samples.

5.1.3 Scanning Electron Microscopy (SEM) of coated samples

The SEM images of coated samples at 1000X magnification are shown in Fig.5.33 to Fig.5.48.

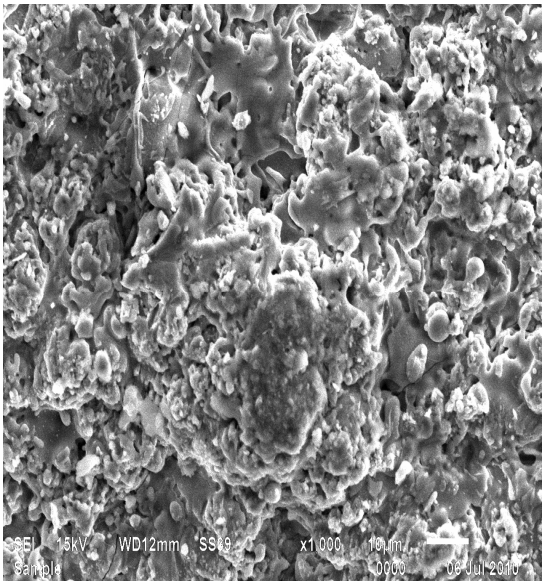

Fig.5.33 SEM image of Sample 1

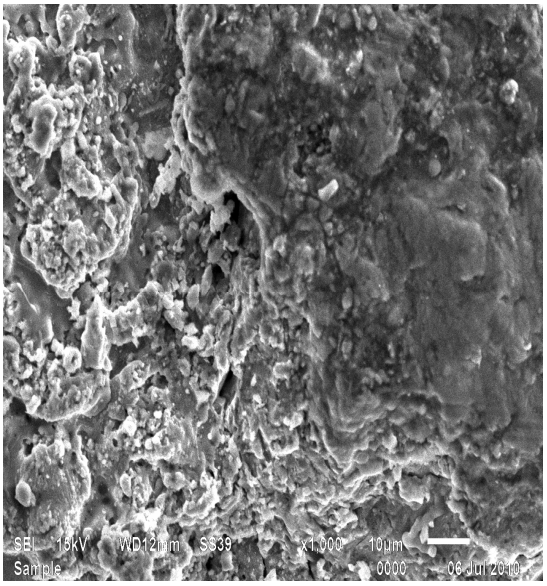

Fig.5.34 SEM image of Sample 2

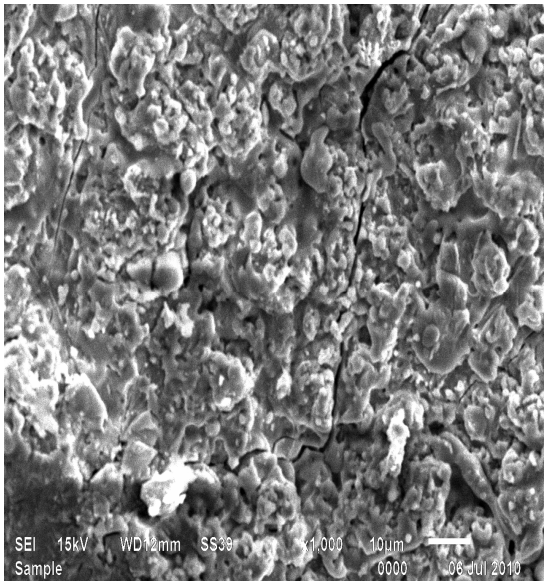

Fig.5.35 SEM image of Sample 3

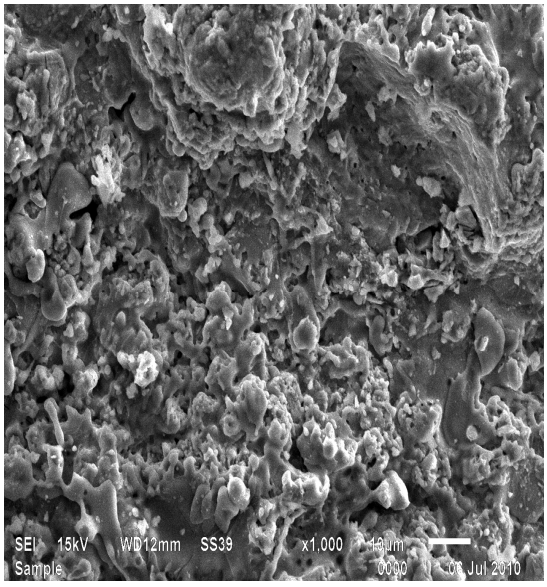

Fig.5.36 SEM image of Sample 4

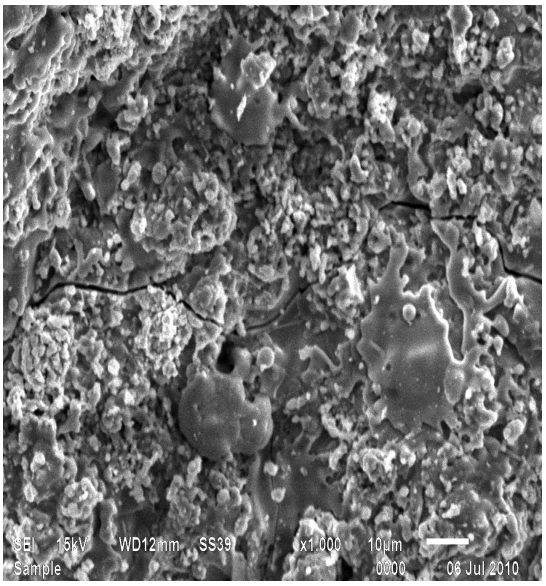

Fig.5.37 SEM image of Sample 5

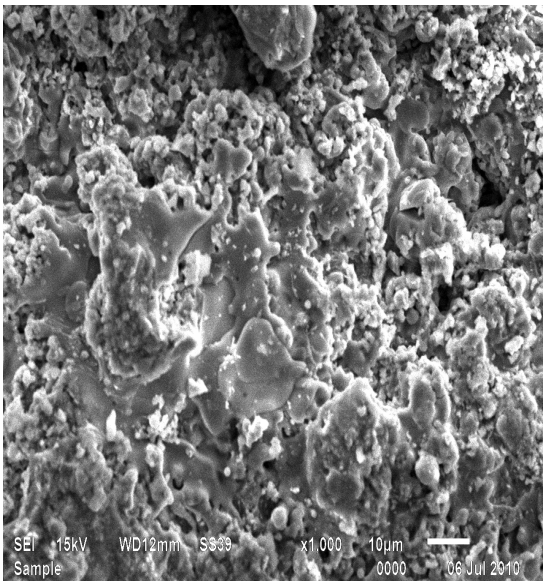

Fig.5.38 SEM image of Sample 6

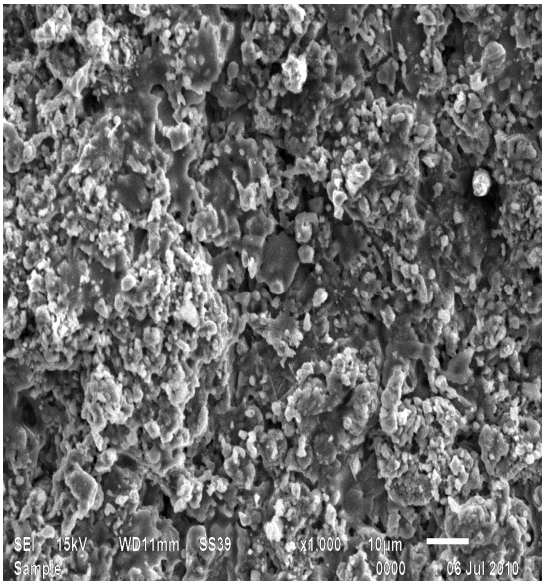

Fig.5.39 SEM image of Sample 7

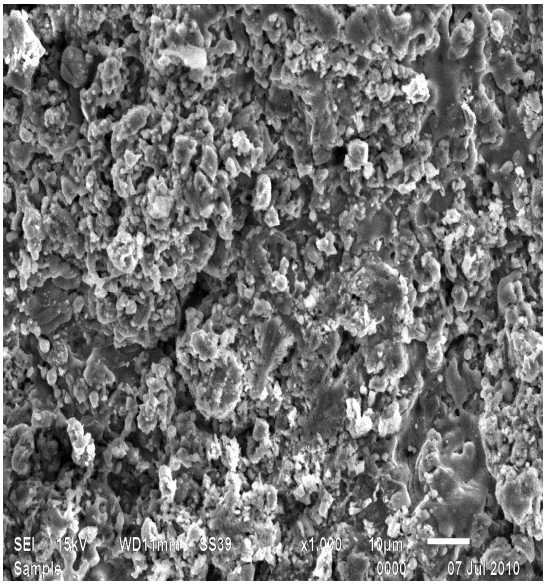

Fig.5.40 SEM image of Sample 8

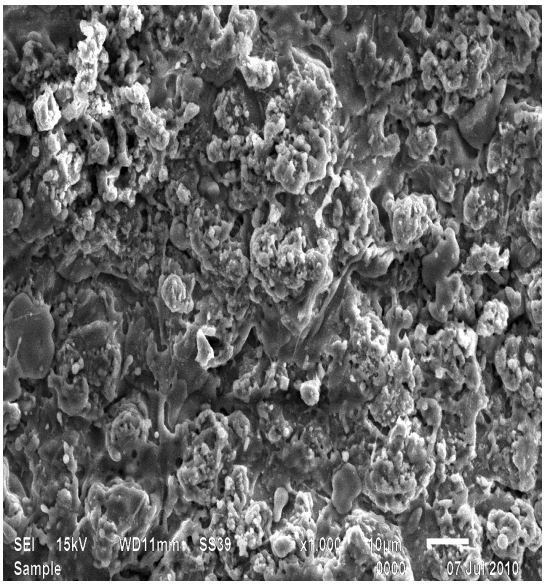

Fig.5.41 SEM image of Sample 9

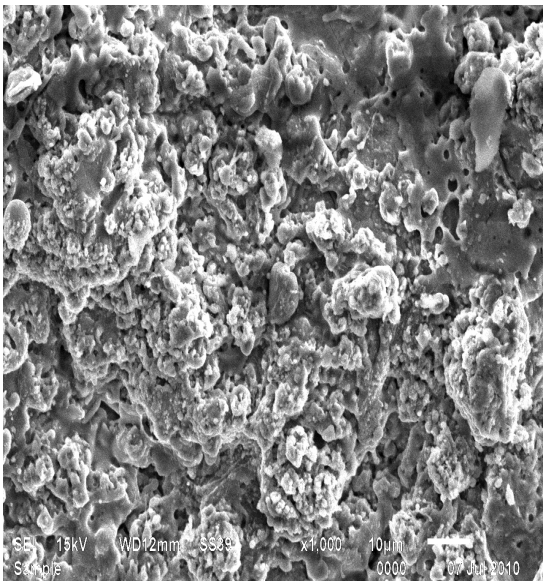

Fig.5.42 SEM image of Sample 10

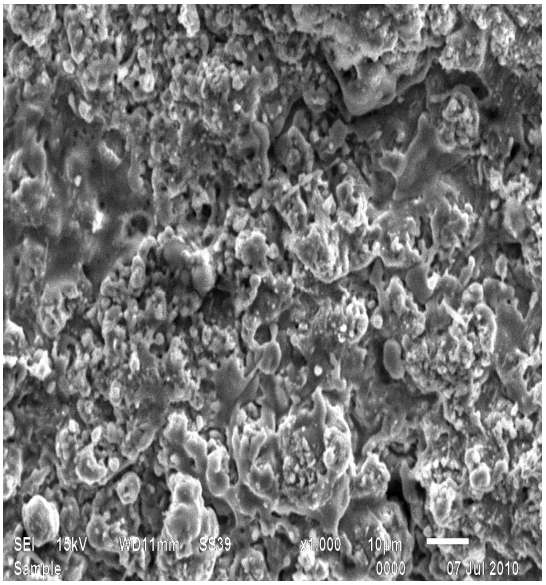

Fig.5.43 SEM image of Sample 11

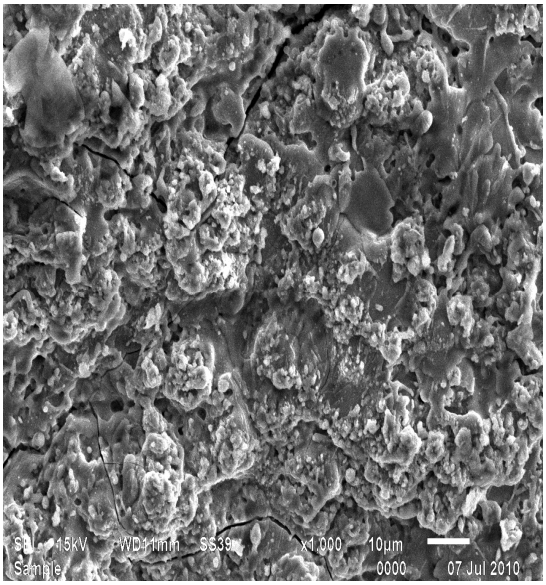

Fig.5.44 SEM image of Sample 12

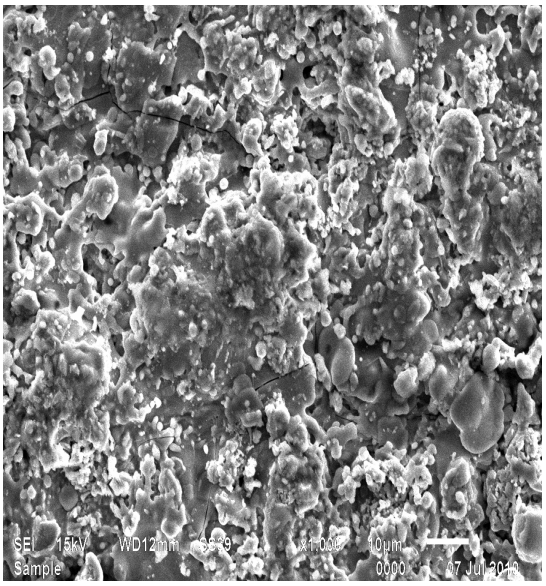

Fig.5.45 SEM image of Sample 13

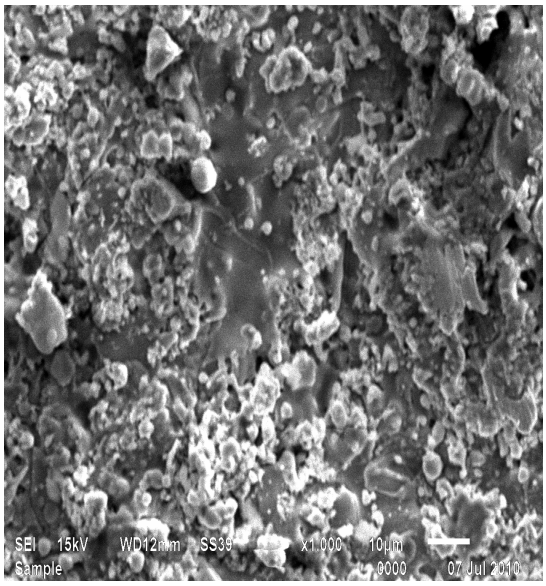

Fig.5.46 SEM image of Sample 14

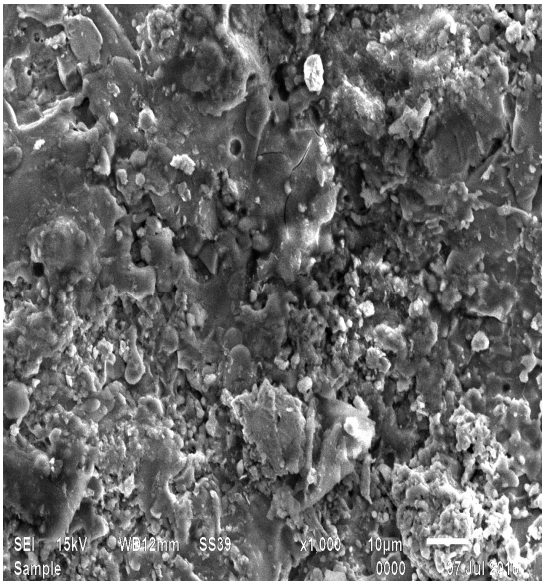

Fig.5.47 SEM image of Sample 15

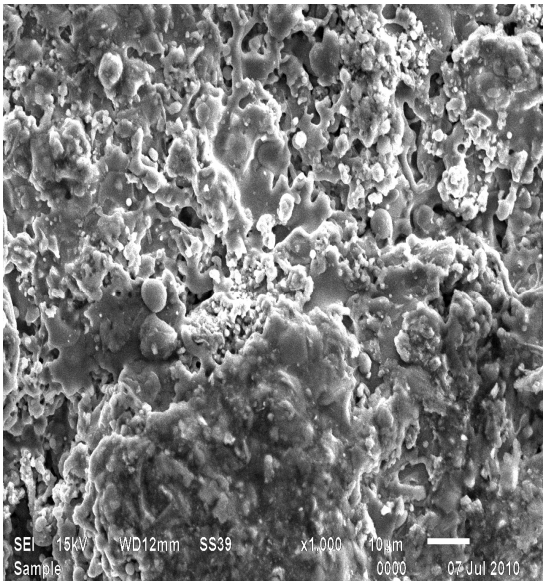

Fig.5.48 SEM image of Sample 16

5.1.4 Image analysis by "Image J" software

The analysis of all SEM image was done in order to find circularity and area fraction. The commercially available software Image J was used for analysis of images. Image J is open source software developed by National Institute of Health. Images of SEM and after analysis by software are shown from Fig.5.49 to Fig.5.80.

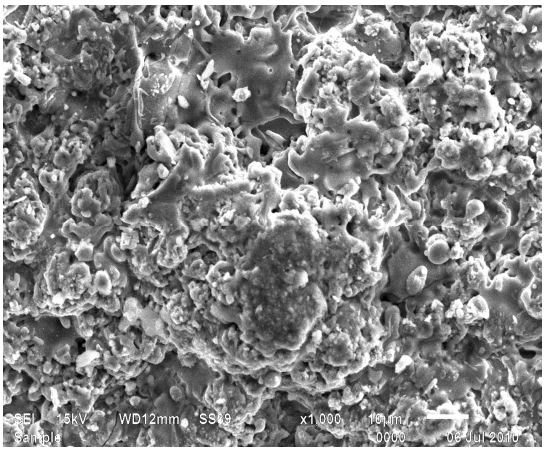

Fig.5.49 SEM image of Sample 1

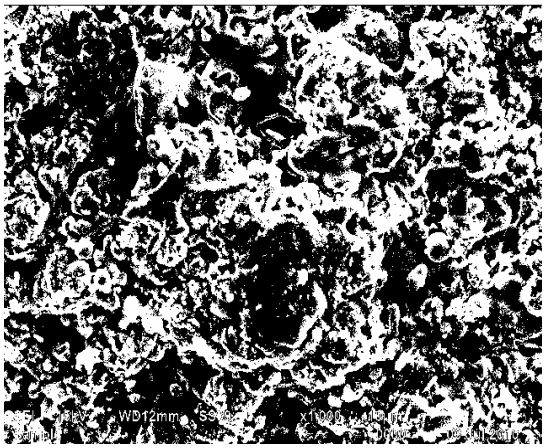

Fig.5.50 Image-J image of Sample 1

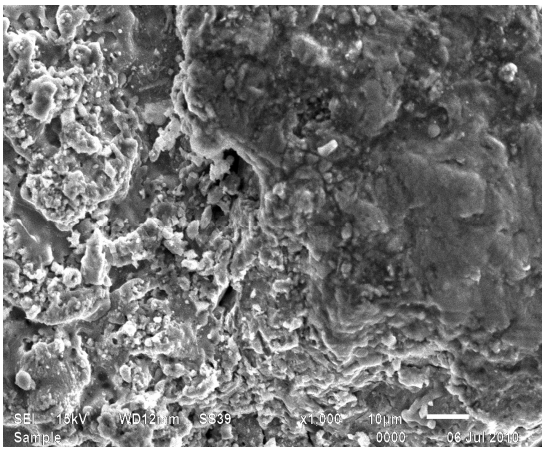

Fig.5.51 SEM image of Sample 2

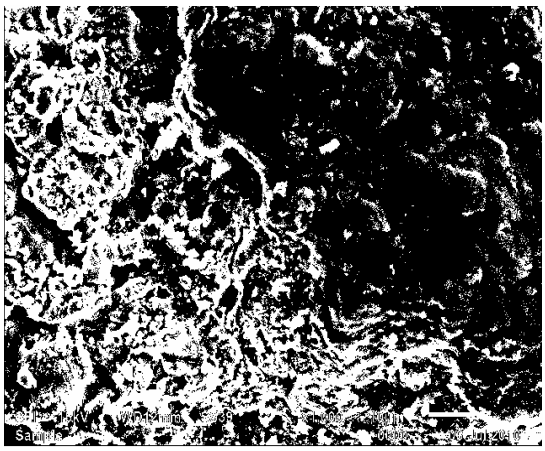

Fig.5.52 Image-J image of Sample 2

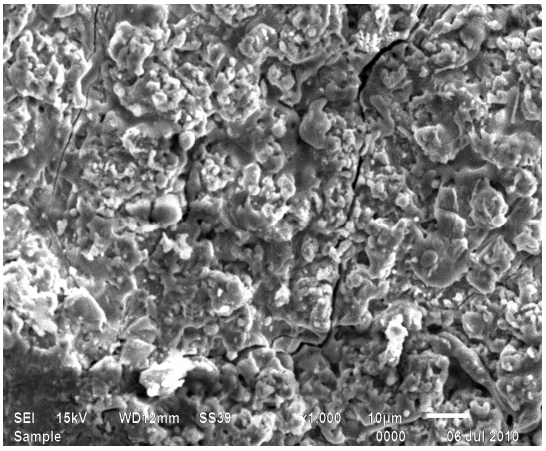

Fig.5.53 SEM image of Sample 3

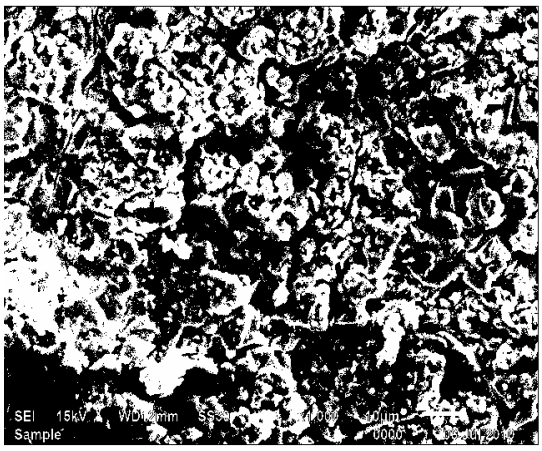

Fig.5.54 Image-J image of Sample 3

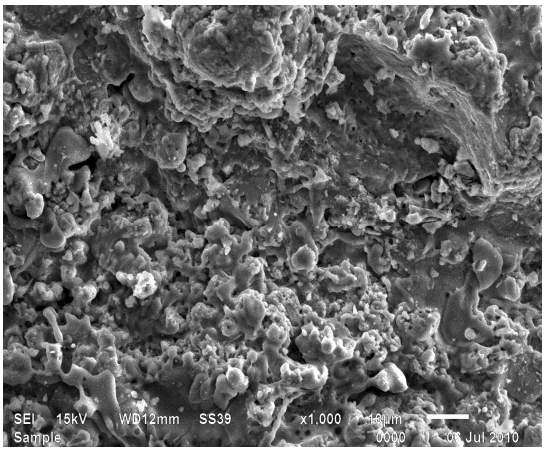

Fig.5.55 SEM image of Sample 4

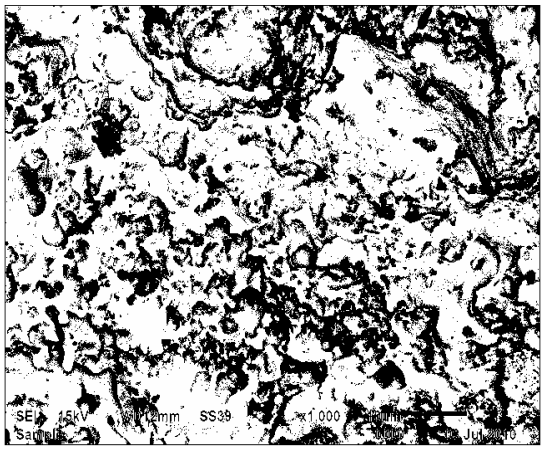

Fig.5.56 Image-J image of Sample 4

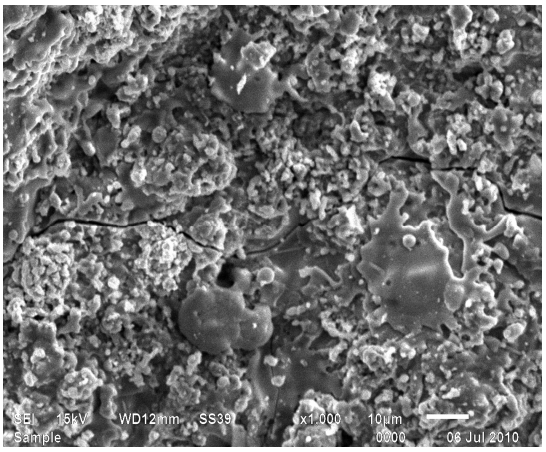

Fig.5.57 SEM image of Sample 5

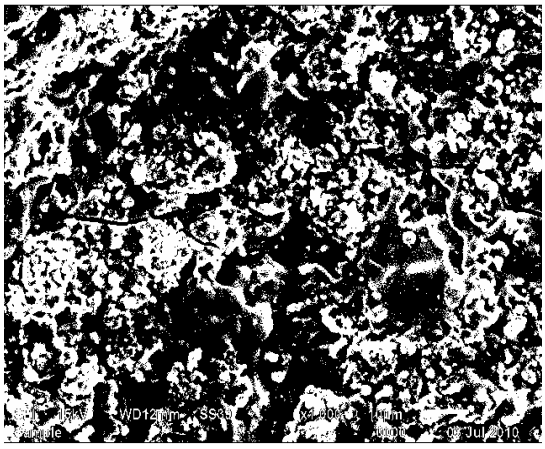

Fig.5.58 Image-J image of Sample 5

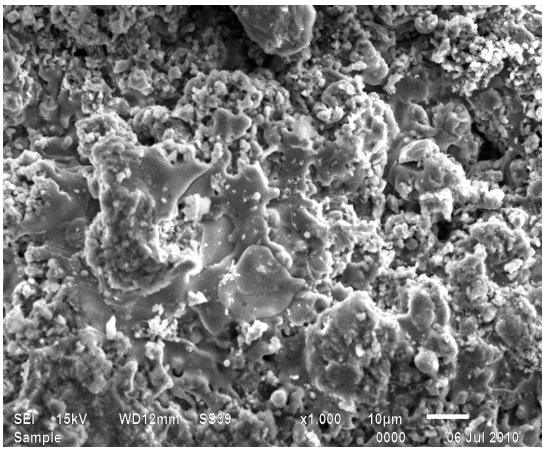

Fig.5.59 SEM image of Sample 6

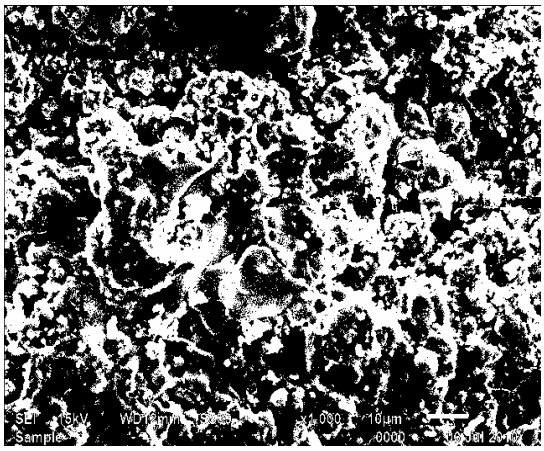

Fig.5.60 Image-J image of Sample 6

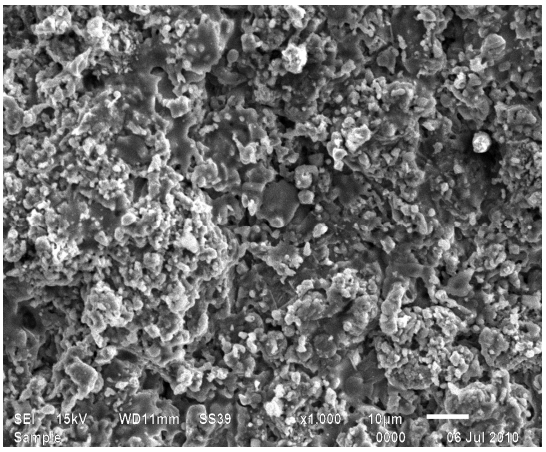

Fig.5.61 SEM image of Sample 7

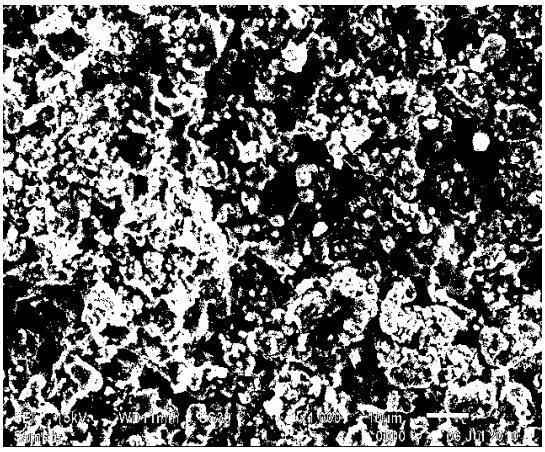

Fig.5.62 Image-J image of Sample 7

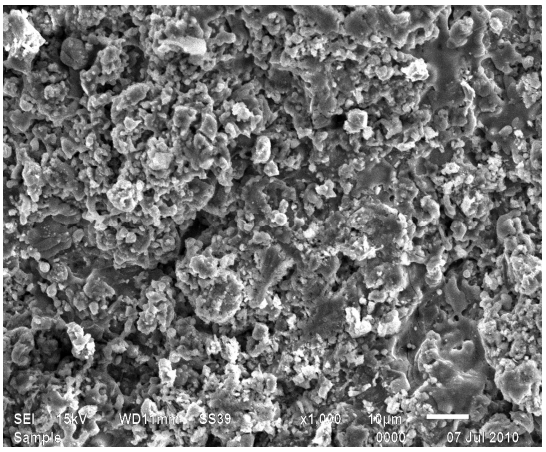

Fig.5.63 SEM image of Sample 8

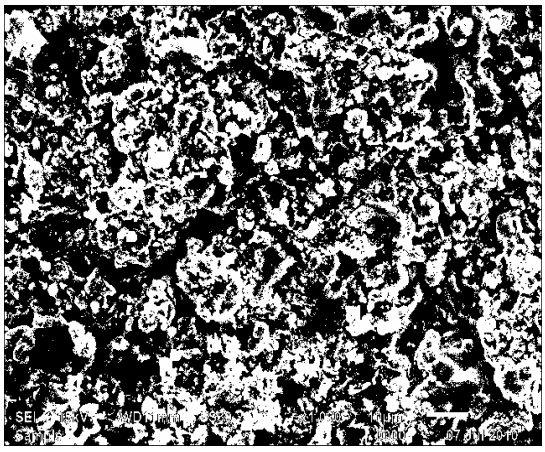

Fig.5.64 Image-J image of Sample 8

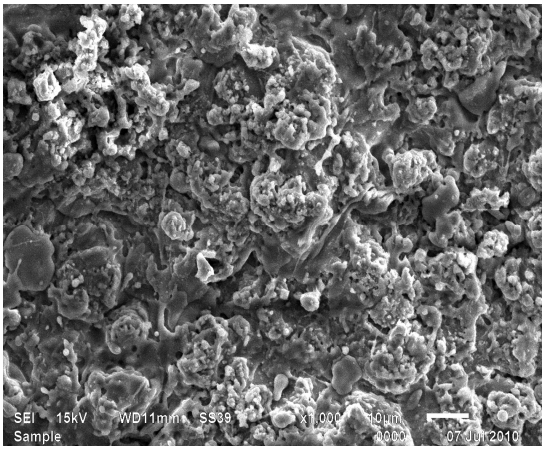

Fig.5.65 SEM image of Sample 9

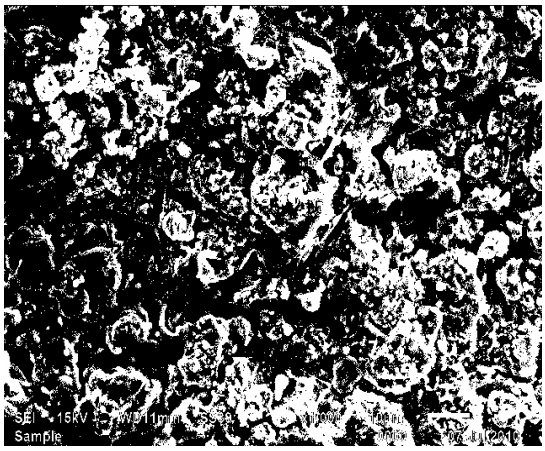

Fig.5.66 Image-J image of Sample 9

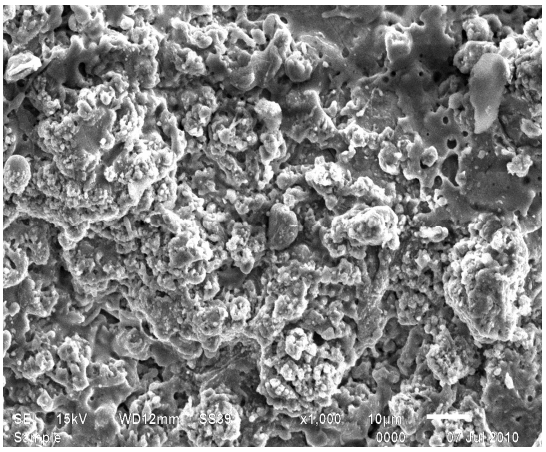

Fig.5.67 SEM image of Sample 10

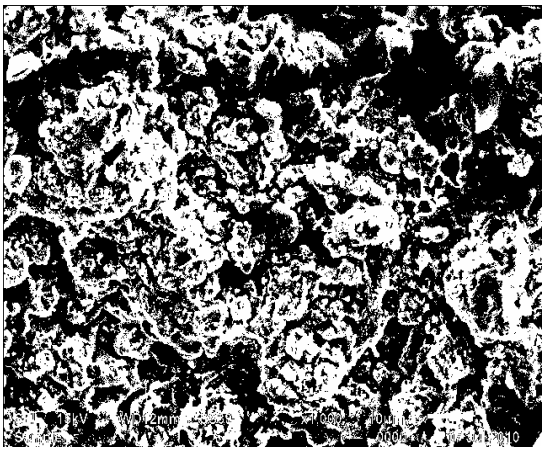

Fig.5.68 Image-J image of Sample 10

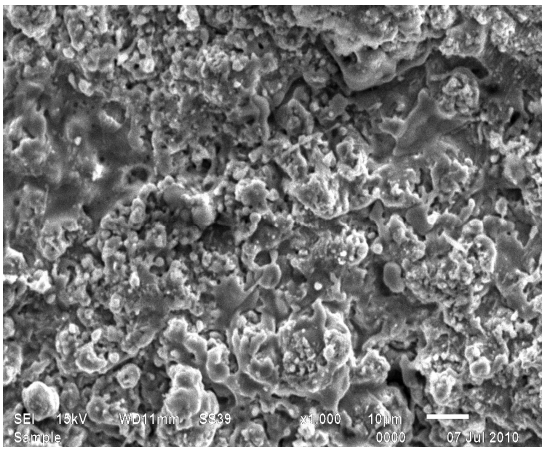

Fig.5.69 SEM image of Sample 11

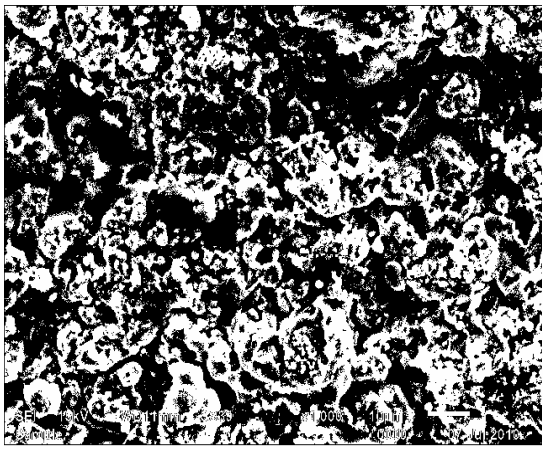

Fig.5.70 Image-J image of Sample 11

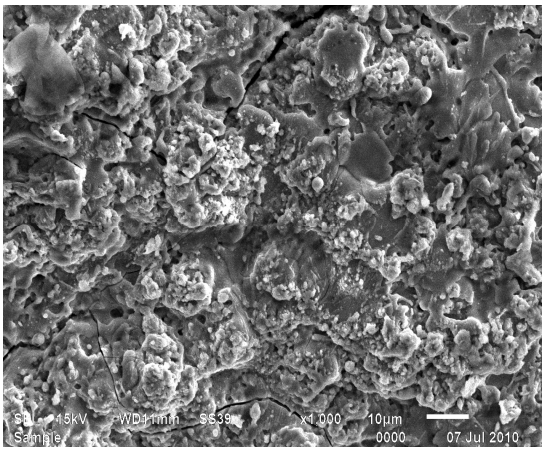

Fig.5.71 SEM image of Sample 12

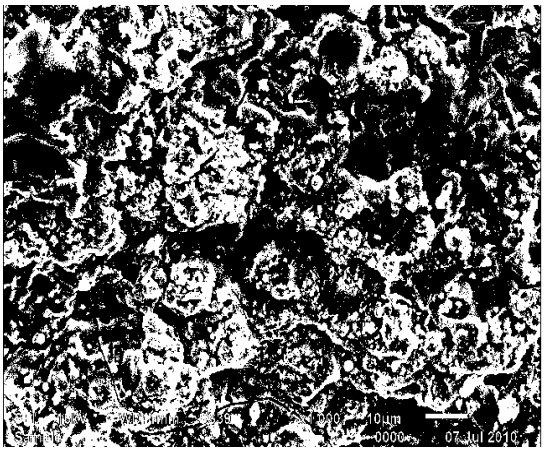

Fig.5.72 Image-J image of Sample 12

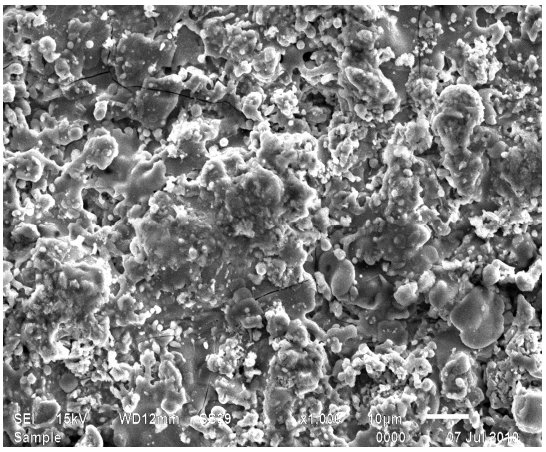

Fig.5.73 SEM image of Sample 13

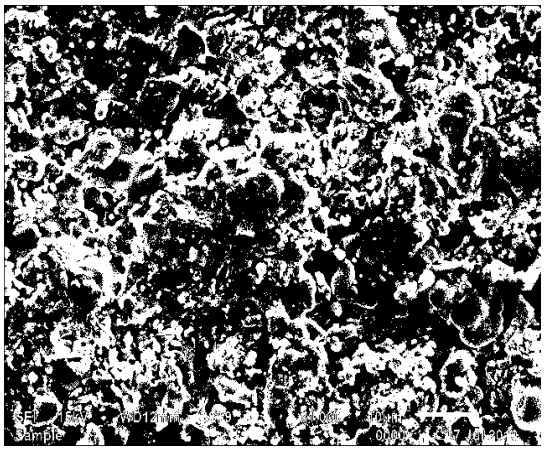

Fig.5.74 Image-J image of Sample 13

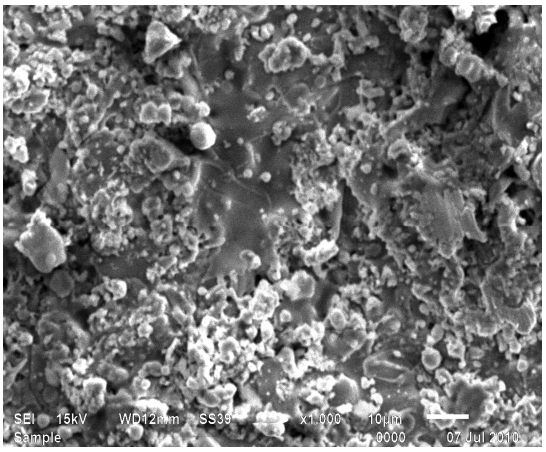

Fig.5.75 SEM image of Sample 14

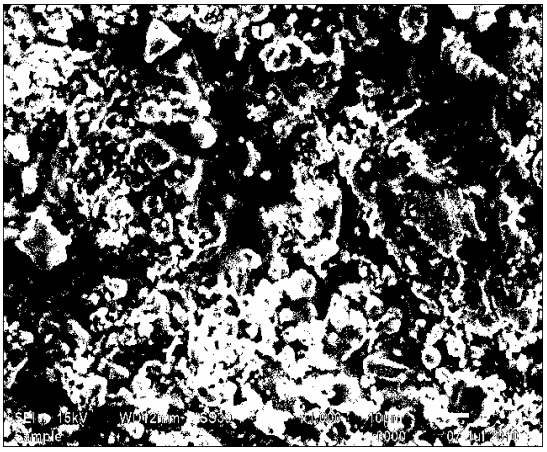

Fig.5.76 Image-J image of Sample 14

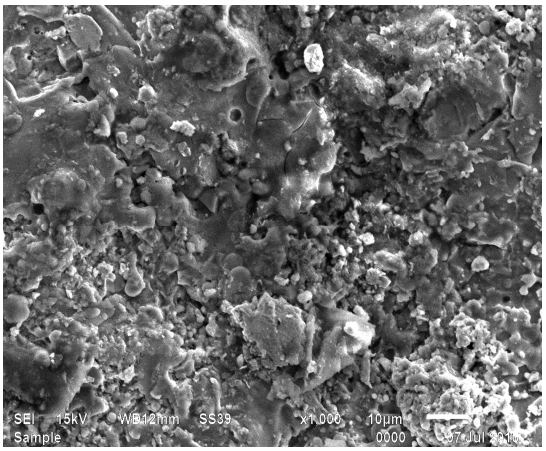

Fig.5.77 SEM image of Sample 15

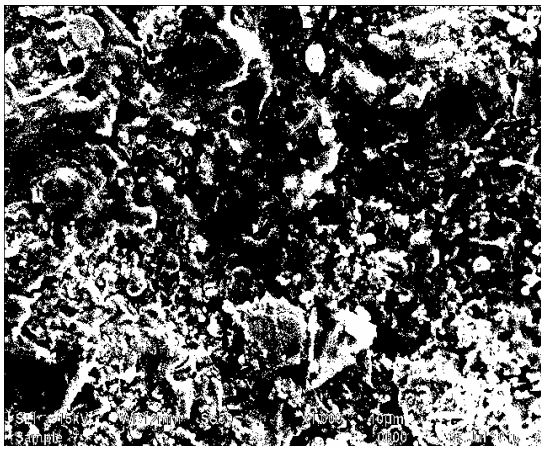

Fig.5.78 Image-J image of Sample 15

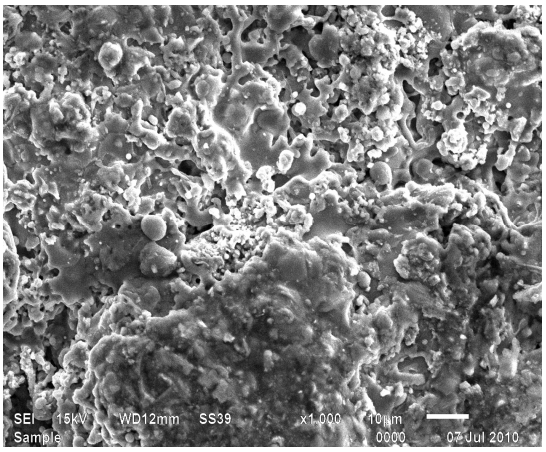

Fig.5.79 SEM image of Sample 16

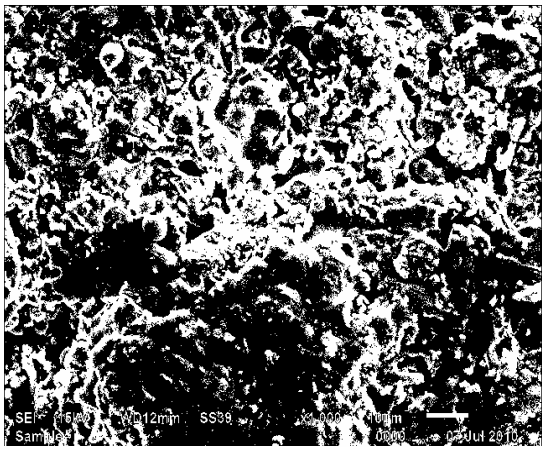

Fig.5.80 Image-J image of Sample 16

Result and discussion of analysis done by "Image J" software

Following are the results of area fraction and circularity shown in Table5.2 obtained by Image-J software.

Sample No	Area Fraction	Circularity
Sample1	58.4	0.893
Sample2	66.7	0.887
Sample3	59.5	0.92
Sample4	35.8	0.898

Sample5	62.6	0.912
Sample6	60.7	0.911
Sample7	61.6	0.902
Sample8	59.1	0.895
Sample9	65.8	0.901
Sample10	57.8	0.884
Sample11	60.7	0.91
Sample12	63.4	0.899
Sample13	60.2	0.908
Sample14	62.4	0.914
Sample15	66.5	0.906
Sample16	60.5	0.904

Table5.2 Results of area fraction and circularity

Maximum area fraction is 66.7 obtained for Sample2 and minimum area fraction is 35.8 obtained for Sample4. Maximum circularity is 0.92 obtained for Sample3 and minimum circularity is 0.893 obtained for Sample1.

Circularity - Calculate the shape descriptors like value of 1.0 indicates a perfect circle. Area Fraction - Percentage of pixels in the image or selection that have been highlighted in red.

5.2 Macroscopic Behaviour

5.2.1 Sliding wear performance of coated samples

The specific wear rates for the materials were obtained by

$$W = \Delta w / L\rho F$$

Where W denotes specific wear rates in mm^3/N-m, Δw is the weight loss measured in grams, L is the sliding distance in meters, ρ is the density of the worn material in g/mm^3, and F is the applied load in N. Weight loss of the coating in grams of 1-16 coated samples and 17 sample uncoated is shown in Table5.3.

Distance	0	300	600	900	1200	1500	1800	2100	2400	2700
Sample1	19.3743	19.3731	19.3722	19.3719	19.3716	19.3713	19.371	19.3708	19.3706	19.3692
Sample2	19.0389	19.0383	19.0364	19.0326	19.0311	19.0293	19.0267	19.0254	19.023	19.201
Sample3	19.4508	19.4498	19.4494	19.4466	19.446	19.4457	19.445	19.4446	19.4442	19.4425
Sample4	19.463	19.4612	19.4606	19.4601	19.4589	19.4581	19.4579	19.4578	19.4578	19.455
Sample5	19.6212	19.6174	19.617	19.6166	19.6154	19.6148	19.6147	19.6145	19.6143	19.6129
Sample6	19.3088	19.308	19.3067	19.3063	19.3053	19.3049	19.3049	19.3049	19.3049	19.3037
Sample7	19.5483	19.548	19.5476	19.5469	19.546	19.5457	19.5451	19.5449	19.5449	19.5437
Sample8	19.6285	19.6279	19.6276	19.6273	19.6264	19.6254	19.6238	19.6238	19.6238	19.6215
Sample9	19.5888	19.588	19.5878	19.5875	19.5874	19.5871	19.5866	19.5864	19.5864	19.5851
Sample10	19.4927	19.4926	19.4923	19.4916	19.4914	19.4911	19.4907	19.4902	19.4901	19.4894
Sample11	19.4992	19.4986	19.4984	19.4979	19.4979	19.4976	19.4964	19.4964	19.4964	19.4964
Sample12	19.3999	19.3994	19.3979	19.395	19.3947	19.394	19.3935	19.3932	19.3932	19.3918
Sample13	19.5824	19.5822	19.582	19.5808	19.5807	19.5807	19.5797	19.5797	19.5794	19.5793
Sample14	19.4343	19.4341	19.4332	19.4321	19.4321	19.4316	19.4314	19.4313	19.431	19.4308
Sample15	19.4198	19.4189	19.4188	19.4188	19.4185	19.4165	19.4158	19.4157	19.4156	19.4143
Sample16	19.4199	19.4198	19.4197	19.4193	19.4193	19.4186	19.4186	19.4186	19.4184	19.418
Sample17	19.2796	19.1251	19.1178	19.1168	19.1143	19.1128	19.1091	19.1056	19.105	19.1024

Table5.3 Weight loss of the coating (in grams) V/S Sliding distance

5.2.1.1 Graphs showing the trend of Wear Performance, W at various Detonation parameters.

Graphs cumulative wear rate and sliding distance of 16 coated samples and 1 uncoated sample is given from Fig.5.81 to Fig.5.97.

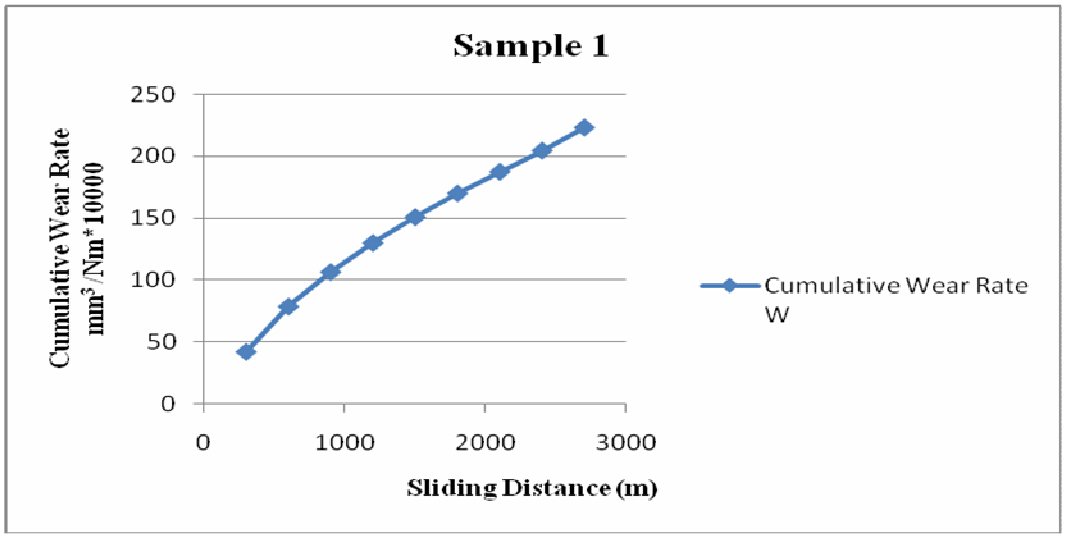

Fig.5.81 Cumulative wear rate (W) V/s Sliding distance (L) of Sample 1

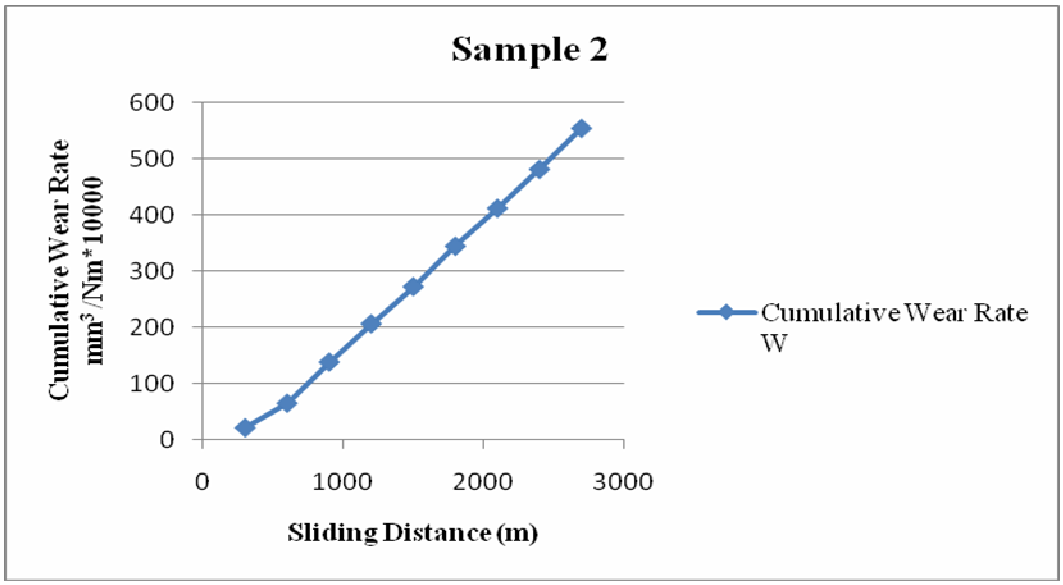

Fig.5.82 Cumulative wear rate (W) V/s Sliding distance (L) of Sample 2

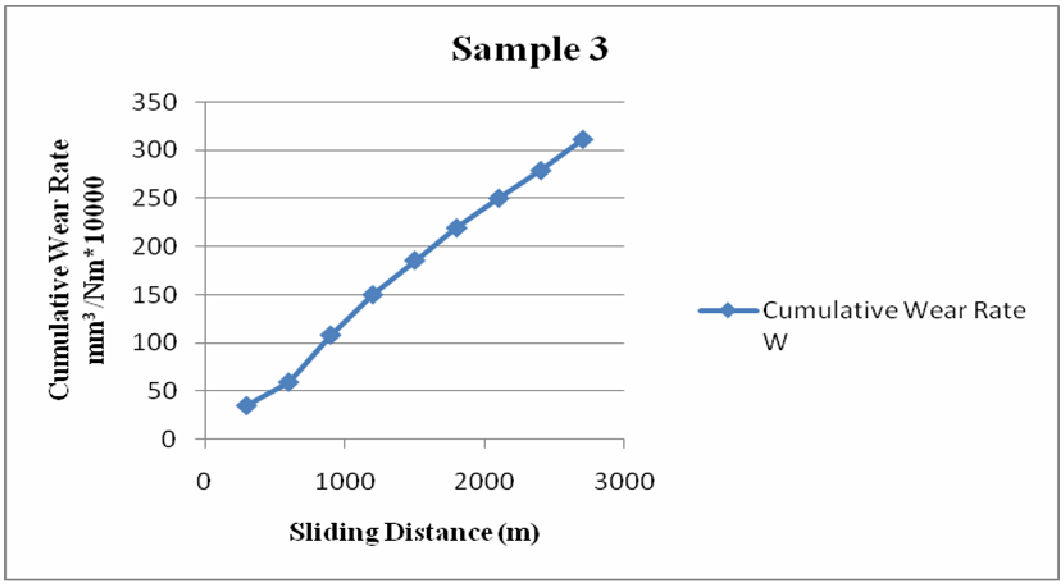

Fig.5.83 Cumulative wear rate (W) V/s Sliding distance (L) of Sample 3

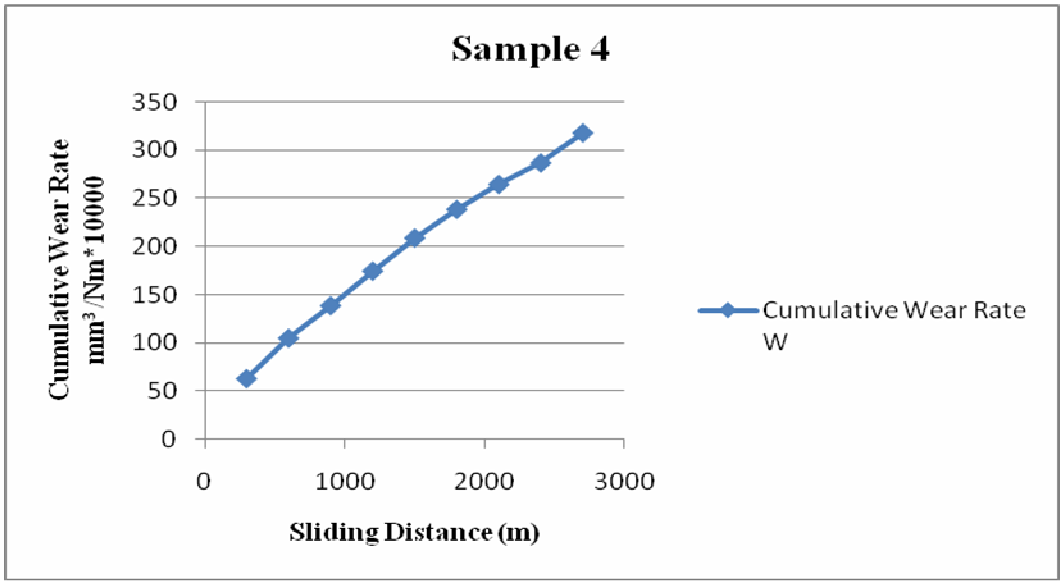

Fig.5.84 Cumulative wear rate (W) V/s Sliding distance (L) of Sample 4

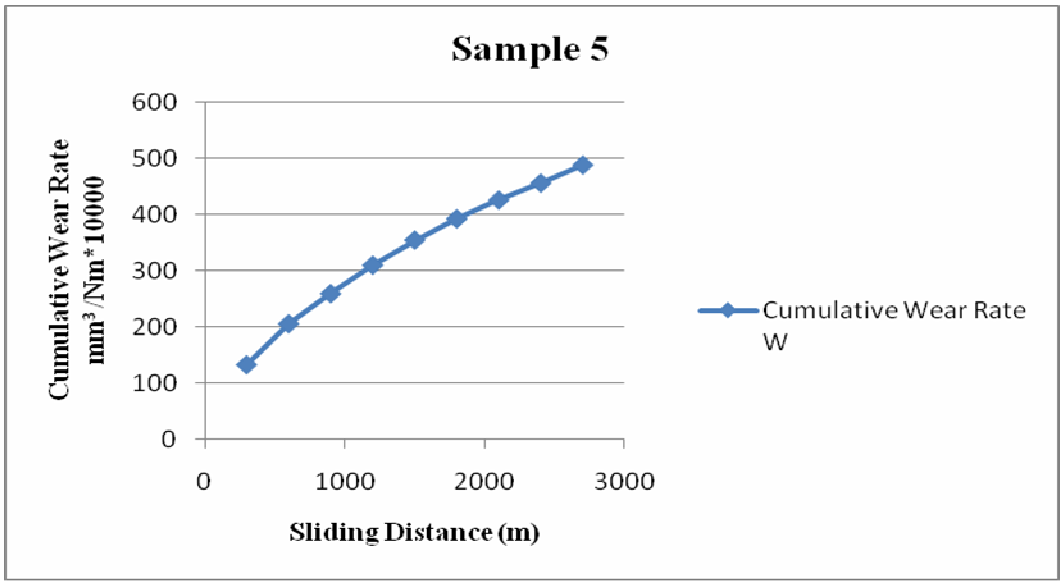

Fig.5.85 Cumulative wear rate (W) V/s Sliding distance (L) of Sample 5

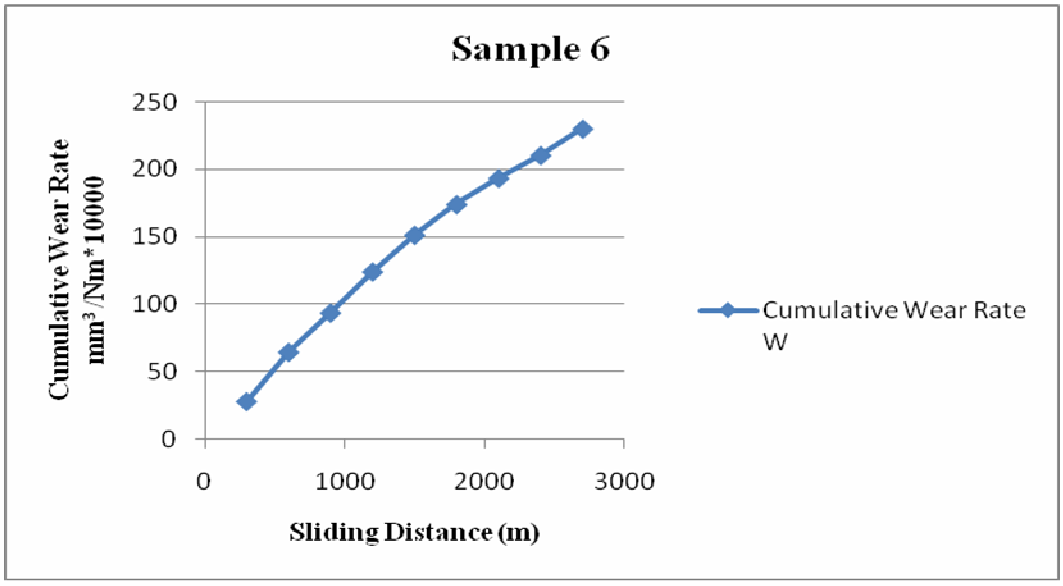

Fig.5.86 Cumulative wear rate (W) V/s Sliding distance (L) of Sample 6

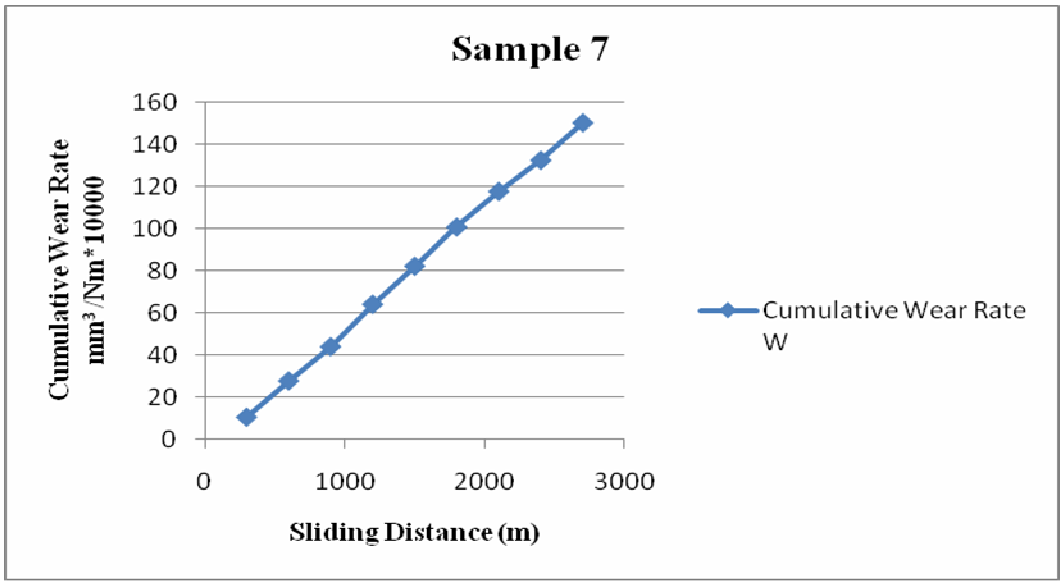

Fig.5.87 Cumulative wear rate (W) V/s Sliding distance (L) of Sample 7

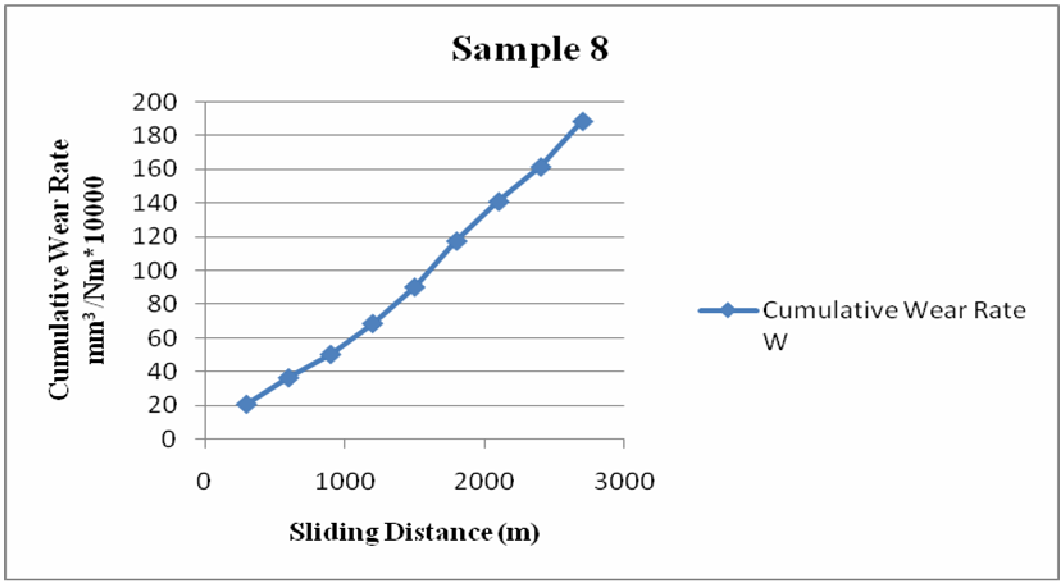

Fig.5.88 Cumulative wear rate (W) V/s Sliding distance (L) of Sample 8

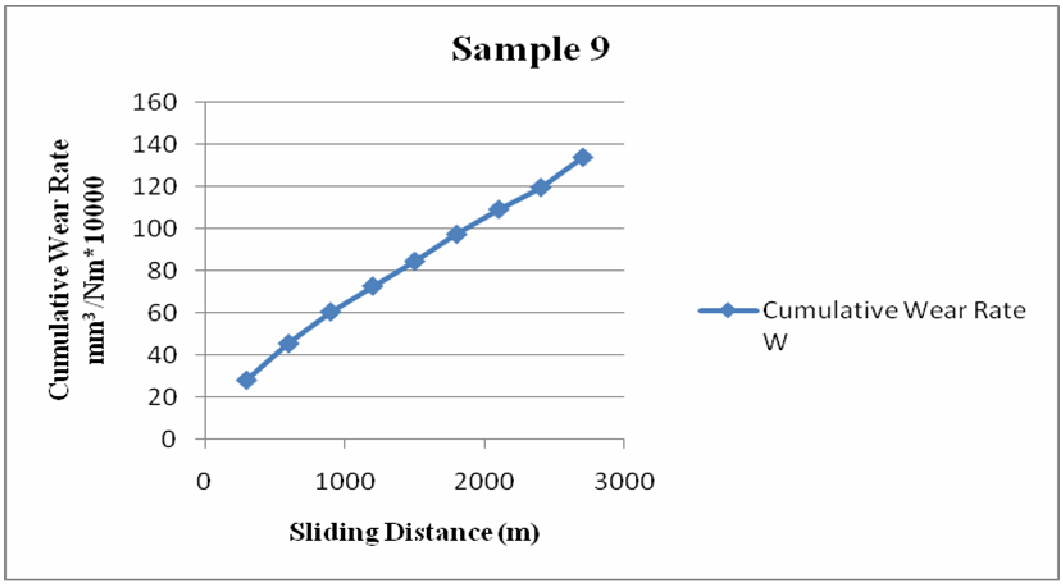

Fig.5.89 Cumulative wear rate (W) V/s Sliding distance (L) of Sample 9

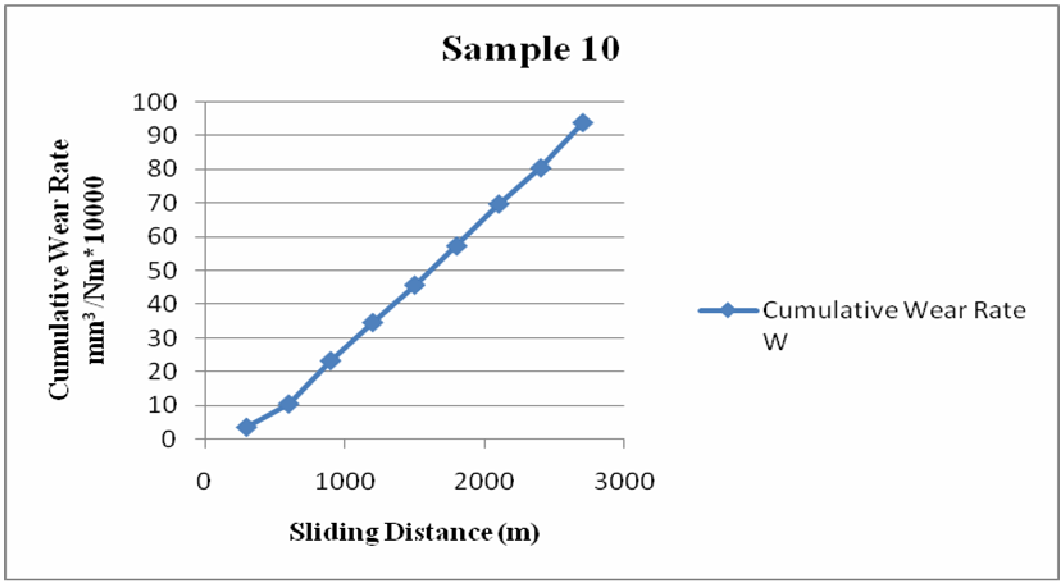

Fig.5.90 Cumulative wear rate (W) V/s Sliding distance (L) of Sample 10

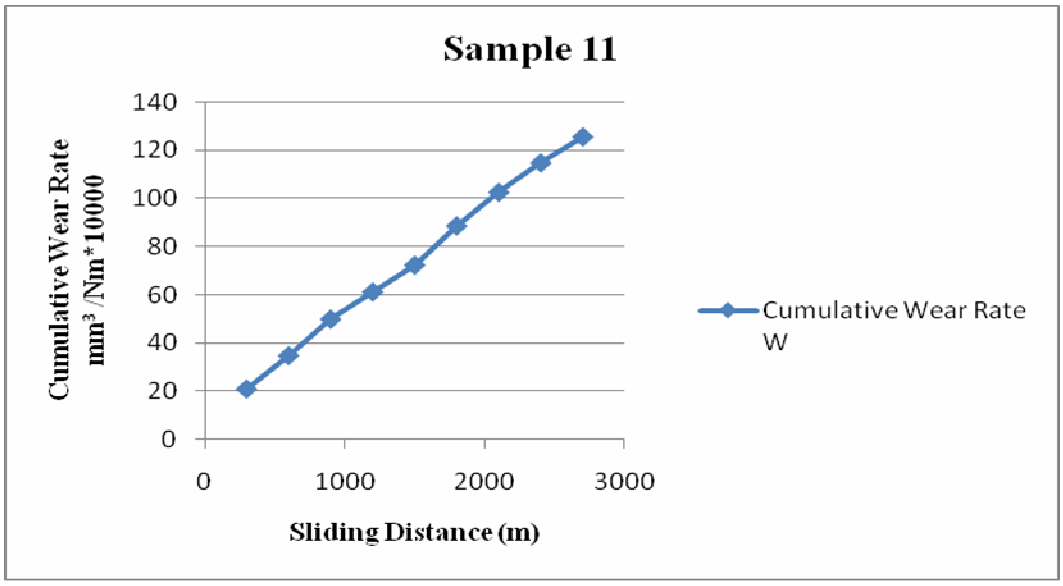

Fig.5.91 Cumulative wear rate (W) V/s Sliding distance (L) of Sample 11

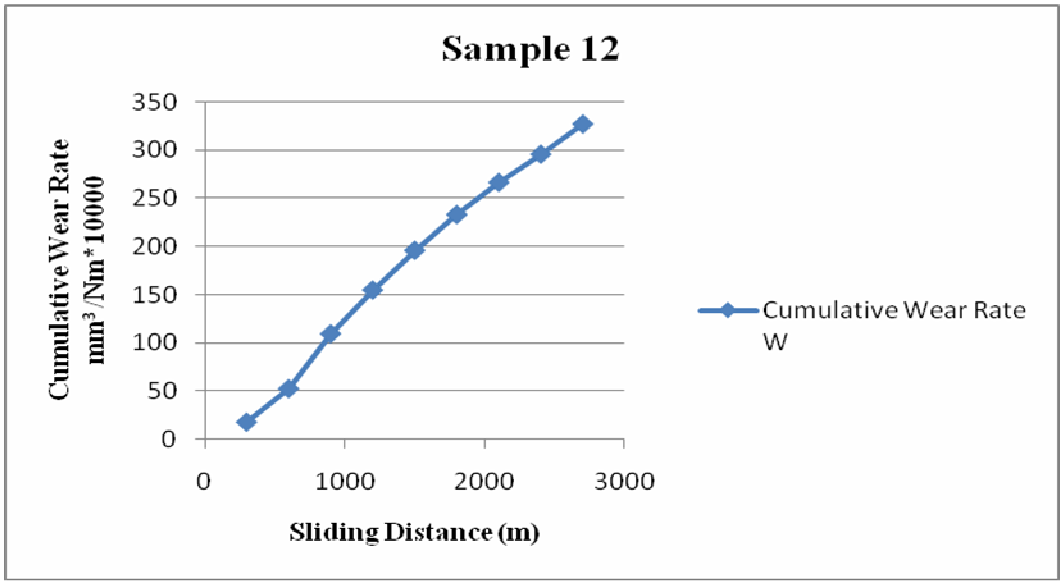

Fig.5.92 Cumulative wear rate (W) V/s Sliding distance (L) of Sample 12

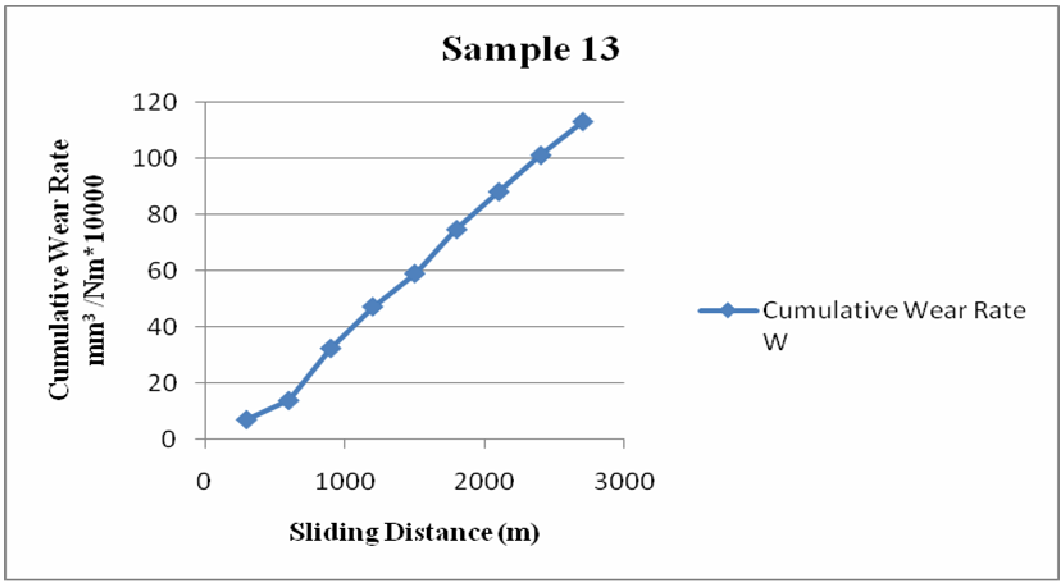

Fig.5.93 Cumulative wear rate (W) V/s Sliding distance (L) of Sample 13

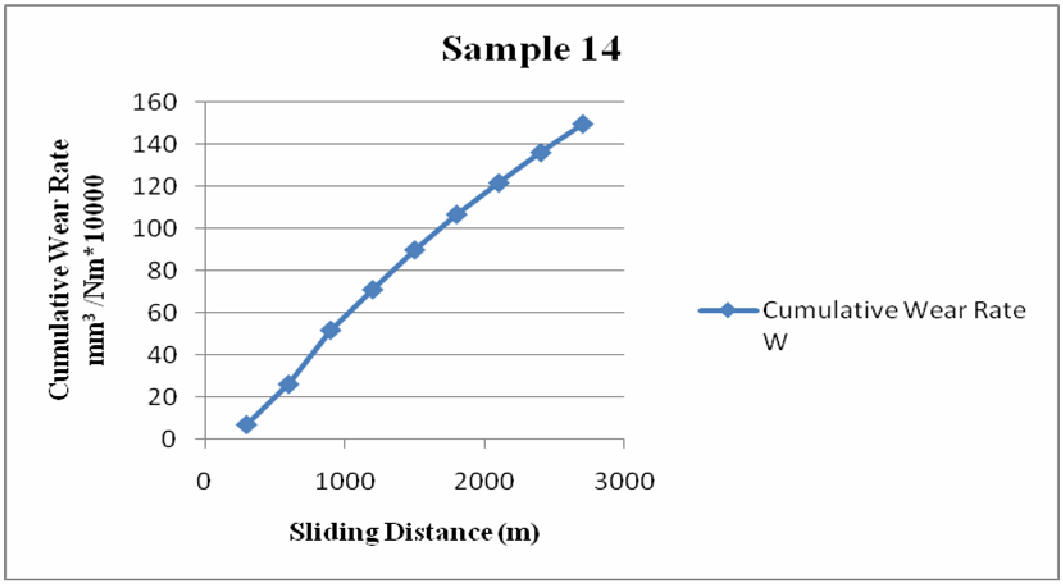

Fig.5.94 Cumulative wear rate (W) V/s Sliding distance (L) of Sample 14

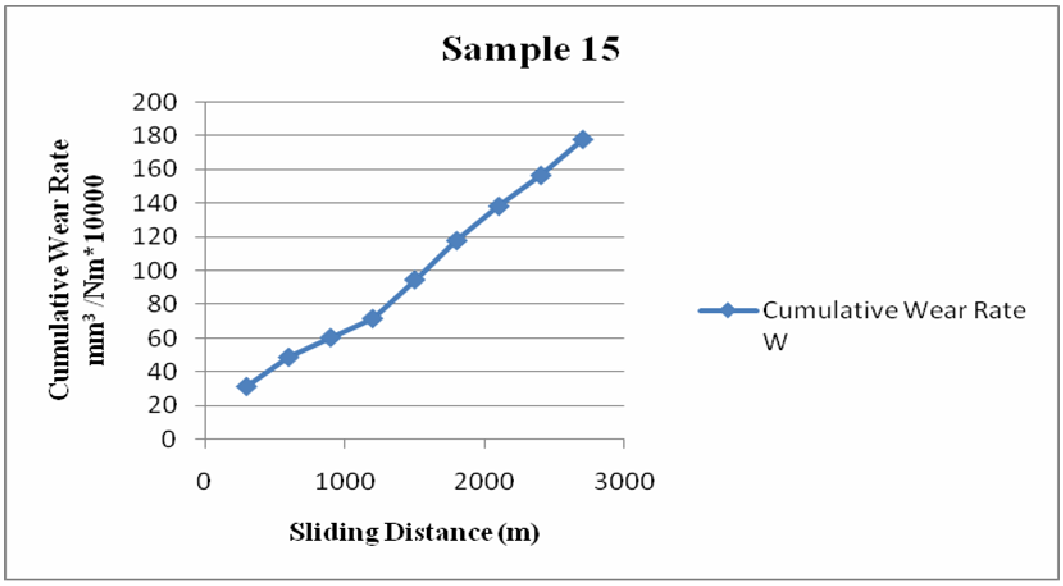

Fig.5.95 Cumulative wear rate (W) V/s Sliding distance (L) of Sample 15

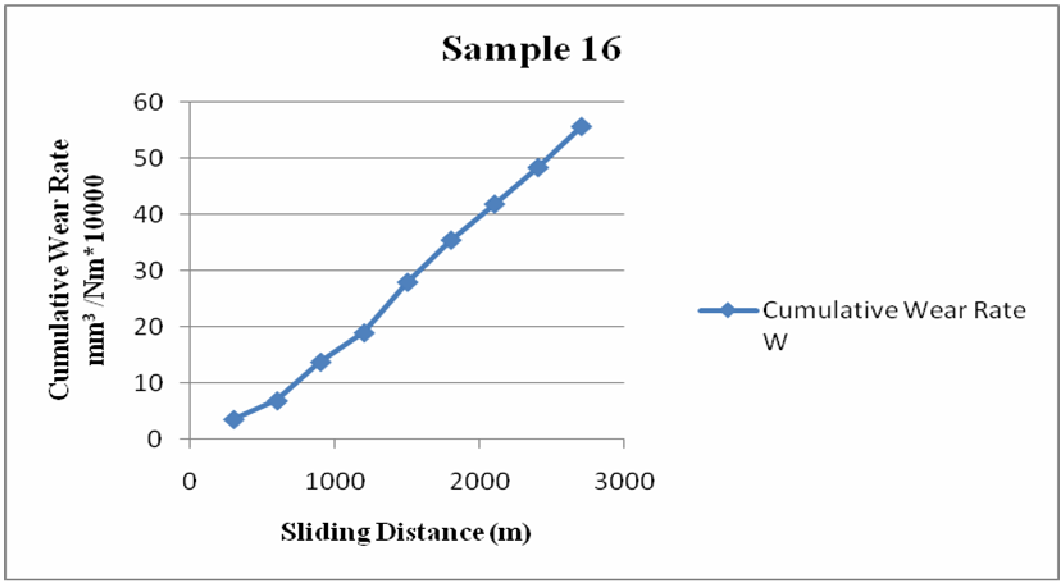

Fig.5.96 Cumulative wear rate (W) V/s Sliding distance (L) of Sample 16

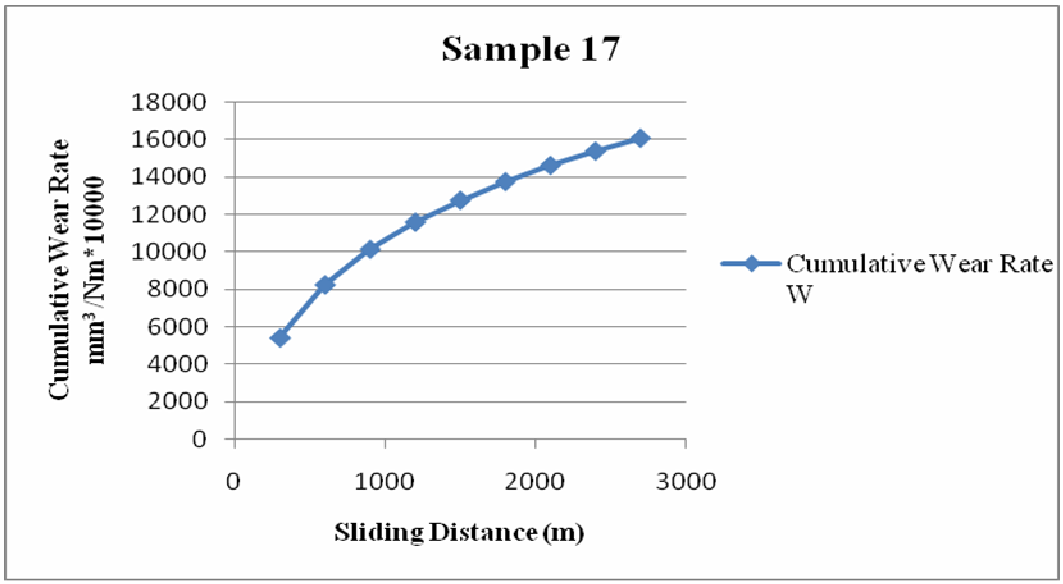

Fig.5.97 Cumulative wear rate (W) V/s Sliding distance (L) of Sample 17 (uncoated)

Maximum cumulative wear rate and Wear slope of coated samples with detonation parameters are given in Table5.4. 'SLPH' means 'Standard Litres per Hour', Powder 1 means (20%HA+40%TiO_2+40%Al_2O_3) and Powder 2 means (30%HA+35%TiO_2+35%Al_2O_3).

Sample No.	D-Gun Spray Parameters				Max. Cumulative Wear Rate	Wear Slope
	Oxygen (SPLH)	Acetylene (SPLH)	Nitrogen (SPLH)	Powder Composition		
1	5040	710	2160	Powder 1	223.1	0.075
2	5120	710	2160	Powder 1	553.5	0.22
3	5040	800	2160	Powder 1	311.3	0.11
4	5120	800	2160	Powder 1	317.1	0.1
5	5040	710	2160	Powder 1	488	0.14
6	5120	710	2160	Powder 1	230.1	0.08
7	5040	800	2160	Powder 1	150.2	0.05
8	5120	800	2160	Powder 1	188.7	0.06
9	5040	710	2240	Powder 2	133.8	0.04
10	5120	710	2240	Powder 2	93.7	0.03
11	5040	800	2240	Powder 2	125.5	0.04
12	5120	800	2240	Powder 2	327.1	0.12
13	5040	710	2240	Powder 2	113.1	0.04

14	5120	710	2240	Powder 2	149.3	0.05
15	5040	800	2240	Powder 2	177.9	0.06
16	5120	800	2240	Powder 2	55.6	0.02

Table 5.4 Maximum cumulative wear rate and Wear slope of samples with detonation parameters

Result and discussion of graphs between cumulative wear rate and sliding distance

Minimum cumulative wear rate is 55.6 observed for Sample 16 at Oxygen flow rate 5120 SPLH, Acetylene flow rate 800 SPLH, Nitrogen flow rate 2240 SPLH and Powder 2 (30%HA+35%TiO_2+35%Al_2O_3). Maximum cumulative wear rate is 553.5 observed for Sample 2 at Oxygen flow rate 5120 SPLH, Acetylene flow rate 710 SPLH, Nitrogen flow rate 2160 SPLH.

5.2.2 Hardness and Microhardness Measurement

Sample No.1 to 16 are coated samples and Sample No.17 is uncoated sample as shown in Table 5.5.

Sample No.	**Mean Rockwell hardness No. R_c**	**Mean Micro hardness VHN No.**
1	52.2	172.05
2	56.4	153.6
3	55	149.4
4	53.8	129.5
5	56.6	148.7
6	58	151.6
7	60.8	128.4
8	49.4	166
9	52.6	190.8
10	52.2	136.7
11	50.6	133.6
12	51.6	138.1
13	54.2	127.2
14	54.8	157.5
15	55.2	131
16	57.8	134.9
17	48.1	110

Table 5.5 Hardness and Micro hardness measurement

5.2.2.1 Graphs showing the trend of Rockwell hardness number and Micro hardness number at various Detonation parameters.

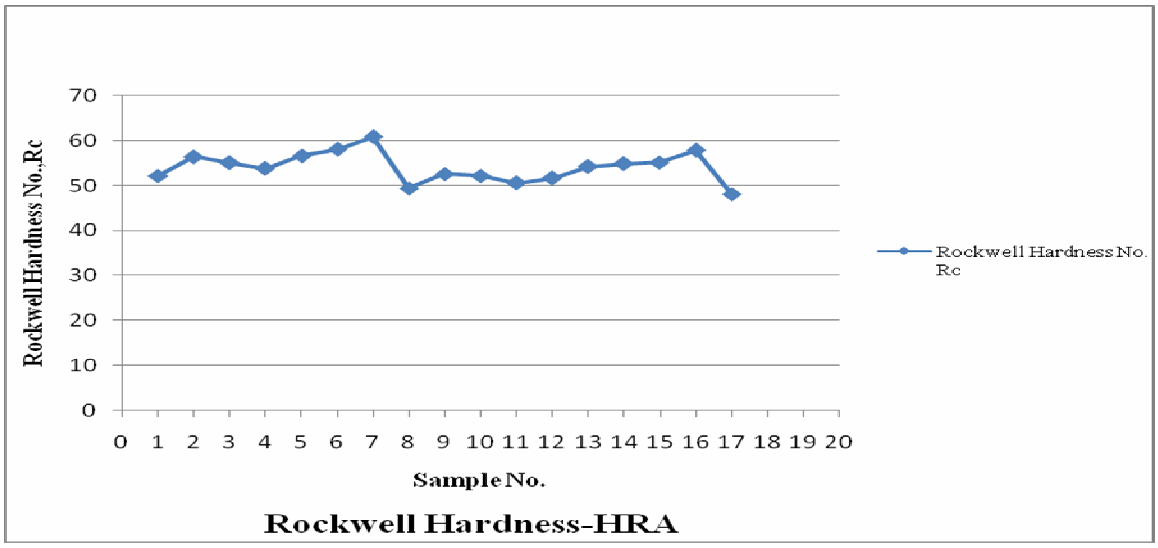

Fig.5.98 Graphs showing the trend of Hardness number at various Detonation parameters.

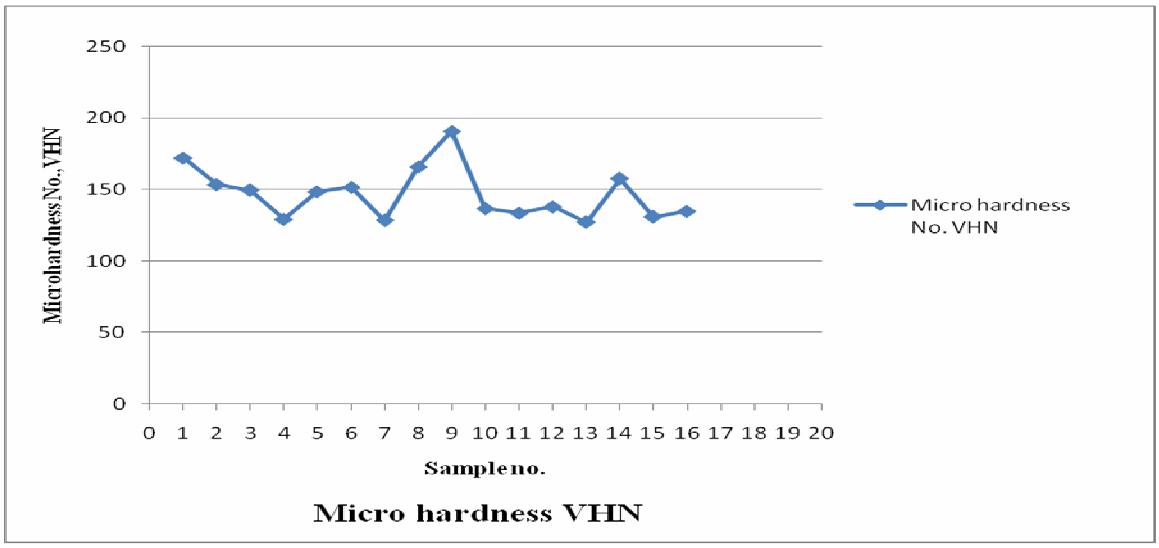

Fig.5.99 Graphs showing the trend of Micro hardness number at various Detonation parameters.

Result and discussion of Rockwell hardness number and micro hardness number of coated samples

As shown in Fig.5.98 maximum value of Rockwell hardness number for coated sample, Rc is 60.8 for Sample No.7 obtained at Oxygen flow rate 5040 SPLH, Acetylene flow rate 800 SPLH, Nitrogen flow rate 2160 SPLH and Powder 1 (20%HA+40%TiO_2+40%Al_2O_3). The minimum value of Rockwell hardness number for coated sample, Rc is 49.4 for Sample No.8 obtained at Oxygen flow rate 5120 SPLH, Acetylene flow rate 800 SPLH, Nitrogen flow rate 2160 SPLH and Powder 1 (20%HA+40%TiO_2+40%Al_2O_3). For uncoated Sample No.17, Rockwell hardness number is 48.1. So, increase in Rockwell hardness is obtained after coating.

As shown in Fig.5.99 maximum value of Micro hardness number for coated sample, Rc is 190.8 for Sample No.9 obtained at Oxygen flow rate 5040 SPLH, Acetylene flow rate 710 SPLH, Nitrogen flow rate 2240 SPLH and Powder 2 (30%HA+35%TiO_2+35%Al_2O_3). The minimum value of Micro hardness number for coated sample, Rc is 128.4 for Sample No.7 obtained at Oxygen flow rate 5040 SPLH, Acetylene flow rate 800 SPLH, Nitrogen flow rate 2160 SPLH and Powder 1 (20%HA+40%TiO_2+40%Al_2O_3). For uncoated Sample No.17, Micro hardness number is 110. So, increase in Micro hardness is obtained after coating.

5.3 Relation between Microscopic and Macroscopic behaviour

Graph is drawn to show the relation between wear slope and microhardness, wear slope and area fraction, wear slope and circularity as shown in Fig.5.100, Fig.5.101 and Fig.5.102 respectively.

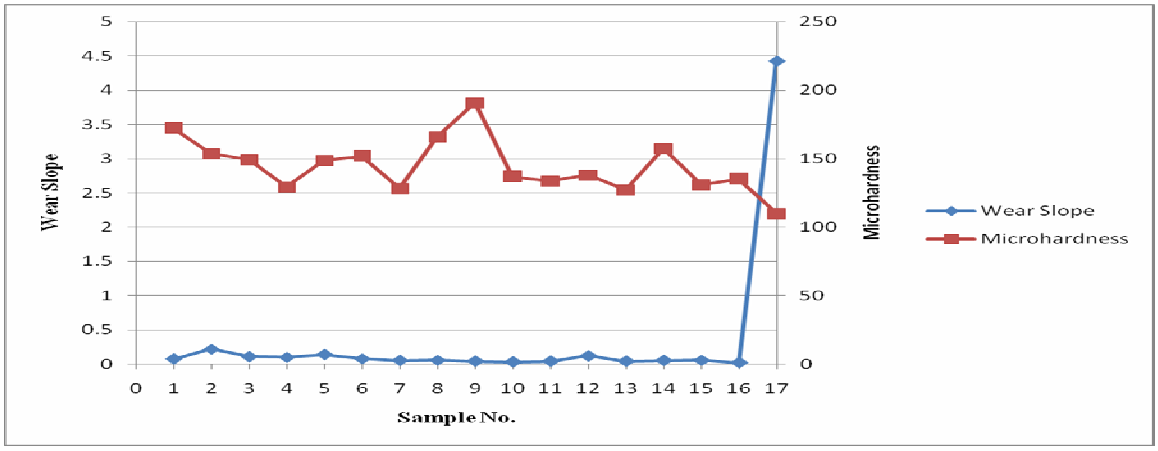

Fig.5.100 Graph between Wear Slope, Sample No. and Micro hardness

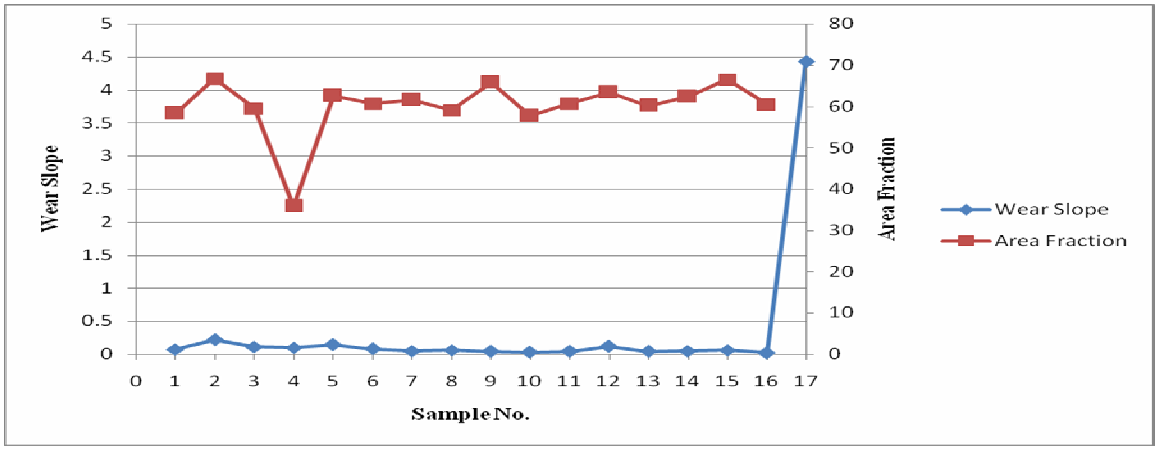

Fig.5.101 Graph between Wear Slope, Sample No. and Area Fraction

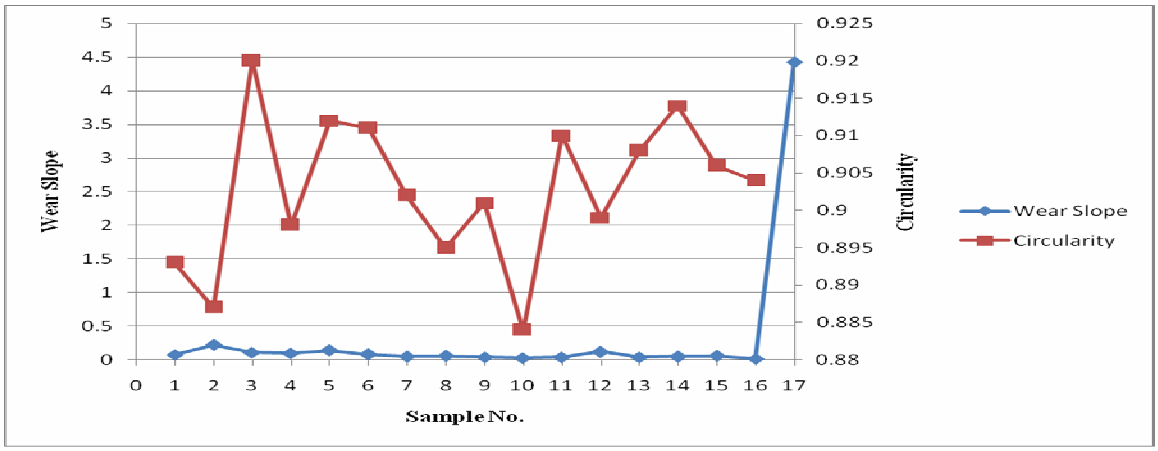

Fig.5.102 Graph between Wear Slope, Sample No. and Circularity

Result and discussion of graph between wear slope and microhardness, wear slope and area fraction, wear slope and circularity

As shown in Fig.5.100, results predict that more is the Wear slope less is the micro hardness. Wear slope for uncoated Sample No. 17 is large as compared to coated samples. Micro hardness for uncoated Sample No.17 is small as compared to coated samples.

As shown in Fig.5.101, results predict that more is the Wear slope more is the Area fraction. Wear slope for uncoated Sample No. 17 is large as compared to coated samples.

As shown in Fig.5.102, results predict that more is the Wear slope less is the Circularity. Wear slope for uncoated Sample No. 17 is large as compared to coated samples.

Chapter 6 CONCLUSIONS AND FUTURE SCOPE

6.1 Conclusions

Following are the main conclusions drawn from the present research work:

- The XRD peaks of eggshell powder at 900^0C shows Hydroxyapatite (HA) as per following:

  Peak No.1: 32.8 ^{o}
  Peak No.2: 54.5 ^{o}
  Peak No.3: 65.3 ^{o}
  Peak No.4: 67.0 ^{o}

- In the FTIR, The OH group is found at 3514.20cm^{-1} and 654.03 for eggshell powder at 900^0C, and the same peak is also traced in HA powder. Similarly, the P-O group is also found at 1084.02cm^{-1} and 874.82cm^{-1} for egg shell powder at 300^0C, 872.39cm^{-1} for eggshell powder at 600^0C, 1098.99cm^{-1} and 873.45cm^{-1} for eggshell powder at 900^0C and the same peak is also traced in HA powder. So, it is clear from the above comparison that both the powders shows the traces of HA phase.

- During the biocompatibility test, the Powder 1 produces blood clotting in 8 seconds and the Powder 2 makes blood clotting in 28 seconds which shows that both the powders are efficient and compatible with human blood and clotting capacity is good for Powder 1.

- Both the Powder 1 and Powder 2 are successfully sprayed by detonation gun.

- The microstructure examination of the coated samples shows the uniform distribution of Powder 1(20%HA+40%TiO_2+40%Al_2O_3) on SS 304L metal substrate. It is due to good flowability of Powder 1 as compared to Powder 2(30%HA+35%TiO_2+35%Al_2O_3).

- The XRD peaks of coated samples shows formation of various elements from hybrid powder like $Ca(TiO_3)$, $Al(OH)_3$,$AlPO_4$, $CaTi_2O_4(OH)_2$,MgO,CaO etc.

- The coated samples show very good resistance to wear as compared to uncoated samples. Minimum cumulative wear is obtained for Sample16.

- The maximum amount of Rockwell Hardness Number, Rc i.e.60.8 is obtained at Oxygen flow rate 5040 SPLH, Acetylene flow rate 800 SPLH., Nitrogen flow rate 2160 SPLH and Powder 1 (20%HA+40%TiO_2+40%Al_2O_3).

- The maximum amount of Micro Hardness Number, VHN i.e.190.8 is obtained at Oxygen flow rate 5040 SPLH, Acetylene flow rate 710 SPLH., Nitrogen flow rate 2160 SPLH and Powder 1 (20%HA+40%TiO_2+40%Al_2O_3).

- Maximum area fraction is 66.7 obtained for Sample2 and minimum area fraction is 35.8 obtained for Sample4.

- Maximum circularity is 0.92 obtained for Sample3 and minimum circularity is 0.893 obtained for Sample1.

- Wear slope is inversely proportional to micro hardness i.e more is the Wear slope less is the micro hardness.

- Wear slope is proportional to Area fraction i.e more is the Wear slope more is the area fraction.

- Wear slope is inversely proportional circularity i.e more is the Wear slope less is the circularity.

6.2 Scope for future work

- Coating characteristics of Detonation spraying technique may be compared with other thermal spray techniques like HVOF, Plasma spraying etc.
- Base metal may be varied like SS 316L, cobalt-chromium alloys and titanium to enhanced mechanical properties.
- Instead of TiO_2 and Al_2O_3, some other biocompatible material may be included in future.
- Coated samples may be implanted in SBF (stimulated body fluid) to see the blood and saliva compatibility.

REFERENCES

1. K Prabakaran, A Balamurugan and S Rajeswari, ***Development of calcium phosphate based apatite from hen's eggshell***, Bull. Mater. Science, Vol. 28, No. 2, pp. 115–119, April 2005.

2. Csaba Balazsi, Zsuzsanna Kover, Eniko Horvath, Csaba Nemeth, Zsolt Kasztovszky, Sandor Kurunczi and Ferenc Weber, ***Examination of calcium phosphates prepared from eggshell***, Materials science forum, Vol. 537-538, pp 105-112, 2007.

3. Su-Hee Lee, Hae-Won Kim, Eun-Jung Lee, Long-Hao Li and Hyoun-Ee Kim, ***Hydroxyapatite–TiO_2 hybrid coating on Ti implant***, Journal of Biomaterials Applications, Vol. 20, pp 195-208, January, 2006.

4. R.S. Lima, C. Moreau, and B.R. Marple, ***HVOF-Sprayed coatings engineered from mixtures of nanostructured and submicron Al_2O_3-TiO_2 powders: An enhanced wear performance***, Journal of Thermal Spray Technology Volume 16, pp 866-872, December 2007.

5. Aravind Vadiraj and M. Kamaraj***, Fretting fatigue studies of titanium nitride coated biomedical titanium alloys***, Journal of Materials Engineering and Performance, Vol. 15(5), pp 553-557, October 2006.

6. R. Jaworski, L. Pawlowski and C. Pierlot***, Suspension plasma sprayed titanium oxide and hydroxyapatite coatings***, Thermal Spray 2009, pp 156-161, 2009.

7. Heleno R.A, Wagner N. S and J. R. T. Branco, ***Performance evaluation of hydroxyapatite coatings thermally sprayed on surgical fixation pins***, Key Engineering Materials, Vol. 396-398, pp 396-398, 2009.

8. F.-X. Ye, A. Ohmori, T. Tsumura, K. Nakata and C.-J. Li, ***Microstructural analysis and photocatalytic activity of plasma sprayed titania-hydroxyapatite coatings***, Volume 16(5-6), pp 776-782, December 2007.

9. Kobayashi Akira and Jiang Wei, ***Preparation of plasma sprayed Titania/Hydroxyapatite photocatalytic coatings with nanostructured powder***, Transactions of JWRI, Vol. 34, No.1, 2005.

10. Celaletdin Ergun and Robert H. Doremus, ***Thermal stability of hydroxylapatite-titanium and hydroxylapatite-titania composites***, Env. Sci., Vol. 27, pp 423-429, 2003.

11. M. Gaona, R.S. Lima and B.R. Marple, ***Influence of particle temperature and velocity on the microstructure and mechanical behavior of high velocity oxy-fuel (HVOF)-sprayed nanostructured titania coatings***, Journal of materials processing technology, pp 426–435, July 2007.

12. Arjun Dey, Anoop K. Mukhopadhyay, S. Gangadharan, Mithilesh K. Sinha, and Debabrata Basu, ***Characterization of microplasma sprayed hydroxyapatite coating***, Journal of Thermal Spray Technology, September 2009.

13. P. Suresh Babu, Bikramjit Basu and G. Sundararajan, ***Processing–structure–property correlation and decarburization phenomenon in detonation sprayed WC–12Co coatings***, Acta Materialia, Vol. 56, pp 5012–5026, July 2008.

14. Kantesh Balani, Rebecca Anderson, Tapas Laha, Melanie Andara, Jorge Tercero, Eric Crumpler and Arvind Agarwal, ***Plasma-sprayed carbon nanotube reinforced hydroxyapatite coatings and their interaction with human osteoblasts in vitro***, Biomaterials, Vol.28, pp 618–624, 2007.

15. Dean-Mo Liu, Quanzu Yang and Tom Troczynski, ***Sol–gel hydroxyapatite coatings on stainless steel substrates***, Biomaterials, Vol. 23, pp 691–698, 2002.

16. H. Singh, M.S. Grewal, H.S. Sekhon and R.G. Rao, ***Sliding wear performance of high-velocity oxy-fuel spray Al_2O_3/TiO_2 and Cr_2O_3 coatings***, Proc. IMechE Part J: Engineering Tribology, Vol. 222, pp 601–610, 2008.

17. Maninder Kaur, Harpreet Singh, Balraj Singh, and Bhupinder Singh, ***Studies on the Sliding Wear Performance of Plasma Spray Ni-20Cr and Ni_3Al Coatings***, Journal of Thermal Spray Technology, Vol. 19, pp 378–383, January 2010.

18. G. Sundararajan, D. Sen and G. Sivakumar, ***The tribological behaviour of detonation sprayed coatings: the importance of coating process parameters***, Wear, Vol. 258, pp 377–391, *2005*.

19. Margaret A. McGee , Donald W. Howie , Kerry Costi , David R. Haynes , Corinna I. Wildenauer , Mark J. Pearcy and Jean D. McLean, ***Implant retrieval studies of the wear and loosening of prosthetic joints: a review***, Wear, Vol. 241, pp 158–165, 2000.

20. U Kamachi Mudali, T M Sridhar and Baldev Raj, ***Corrosion of bio implants***, Metallurgy and Materials Group, Sadhana, Vol. 28, Parts 3 & 4, pp 601-637, June 2003.

21. J.J. Ramsden, D.M. Allen, D.J. Stephenson, J.R. Alcock, G.N. Peggs, G. Fuller and G. Goch, ***The design and manufacture of biomedical surfaces***, Annals of the CIRP, Vol. 56, pp 687-711, February 2007.

22. J.P. Simon and G. Fabry, ***An overview of implant materials***, Acta Orthopaedica Belgica, Vol. 57, pp 1-5, January 1991.

23. Daniel Lin, Qing Li, Wei Li and Michael Swain**,** ***Dental implant induced bone remodeling and associated algorithms (review article)*****,** Journal of the mechanical behavior of biomedical materials, Vol.2, pp 410-432, 2009.

24. Naresh Chaudhary, Scott T. Lovald, Jon Wagner, Tariq Khraishi and Bret Baack**,** ***Experimental and numerical modeling of screws used for rigid internal fixation of mandibular fractures*****,** Modeling and Simulation in Engineering, Vol. 2008, pp 1-11, February 2008.

25. Sachiko Hiromoto**, Corrosion of Metallic Biomaterials in Cell Culture Environments,** The Electrochemical Society Interface, pp 41-44, Summer 2008.

26. Joyce Y.Wong, ***Biomaterials*** (Book), pp 13-17, 2007.

27. Jeremy Ramsden, ***Biomedical surface*** (Book), pp 51-52, 2008.

28. Teoh Swee Hin, ***Engineering materials for biomedical applications*** (Book), pp 1-3, 2004.

29. Gordon England, ***Independent metallurgist & consultant to the thermal spray coating industry***, *www.gordonengland.co.uk.*

30. Efunda, ***The ultimate online reference for engineers***, *www.efunda.com*.

31. Emedicine, ***Medical reference***, *www.emedicine.medscape.com*.

32. The Molecular Material Research Center, ***Introduction to Fourier transform infrared spectrometry***, *www.mmrc.caltech.edu/FTIR/FTIRintro.pdf*.